National Library of Canada
Bibliothèque nationale du Canada

Canadian Theses Service
Services des thèses canadiennes

Ottawa, Canada
K1A 0N4

CANADIAN THESES
THÈSES CANADIENNES

NOTICE

The quality of this microfiche is heavily dependent upon the quality of the original thesis submitted for microfilming. Every effort has been made to ensure the highest quality of reproduction possible.

If pages are missing, contact the university which granted the degree.

Some pages may have indistinct print especially if the original pages were typed with a poor typewriter ribbon or if the university sent us an inferior photocopy.

Previously copyrighted materials (journal articles, published tests, etc.) are not filmed.

Reproduction in full or in part of this film is governed by the Canadian Copyright Act, R.S.C. 1970, c. C-30. Please read the authorization forms which accompany this thesis.

AVIS

La qualité de cette microfiche dépend grandement de la qualité de la thèse soumise au microfilmage. Nous avons tout fait pour assurer une qualité supérieure de reproduction.

S'il manque des pages, veuillez communiquer avec l'université qui a conféré le grade.

La qualité d'impression de certaines pages peut laisser à désirer, surtout si les pages originales ont été dactylographiées à l'aide d'un ruban usé ou si l'université nous a fait parvenir une photocopie de qualité inférieure.

Les documents qui font déjà l'objet d'un droit d'auteur (articles de revue, examens publiés, etc.) ne sont pas microfilmés.

La reproduction, même partielle, de ce microfilm est soumise à la Loi canadienne sur le droit d'auteur, SRC 1970, c. C-30. Veuillez prendre connaissance des formules d'autorisation qui accompagnent cette thèse.

THIS DISSERTATION
HAS BEEN MICROFILMED
EXACTLY AS RECEIVED

LA THÈSE A ÉTÉ
MICROFILMÉE TELLE QUE
NOUS L'AVONS REÇUE

Canada

NL 339 (r. 86/01)

National Library of Canada / Bibliothèque nationale du Canada

174 Ottawa, Canada K1A 0N4

TC –

I 0-315-23368-0

CANADIAN THESES ON MICROFICHE SERVICE – SERVICE DES THÈSES CANADIENNES SUR MICROFICHE

PERMISION TO MICROFILM – AUTORISATION DE MICROFILMER

• Please print or type – Écrire en lettres moulées ou dactylographier

AUTHOR – AUTEUR

Full Name of Author – Nom complet de l'auteur

DARWIN EDWARD KIFL

Date of Birth – Date de naissance	Canadian Citizen – Citoyen canadien
Sept 20, 1957	☑ Yes / Oui ☐ No / Non
Country of Birth – Lieu de naissance	**Permanent Address – Résidence fixe**
Canada	11315 – 130 ST Edmonton, AB. T5M 1A3

THESIS – THÈSE

Title of Thesis – Titre de la thèse

MEASURING AND MODELLING AIR FLOW THROUGH DOORWAYS

Degree for which thesis was presented Grade pour lequel cette thèse fut présentée	Year this degree conferred Année d'obtention de ce grade
M.Sc.	1985
University – Université	**Name of Supervisor – Nom du directeur de thèse**
University of Alberta	Dr. D.J. Wilson

AUTHORIZATION – AUTORISATION

Permission is hereby granted to the NATIONAL LIBRARY OF CANADA to **microfilm** this thesis and to **lend** or **sell copies of the film.**

The author reserves other publication rights, and neither the thesis nor extensive extracts from it may be printed or otherwise reproduced without the author's written permission.

L'autorisation est, par la présente, accordée à la BIBLIOTHÈQUE NATIONALE DU CANADA de **microfilmer** cette thèse et de **prêter** ou de **vendre des exemplaires du film.**

L'auteur se réserve les autres droits de publication; ni la thèse ni de longs extraits de celle-ci ne doivent être imprimés ou autrement reproduits sans l'autorisation écrite de l'auteur.

ATTACH FORM TO THESIS – VEUILLEZ JOINDRE CE FORMULAIRE À LA THÈSE

Signature	Date
Darwin Kifl	Sept 26 / 85

NL-91 (r. 84/03)

Canada

THE UNIVERSITY OF ALBERTA

MEASURING AND MODELLING AIR FLOW THROUGH DOORWAYS

by

(C) DARWIN EDWARD KIEL

A THESIS

SUBMITTED TO THE FACULTY OF GRADUATE STUDIES AND RESEARCH

IN PARTIAL FULFILMENT OF THE REQUIREMENTS FOR THE DEGREE

OF MASTER OF SCIENCE

DEPARTMENT OF MECHANICAL ENGINEERING

EDMONTON, ALBERTA

FALL, 1985

THE UNIVERSITY OF ALBERTA

Release Form

NAME OF AUTHOR: Darwin Edward Kiel

TITLE OF THESIS: Measuring And Modelling Air Flow Through Doorways

DEGREE: Master Of Science

YEAR THIS DEGREE GRANTED: 1985

Permission is hereby granted to THE UNIVERSITY OF ALBERTA LIBRARY to reproduce single copies of this thesis and to lend or sell such copies for private, scholarly or scientific purposes only.

The author reserves other publication rights, and neither the thesis nor extensive extracts from it may be printed or otherwise reproduced without the author's written permission.

C. Darwin Kiel

11315 - 130 St.
Edmonton, Alberta.
T5M 1A3

DATE: Sept. 26, 1985

THE UNIVERSITY OF ALBERTA

FACULTY OF GRADUATE STUDIES AND RESEARCH

The undersigned certify that they have read, and recommend to the Faculty of Graduate Studies and Research, for acceptance, a thesis entitled Measuring And Modelling Air Flow Through Doorways submitted by Darwin Edward Kiel in partial fulfilment of the requirements for the degreé of Master of Science in Mechanical Engineering.

David J Wilson

Supervisor

Date: August 28, 1985

ABSTRACT

Full scale and model studies were performed to examine air exchange flows through residential doors. Buoyancy-driven flow produced by an indoor-outdoor temperature difference was found to dominate the exchange process except for small temperature differences. Pumping exchange produced by the swing effect of the exterior door was found to be significant only at these small temperature differences and therefore negligible when estimating heating energy losses.

Full scale exchange experiments using tracer gas and thermocouples were conducted at the Alberta Home Heating Research Facility. Steady buoyancy-driven flow was found to be proportional to the square root of indoor-outdoor temperature difference with a discharge coefficient C_d, of approximately 0.6. Interfacial mixing between the incoming and outgoing streams was found to reduce the net exchange rates and an orifice coefficient K was defined including a mixing coefficient C_m as $K=C_d(1-C_m)$. Under relatively calm outdoor conditions, C_m was found to vary from 0.35 at small temperature differences to approximately zero at large temperature differences. Wind induced exterior turbulence was found to increase interfacial mixing, thereby reducing the net exchange rate.

Buoyancy driven exchange flow during the opening and closing periods could be accurately approximated by integrating the steady buoyancy flow equations with a variable orifice width as a function of time.

The flow rate was found to decrease when the cold gravity current

wave front had traveled across the interior floor surface, was reflected off the interior walls or partitions, and returned to the entrance. The wave return time was found to be inversely proportional to the square root of the fractional density difference. Theoretical prediction of the wave return time agreed well with experimental results. An expression for decreasing flow was developed to predict the total exchange volume after the wave return.

An empirical relationship between swing speed, temperature difference and pumping exchange was found for residential doors. Although the additional exchange contribution due to door-swing pumping was found to be insignificant in the context of energy losses, it may have important applications for air quality and contaminant transport.

A 1:20 scale model using salt water and fresh water was used to simulate full scale experiments. Model and full scale densimetric Froude numbers were matched and a theoretical time scale of 4.47 determined. Experimental measurements of model and full scale gravity current flows confirmed similitude using this theoretical time scale.

The model densimetric Reynolds number was approximately seven times smaller than the full scale densimetric Reynolds number, causing reduced interfacial mixing between the counterflowing streams in the model. This conclusion was substantiated by comparisons of model salinity profiles with full scale temperature profiles. Reduced interfacial mixing resulted in increased net exchange rates in the model compared to full scale, particularly at small fractional density differences. The scale model studies supported and helped confirm many of the full scale observations concerning the effect of interior volume on flow rate.

ACKNOWLEDGEMENTS

The author would like to extend his deep gratitude to Dr. D.J. Wilson for his guidance and support throughout this project, it has been a valuable and rewarding experience. I would also like to extend may thanks to Dr. J.D. Dale for guidance during Dr. Wilson's absence.

Financial support was provided through a scholarship from Canada Mortgage and Housing Corporation, an ASHRAE Grant-In-Aid, and the R.M. Hardy Engineering Enrichment Fund. Research grants to Dr. D.J. Wilson from Canada Energy Mines and Resources, and NSERC, made this research possible. The author is very grateful for this support.

I would also like to thank Mark Ackerman, Wayne Pittman, Eddy Chui and Brian Zelt for their technical and moral support, as well as the Department of Mechanical Engineering machine shop staff for their high quality of workmanship.

Finally, I would like to extend a special thanks to my family and Sue McKenzie for their constant and patient support throughout this project.

TABLE OF CONTENTS

CHAPTER		PAGE
1.	INTRODUCTION	1
	Buoyancy-Driven Exchange Flow	2
	Inertia-Driven Exchange Flow	3
	Development of Exchange Equations	3
	Full Scale Exchange Flow Experiments	4
	Scale Modelling of Exchange Flows	4
2.	AIR EXCHANGE THEORY	6
	Buoyancy-Driven Exchange During a Typical Door Cycle	7
	Inviscid Stratified Orifice Flow	9
	Energy Losses	15
	Interfacial Mixing	15
	Asymmetric Interfacial Mixing	19
	Nondimensional Numbers	21
	Orifice Coefficient	23
	Buoyancy-Driven Exchange During Door Opening and Closing	27
	Departure From Steady State Flow	29
	Cold Front Flow Down a Long Hall	31
	Cold Front Flow Into a Complicated Interior Geometry	32
	Decreasing Flow Rate Caused by a Finite Interior Volume	34
	Interior and Exterior Turbulence	37

Door Pumping Exchange..... 38

Occupant Motion..... 41

3. FULL SCALE EXPERIMENTS..... 42

Experimental Parameters..... 42

Exchange Flow Measurement Techniques..... 43

Test Facility..... 45

Experimental Equipment..... 48

Experimental Procedure..... 53

ΔT-Sets of Exchange Tests..... 54

Temperature Measurements..... 56

4. FULL SCALE DATA ANALYSIS AND RESULTS..... 58

Data Reduction..... 58

Thermal Expansion of Incoming Air..... 60

Steady State Flow for the Fully Open Door Position..... 62

Orifice Coefficient Analysis..... 66

Temperature Profiles and Interfacial Mixing..... 75

Air Exchange During Door Opening and Closing Periods..... 78

Pumping Exchange..... 79

Cold Front Velocity..... 84

Prediction of Critical Departure Time..... 87

Critical Departure Time from Experimental Data..... 88

Critical Departure Volume..... 90

Decreasing Exchange Rate..... 93

Summary..... 100

5. SCALE MODELLING THEORY AND EXPERIMENTS..... 101

Dynamic Similarity..... 101

Selection of Model Parameters..... 103

Model Design..... 106

Temperature, Density, Salinity and Mass Relationships..... 108

Exchange Flow Measurements..... 113

Model Experimental Procedures..... 117

6. SCALE MODEL RESULTS AND ANALYSIS..... 125

Steady State Buoyancy-Driven Flow..... 125

Interfacial Mixing..... 132

Interfacial Stability and Reynolds Number Mismatch..... 138

Effect of Outside Wind on Model Exchange Rate..... 138

Modelling of Cold Front Flow..... 140

Decreasing Exchange Rate..... 144

Equivalent Opening and Closing Time..... 146

Inertial Pumping..... 149

7. CONCLUSIONS AND RECOMMENDATIONS..... 155

Steady State Buoyancy-Driven Flow..... 155

Steady State Departure and Decreasing Flow Rate..... 156

Inertial Pumping Exchange..... 157

Model Similitude..... 158

Recommendations..... 160

****

REFERENCES..... 161

APPENDIX A DENSITY-DRIVEN FLOW THROUGH AN OPEN DOOR - AN INVISCID ANALYSIS..... 164

APPENDIX B. MIRAN 1A INFRARED ABSORPTION GAS ANALYSER CALIBRATION..... 169

LIST OF TABLES

Table	Description	Page
3-1	Interior Volumes of Test Geometries	50
3-2	Fully Open Hold Times in Each ΔT-Set	55

LIST OF FIGURES

Figure	Description	Page
2-1	Idealized Flow Rate and Volume Exchange for a Typical Door Cycle	8
2-2	Velocity and Temperature Difference Profiles on the Vertical Centerline of an Opening into a Sealed Room for Stratified Counterflow without Interfacial Mixing	10
2-3	Velocity and Temperature Difference Profiles on the Vertical Centerline of an Opening into a Sealed Room for Stratified Counterflow with and without Interfacial Mixing	16
2-4	Velocity and Temperature Difference Profiles for a Long Hall with Interfacial Mixing	20
2-5	Gravity Current Flow Down a Long Hall with Reflection and Return Wave	30
2-6	Idealized Decreasing Flow Assuming a Series of Discrete Gravity Current Inflows; See Figure 2.7 for Time Definitions	35
2-7	Volume Exchange as a Function of Time for the Series of Discrete Gravity Current Inflows in Figure 2.6	36
2-8	Idealized Pumping, Buoyancy and Residual Exchange Curves	40
3-1	Physical Layout of the Alberta Home Heating Research Facility, All Dimensions in Meters	46
3-2	Physical Dimensions of Module #3, All Dimensions in Meters	47
3-3	Interior Test Geometries; Full-House, Hall and Entry	49
3-4	Typical Door Motion Curve Measured with Position Sensor	52
4-1	Measured Tracer Gas Concentration Decays and Exponential Extrapolations for a Typical Exchange Experiment; Entry Geometry, Hold Time=2 s, $\Delta T=6.5^{o}C$, $T_{i,ref}=22^{o}C$	59
4-2	Effect of Thermal Expansion of Outdoor Air on Tracer Gas Concentration During Final Decay Measurement	61

4-3 Typical ΔT-Sets of Exchange Volumes Correlated with Fully Open Hold Time; Full-House Geometry..... 64

4-4 Variation in the Full-House Steady State Flow Rate with Temperature Difference; $T_{i,ref}=22^{o}C$..... 65

4-5 Variation in the Full-House Orifice Coefficient with Temperature Difference; $T_{i,ref}=22^{o}C$..... 67

4-6 Variation in the Hall Orifice Coefficient with Temperature Difference; $T_{i,ref}=22^{o}C$..... 68

4-7 Variation in the Entry Orifice Coefficient with Temperature Difference; $T_{i,ref}=22^{o}C$..... 69

4-8 Orifice Coefficient Variation with Temperature Difference for Full-House, Hall and Entry Geometries, Wind Speeds less than 10 km/hr; $T_{i,ref}=22^{o}C$..... 70

4-9 Orifice Coefficient Correlation with Average Flow Reynolds Number for Full-House and Hall Geometries, Wind Speeds less than 10 km/hr..... 72

4-10 Orifice Coefficient Correlation with Densimetric Reynolds Number for Full-House and Hall Geometries, Wind Speeds less than 10 km/hr; Cold Room Data by Fritzsche (1968)..... 73

4-11 Orifice Coefficient Correlation with Temperature Difference for Full-House and Hall Geometries, Wind Speeds less than 10 km/hr, $T_{i,ref}=22^{o}C$; Cold Room Data by Fritzsche (1968)..... 74

4-12 Normalized Temperature Profiles on the Doorway Vertical Centerline for the Full-House Geometry..... 77

4-13 Ratio of Total Exchange to Buoyancy Predicted Exchange Using Equivalent Time and Zero Hold Time..... 80

4-14 Correlation of Short Duration Exchanges with Temperature Difference, $T_{i,ref}=22^{o}C$; Swing Time=3.75 s, Hold Time=0.5 s..... 81

4-15 Critical Fractional Density Difference Determined from the Ratio of Total Exchange to Buoyancy Predicted Exchange; Swing Time=3.75 s, Hold Time=0.5 s..... 83

4-16 Typical Frontal Position Curves from Hall Thermocouple Experiments, Time and Position Relative to First Thermocouple..... 85

4-17 Hall Frontal Velocity Correlation with Temperature Difference, $T_{i,ref}=22^{o}C$..... 86

4-18 Critical Departure Time from Steady Flow for the Hall Geometry..... 89

4-19 Critical Departure Time from Steady Flow for the Entry Geometry..... 91

4-20 Critical Departure Time from Steady Flow for the Full-House Geometry..... 92

4-21 Single Reflected Wave Departure Compared to Multiple Reflected Wave Departure..... 94

4-22 Normalized Volume Exchange and Decreasing Flow Correlation for the Hall Geometry..... 96

4-23 Normalized Volume Exchange and Decreasing Flow Correlation for the Entry Geometry..... 97

4-24 Normalized Volume Exchange and Decreasing Flow Correlation for the Hall and Entry Geometries..... 99

5-1 1:20 Scale Model House, Interior Dimensions 35.6 cm x 32.5 cm x 12.0 cm..... 109

5-2 Illustration of Inverted Scale Model..... 110

5-3 Typical Door Motion Calibration Curve Measured in the 1:20 Scale Model..... 111

5-4 Counterweight and Differential Load Transducer System..... 115

5-5 Typical Load Cell Calibration Curve..... 120

5-6 Inverted Model in Channel During Exchange Experiment..... 121

6-1 Indicated Volume Exchange Determined by the Model Load Cell Measurement System, Shown in Full Scale Units; Full-House Geometry; $\Delta T=44.4^{o}C$, $T_{i,ref}=22^{o}C$..... 126

6-2 Indicated Volume Exchange Determined by the Model Load Cell Measurement System, Shown in Full Scale Units; Full-House Geometry; $\Delta T=1.5^{o}C$, $T_{i,ref}=22^{o}C$..... 127

6-3 Comparison of Model and Full Scale Steady State Flow Rate Variation with Temperature Difference, Full-House Geometry; $T_{i,ref}=22^{o}C$..... 130

6-4 Comparison of Model and Full Scale Orifice Coefficient Variation with Temperature Difference, Full-House Geometry; Full Scale Wind Speeds less than 10 km/hr; $T_{i,ref}=22^{o}C$..... 131

6-5 Comparison of a Model Salinity Profile with a Full Scale Temperature Profile Measured on the Doorway Vertical Centerline at an Equivalent Full Scale ΔT Model =24.4°C and ΔT Full Scale =28.6°C..... 134

6-6 Comparison of a Model Salinity Profile with a Full Scale Temperature Profile Measured on the Doorway Vertical Centerline at an Equivalent Full Scale ΔT Model =18.9°C and ΔT Full Scale =18.5°C..... 135

6-7 Comparison of a Model Salinity Profile With a Full Scale Temperature Profile Measured on the Doorway Vertical Centerline at an Equivalent Full Scale ΔT Model =5.7°C and ΔT Full Scale =5.8°C..... 136

6-8 Comparison of Model and Full Scale Orifice Coefficients with Densimetric Reynolds Number; Stability Limits from Rozovsky, Shabrin and Markov (1972)..... 139

6-9 Reduction in Model Orifice Coefficient Due to a Parallel Wind Past the Opening at a Full Scale Equivalent Rate of 20 km/hr, Geometrically Similar to a Full Scale South Wind, No Wind Breaks Employed..... 141

6-10 Comparison of Model and Full Scale Hall Frontal Velocity Variation with Temperature Difference..... 143

6-11 Model Exchange Ratio for Full-House Geometry with Exponential Decreasing Flow Correlation..... 145

6-12 Typical Correlation of Short Duration Exchanges with Temperature Difference; Swing Time=1.9 s, Hold Time=1.1 s.... 148

6-13 Critical Fractional Density Difference Determined from the Ratio of Total Exchange to Buoyancy Predicted Exchange for Short Duration Openings; Swing Time=1.9 s, Hold Time=1.1 s... 150

6-14 Correlation of Residual Pumping Exchange Volume with Door Swing Time and Fractional Density Difference..... 153

A1 Double Weir Model of Inviscid Buoyancy-Driven Flow Through a Vertical Opening into a Sealed Room..... 166

B1 Miran 1A Infrared Gas Analyser Calibration Curve..... 171

NOMENCLATURE

A_f	Floor area
C_c	Contraction coefficient
C_d	Discharge coefficient
C_v	Velocity coefficient
C_m	Mixing coefficient
$C_{m,ref}$	Reference mixing coefficient
Cp	Specific heat coefficient
c	Concentration
E	Exchange ratio
E_{cr}	Critical exchange ratio
E_{max}	Maximum exchange ratio
Fr	Froude number
Fr_f	Frontal Froude number
Fr_Δ	Densimetric Froude number
Gr	Grashof number
Gr_Δ	Densimetric Grashof number
g	Local gravitational acceleration
g'	Effective gravitational acceleration
g'_F	Full scale effective gravitational acceleration
g'_M	Model effective gravitational acceleration
g'_{avg}	Average g' for one ΔT-Set of exchange tests
H	Door height
H_{ref}	Reference door height
h	Distance above floor surface

h_i	Thickness of the outgoing flow
h_m	Thickness of the mixing layer
h_o	Thickness of the incoming flow
K	Orifice coefficient
L	Fundamental dimension of length
L_F	Full scale characteristic length
L_M	Model characteristic length
L_S	Model length scale factor
L_f	Frontal flow length
m	Fundamental dimension of mass
P_i	Pressure indoors
P_o	Pressure outdoors
Q	Gross incoming or outgoing flow rate
Q_m	Effective interfacial mixing rate
Q_n	Net inflow and outflow rate
Q_i	Gross flow rate of outgoing indoor air
Q_i'	Inviscid flow rate of outgoing indoor air
Q_o	Gross flow rate of incoming outdoor air
Q_o'	Inviscid flow rate of incoming outdoor air
q	Energy loss rate
Re	Reynolds number
Re_H	Average flow Reynolds number
Re_Δ	Densimetric Reynolds number
SG_f	Final specific gravity of model fluid
SG_i	Initial specific gravity of model fluid
SG_l	Local specific gravity of model fluid

T_o	Outdoor temperature
T_i	Indoor temperature
T_l	Local temperature
$T(h)$	Orifice temperature at height h
$T_{i,ref}$	Indoor reference temperature
t	Fundamental dimension of time
t_F	Full scale time
t_M	Model time
t_S	Model time scale factor
t_c	Time required for door to move from $\theta=90^o$ to $\theta=0^o$
t_{cr}	Time until critical departure from steady flow
t_d	Duration of decreasing flow while $\theta>90^o$
t_{eq}	Equivalent opening or closing time
t_h	Fully open hold time (total time that $\theta>90^o$)
t_o	Time required for the door to move from $\theta=0^o$ to $\theta=90^o$
t_s	Duration of steady flow
t_∞	Infinite time
U	Velocity
$\overline{U}$	Average incoming or outgoing velocity
U_Δ	Densimetric velocity scale
U_i	Velocity of outgoing indoor air
U_i'	Inviscid velocity of outgoing indoor air
U_o	Velocity of incoming outdoor air
U_o'	Inviscid velocity of incoming outdoor air
U_f	Frontal Velocity
V	Total exchange volume
V_B	Predicted total buoyancy driven exchange volume

V_H	Gaseous volume below a horizontal plane at height H
V_I	Gaseous interior volume
V_M	Interior volume of model
V_P	Residual pumping exchange volume
V_{Po}	Residual pumping exchange volume at $\Delta T=0$
V_c	Exchange volume during closing period
V_d	Exchange volume during decreasing flow period
V_h	Exchange volume during hold period
V_o	Exchange volume during opening period
V_s	Exchange volume during steady period
W	Door width
W_f	Frontal flow width
W'	Opening width at door angle less than 90°
z	Absolute distance from neutral level

Greek Symbols

$\bar{\Delta}$	Fractional density difference based on $\bar{\rho}$
Δ'	Fractional density difference based on ρ_i
ΔT	Temperature difference based on $T_{i,ref}$
Δm	Change in mass of suspended model
$\Delta \rho$	Indoor-outdoor density difference
$\bar{\Delta}_{cr}$	Critical fractional density difference
$\bar{\Delta}_F$	Full scale fractional density difference
$\bar{\Delta}_M$	Model fractional density difference
$\bar{\Delta}_S$	Model fractional density difference scale factor
μ	Dynamic viscosity
ν	Kinematic viscosity

ν_F	Full scale kinematic viscosity
ν_M	Model kinematic viscosity
ν_S	Model kinematic viscosity scale factor
θ	Door angle.
ρ_C	Channel water density
ρ_M	Initial model fluid density
ρ_i	Indoor air density
ρ_o	Outdoor air density
$\bar{\rho}$	Average indoor-outdoor density
ρ'	Reference density

CHAPTER 1

INTRODUCTION

The transport of mass and energy through open doors can contribute significantly to the energy loads on structures and enclosures. Energy loss applications range from the flow of warm interior air out of residential structures or industrial hangers, to the flow of cold air out of commercial walk-in freezers. Increasing energy costs, combined with improved thermal insulation standards and reduced air infiltration, are causing the energy losses associated with door openings to represent an increasingly important component of total energy costs.

Air flow through doorways is also important in the fields of air quality and contaminant transport. Applications include the transport of bacteria into or out of operating theaters, transport of dust into microchip clean rooms, escape of contaminated air or gas from containment structures, supply of fresh air to rooms which suffer from insufficient ventilation, and interior transport of life threatening smoke during residential and commercial fires.

Regardless of whether interest lies with energy losses or air quality, an accurate understanding of exchange flows is required to develop methods of estimating exchange rates and flow characteristics. This insight is essential for the development of designs to reduce flow rates or modify flow characteristics. Without this knowledge, it is also impossible to determine energy loads or estimate indoor air quality.

This investigation is devoted to the study of the air exchange flows that occur through exterior entries typical of those found in residential structures. Many of the theories, equations and observations presented, can be applied directly to other similar flow conditions.

Buoyancy-Driven Exchange Flow

Buoyancy-driven exchange flows are caused by a difference between indoor and outdoor air density in the presence of a gravity field. In residential structures, the density difference is generally produced by a temperature difference. This condition causes warm buoyant interior air to flow out the top of the door opening, while cold exterior air flows in the bottom of the opening, across the interior floor surface. Steady flow persists until the door is closed or until the cold gravity current is reflected by interior walls back to the entrance. The arrival of the reflected gravity current at the doorway will be called the wave return time, after which the flow rate begins to decrease.

Steady buoyancy-driven flow will be found to scale with the effective acceleration of gravity, defined as:

$$g' = g\ (\Delta\rho/\rho_{ref})$$

where

g = local gravitational constant

$\Delta\rho$ = the indoor and outdoor density difference

ρ_{ref} = reference density (indoor-outdoor average)

For cold outdoor temperatures of $-20^{o}C$ to $-30^{o}C$, fractional density differences $\Delta\rho/\rho_{ref}$, range from 0.15 to 0.2. The upward flow of air from the top of the door can be compared to the downward pouring of

water into air from a pitcher. The primary difference is that the warm buoyant air flow experiences a gravitational force approximately 1/5 as large as the force experienced by the downward pouring water.

It will be shown that the buoyancy flow rate is approximately proportional to the square root of the temperature difference, so doubling the temperature difference will produce a 40% increase in the flow rate. Energy losses however, depend on the product of flow rate and temperature difference, and thus energy losses vary with the temperature difference to the 1.5 power. So, doubling the temperature difference will increase the energy loss by a factor of 2.8, illustrating the dramatic increase in energy losses at large temperature differences.

Inertia-Driven Exchange Flow

Inertia-driven exchange flows are caused by the input of energy from sources such as the swing motion of an opening door or internal circulation caused by mixing fans. The importance of these contributions compared to buoyancy-driven exchange depends on the relative magnitude of the inertial forces compared to the buoyancy forces. Because inertial forces are almost invariant with temperature difference, their relative contribution will be shown to decrease with increasing temperature difference.

Development of Exchange Equations

An inviscid analysis will provide an equation for stratified counterflow through a typical opening. This equation will then be modified to account for viscous effects, variable orifice size during door opening and closing, and the decreasing flow caused by a limited

interior volume. Classical lock exchange equations will be introduced to estimate the cold gravity current velocity and wave return time. A model will be proposed to describe the decreasing flow rate after the gravity current has returned to the entry.

The importance of buoyancy exchange during door opening and closing compared to inertial pumping exchange will be examined. An empirical relationship will be developed between door swing speed and fractional density difference such that an estimate of the exchange volume over and above that predicted by buoyancy alone can be made.

Full Scale Exchange Flow Experiments

Confirmation of the proposed models and equations is essential to establish confidence in their prediction of exchange rates. In some cases, important parameters can only be determined from experimental results. Experimental measurements of exchange flows were performed at the Alberta Home Heating Research Facility. Tracer gas techniques were used to measure exchange volumes for several interior geometries over a range of door opening durations and temperature differences. Thermocouple measurements were used to obtain an insight into the local characteristics of the exchange process.

Scale Modelling of Exchange Flows

Full scale testing was found to have numerous limitations, including limited measurement accuracy, time consuming tests, uncontrollable environmental influences and a lack of inexpensive ways of testing modified entries or complicated geometries. These problems motivated the development and testing of a 1:20 scale model. The primary objective of the model testing was to examine the degree of similarity

between model and full scale results by repeating tests in the model that had been examined in full scale. These experiments confirmed that scale modelling is a valuable design and experimental tool in studies of exchange flows.

CHAPTER 2

AIR EXCHANGE THEORY

In this chapter theoretical models and equations will be developed to describe air flow through residential doors. An inviscid analysis of buoyancy-driven orifice flow will be used to develop a steady state exchange flow equation. Viscous and turbulent mixing effects will then be discussed and introduced into the basic inviscid equation. The unsteady buoyancy flow that occurs during the door opening and closing period will also be considered in context with the steady state buoyancy equation.

The decrease in flow rate that results from the effect of limited interior volume will then be examined. The analysis will be based on a flow model that assumes that the reduction in flow rate occurs when the cold gravity current has traveled across the interior floor surface, reflects off interior partitions and returns to the entry. The functional form of the decreasing flow will also be considered and a theoretical expression proposed.

Finally, the effect of door pumping will be considered. The idea of a residual pumping volume will be introduced to account for the exchange volume that is in excess of the amount predicted by the steady state equation.

Before beginning the inviscid buoyancy analysis it is instructive to examine first the exchange process for a typical door cycle.

Buoyancy-Driven Air Exchange During a Typical Door Cycle

Figure 2-1 illustrates the volume exchanged as a function of time for an idealized exchange cycle. The curve represents the exchange process that occurs when a residential door is swung open, left open for some period of time and then shut. The interior could be an entry vestibule or large room (without multiple levels). Four time periods have been identified in Figure 2-1.

Opening Period (t_o)- This period begins with the initial motion of the door and ends with its arrival at a 90 degree fully open position. The most important characteristic of this period is the increasing opening width, causing an increasing exchange rate as indicated on Figure 2-1.

Fully Open Steady Flow Period (t_s)- During this period, continuous steady state flow exists for the fully open orifice configuration. This flow rate will persist until the orifice size begins to decrease due to door closure or until the interior volume is partially exchanged and a critical point is reached where the exchange rate starts to decrease. The time at which this occurs depends on the steady state flow rate, the interior volume and interior geometry.

Decay Period (t_d)- The decay period only exists if the door is open sufficiently long that a reduction in flow rate begins due to a limited interior volume. The larger the interior volume, the longer the door must be open for this period to exist. The flow rate decreases such that the total exchange asymptotically approaches a maximum volume.

The total time that the door is open 90 degrees or more is identified on Figure 2-1 as the hold time t_h, and is simply t_s+t_d. If the door is not open long enough for the decay period to exist, then

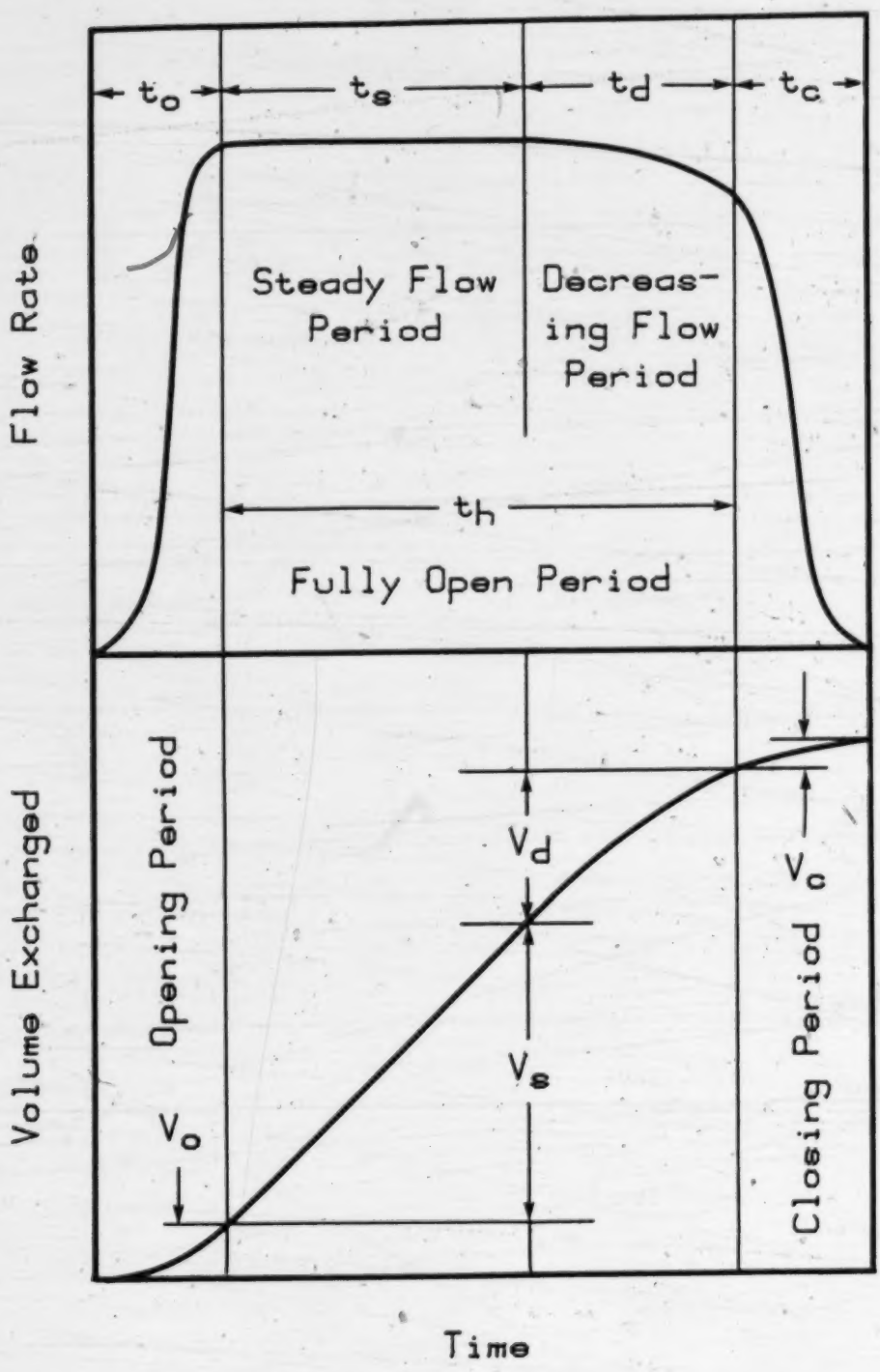

FIGURE 2-1: Idealized Flow Rate and Volume Exchange for a Typical Door Cycle

$t_s=t_h$ and $t_d=0$.

Closing Period (t_c)- This period begins when the opening width starts to decrease as the door is closing. This period is similar to the opening period in reverse, beginning as the door passes the 90 degree open position while closing. The volume exchanged during this period depends both on the variable orifice width and on the steady state flow rate that exists when the door begins to close.

The buoyancy volumes exchanged during each of the respective periods are identified as V_o, V_s, V_d and V_c on Figure 2-1. This typical volume-time curve gives some insight into the factors that effect buoyancy exchange. The development of quantitative relationships to predict the buoyancy exchange flows will now follow.

Inviscid Stratified Orifice Flow

Figure 2-2 illustrates a simple sealed room with one vertical opening of height H, and width W. If the thickness w, of the opening is small in comparison to the height and width of the opening, then a control condition occurs at the entry which sets the flow rates at all other points in the system. This condition of choked orifice flow may be considered as the upper bound on flow rate through the entry. This flow condition will be modelled as two symmetric weirs by making the following assumptions:

- The pressure across the outgoing fluid at ρ_i, is hydrostatic at outdoor conditions across section h_i.
- The pressure across the incoming fluid at ρ_o, is hydrostatic at indoor conditions across section h_o.

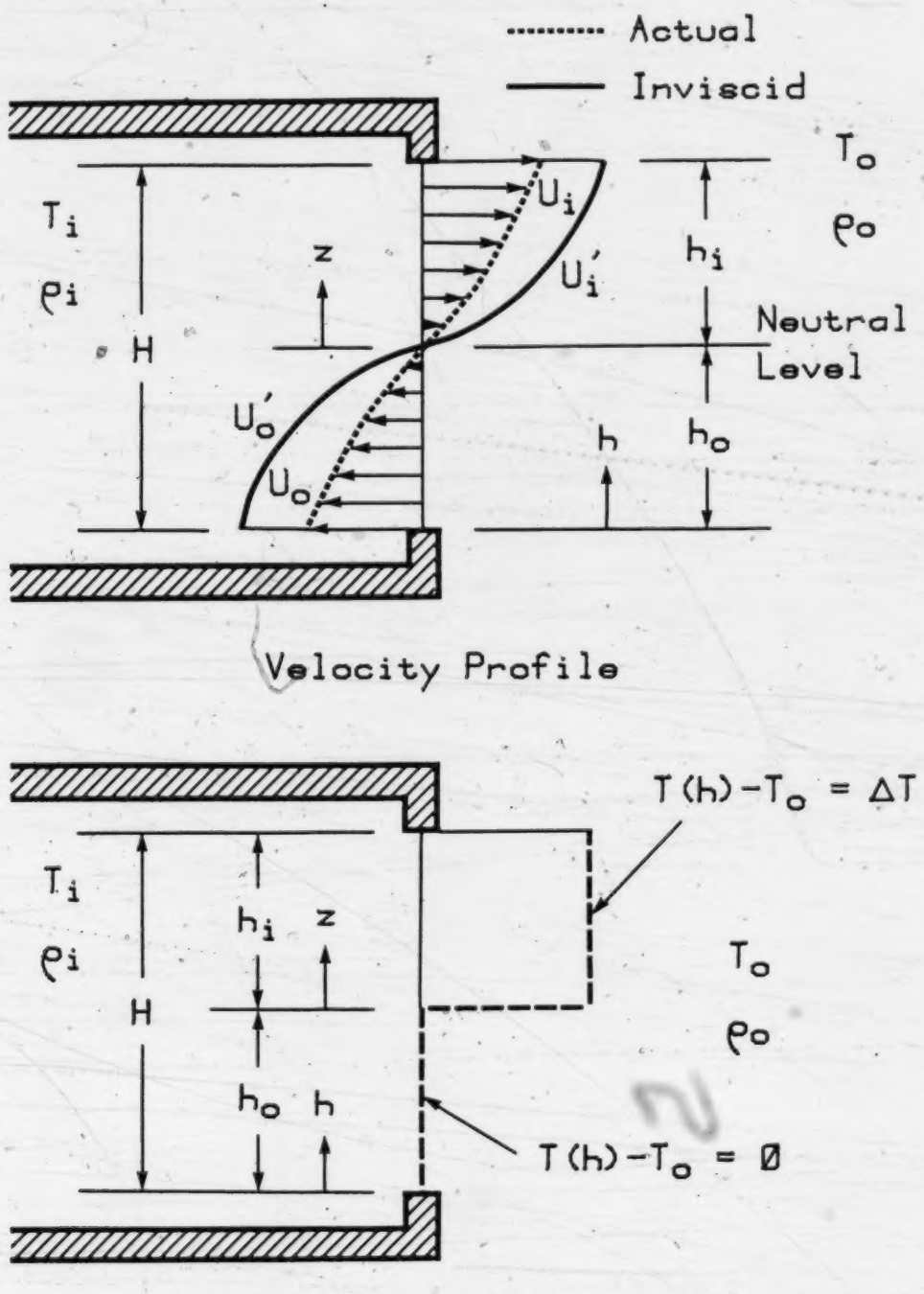

FIGURE 2-2: Velocity and Temperature Difference Profiles on the Vertical Centerline of an Opening into a Sealed Room for Stratified Counterflow without Interfacial Mixing

- The indoor and outdoor pressures P_i and P_o are in equilibrium along the interfacial streamline that divides the incoming and outgoing flows.
- Ideal inviscid Bernoulli flow.

The complete inviscid analysis is shown in Appendix A as developed by D.J. Wilson (personal communication), and results in the following expressions for the inward and outward velocity profiles.

$$U_o' = \left[\frac{2gz\ \Delta\rho}{\rho_o}\right]^{0.5} \qquad (2\text{-}1)$$

$$U_i' = \left[\frac{2gz\ \Delta\rho}{\rho_i}\right]^{0.5} \qquad (2\text{-}2)$$

$$\Delta\rho = \rho_o - \rho_i \qquad (2\text{-}3)$$

where

z = absolute distance from neutral level

U_o' = inviscid incoming outdoor air velocity

U_i' = inviscid outgoing indoor air velocity

g = local gravitational constant (9.81 m/s^2)

ρ_i = indoor air density

ρ_o = outdoor air density

$\Delta\rho$ = indoor-outdoor density difference

Integrating and equating the volume inflow Q_o', with the volume outflow Q_i', yields:

$$Q' = \frac{W}{3}\,(gH^3\ \Delta\rho/\rho')^{0.5} \qquad (2\text{-}4)$$

$$\rho' = \rho_i \frac{(1+(\rho_o/\rho_i)^{1/3})^3}{8} \qquad (2\text{-}5)$$

$$\frac{h_o}{h_i} = \left[\frac{\rho_o}{\rho_i}\right]^{1/3} \qquad (2\text{-}6)$$

where

$Q' = Q_o' = Q_i'$

Q_o' = gross inviscid inflow rate

Q_i' = gross inviscid outflow rate

h_o = thickness of inflow layer

h_i = thickness of outflow layer

ρ' = reference density

The reference density ρ', may be approximated by the average density $\overline{\rho}$, given by Equation 2-7, with a maximum error of 0.4% at a temperature difference of 60°C.

$$\rho' \simeq \overline{\rho} = \frac{(\rho_i+\rho_o)}{2} \qquad (2\text{-}7)$$

where

$\overline{\rho}$ = average indoor-outdoor air density

The fractional density difference may now be defined as:

$$\overline{\Delta} = \Delta\rho / \overline{\rho} \qquad (2\text{-}8)$$

where

$\overline{\Delta}$ = fractional density difference

The ideal gas law holds and Equation 2-8 can be written in terms of a fractional temperature difference as:

$$\bar{\Delta} = \frac{T_i - T_o}{(T_i + T_o)/2} \qquad (2\text{-}9)$$

where

T_i = indoor temperature

T_o = outdoor temperature

For practical applications such as energy losses from homes it is often better to specify temperature difference rather than fractional density difference. From Equation 2-9; however, it is apparent that specifying the absolute temperature difference $(T_i - T_o)$ alone is insufficient. For this reason the temperature difference is specified relative to some indoor reference temperature as given by Equation 2-10.

$$\bar{\Delta} = \frac{\Delta T}{T_{i,ref} - \Delta T/2} \qquad (2\text{-}10)$$

where

ΔT = reference temperature difference

$T_{i,ref}$ = indoor reference temperature; 295 K (22^oC)

As suggested in Chapter 1, it is convenient to think of the fractional density difference as a modifier to the gravitational acceleration such that the effective gravitational acceleration is defined as:

$$g' = \bar{\Delta}\, g \qquad (2\text{-}11)$$

and Equation 2-4 may be written as:

$$Q' = \frac{W}{3} (g' H^3)^{0.5} \qquad (2\text{-}12)$$

The inviscid analysis for orifice flow does not account for viscous energy losses or contraction effects. As illustrated in Figure 2-2, the magnitude of the actual velocity profile U, is smaller than the inviscid profile U'. These effects can be compensated for with a velocity coefficient C_v, and a contraction coefficient C_c, Roberson and Crowe (1980). Only the combined effects of these coefficients can be determined experimentally and therefore it is most convenient to combine them into a single discharge coefficient C_d. The discharge coefficient relates the inviscid flow rate to the actual flow rate.

$$Q = C_d\, Q' \qquad (2\text{-}13)$$

where

Q = is the actual volume inflow or outflow rate

C_d = discharge coefficient

The discharge coefficient applies to the volume flow Q' determined from the integrated inviscid velocity profile and not the local inviscid orifice velocities. The reduced velocity profile U, shown in Figure 2-2 should not therefore be interpreted as directly proportional to the inviscid velocity profile U'.

Discharge coefficients for rectangular weir flows range from 0.58 to 1.00, depending on the amount of flow contraction and on the weir to free flow thickness ratio. Typical entry geometries suggest substantial contraction on the inflow stream and modified contraction on the outflow stream depending on the door position and entry shape, suggesting discharge coefficients closer to the limit of 0.58, ASME (1971).

Energy Losses

Also shown in Figure 2-2 is the temperature profile for a sharp-edged orifice with no mixing between the two counterflows. The total energy loss rate may be expressed in the general from given by:

$$q = \int_{h=0}^{h=H} W\, U(h)\, \rho(h)\, Cp\, (T(h)-T_o)\, dh \qquad (2\text{-}14)$$

where

U(h) = actual flow velocity at some orifice height

T(h) = temperature at some height in the orifice

$\rho(h)$ = density at some height in the orifite

Cp = specific heat of air at (h)

q = energy loss rate

If there is no mixing between the incoming and outgoing streams, as shown in Figure 2-2, Equation 2-14 simplifies due to the zero temperature difference in the inflow stream and constant temperature difference in the outflow stream.

$$q = Q\, \rho_o\, Cp\, (T_i-T_o) \qquad (2\text{-}15)$$

Interfacial Mixing

Although C_d accounts for the viscous energy losses and contraction effects, it does not account for a secondary viscous effect, that of mixing. The derivation of Equation 2-13 and 2-15 assumed that the two counterflowing streams have no mixing across the interface. If interfacial mixing is occurring, as shown in Figure 2-3, momentum transfer across the interface causes a decrease in the velocity

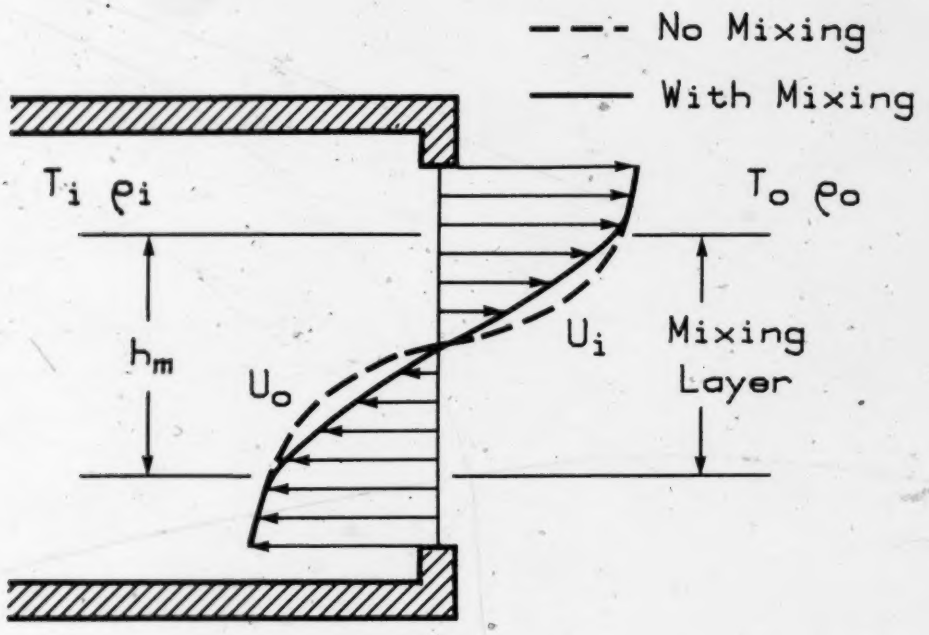

Velocity Profile

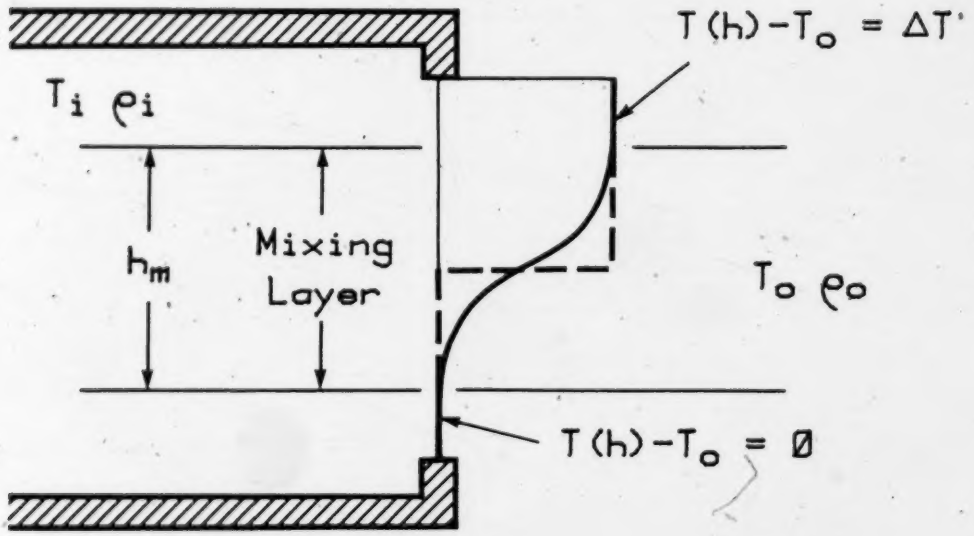

Temperature Difference Profile

FIGURE 2-3: Velocity and Temperature Difference Profiles on the Vertical Centerline of an Opening into a Sealed Room for Stratified Counterflow with and without Interfacial Mixing

magnitudes of both streams within the mixing region. A velocity reduction occurs because the transferred air is traveling in an opposite direction relative to the stream into which it is transferred, resulting in momentum cancellation.

Interfacial mixing also causes a modification of the temperature profile. The outflow stream is now slightly cooler than room temperature in the mixing region due to the presence of upwardly mixed air from the incoming stream. Conversely, the inflow stream is slightly warmer than outdoor temperature in the mixing region due to the presence of downwardly mixed air from the outgoing stream. The amount of indoor and outdoor air at any location can be determined from the local temperature by assuming adiabatic mixing. For example, if $T_i=20^oC$, $T_o=0^oC$ and at some location in the inflow stream a parcel of air has a temperature of $T=5^oC$, 25% of that volume of air must have transferred from the outgoing stream to the incoming stream and is returning inside.

From this discussion it is apparent that interfacial mixing has two effects. First, a reduction in the gross flow rate Q, due to the momentum transfer across the interface. Second, a reduction in the net flow rate because some of the incoming air is returned outdoors and some of the outgoing air is returned indoors. Equation 2-16 is an expression for the resulting net exchange flow rate Q_n. It should be kept in mind that these devivations are all based on conservation of volume not mass.

$$Q_n = \int_{h=0}^{h=H} W\, U(h)\, \frac{T(h)-T_o}{T_i-T_o}\, dh \qquad (2\text{-}16)$$

where

Q_n = net flow rate

Combining Equation 2-16 with Equation 2-14 results in a simple expression for the energy loss based on net flow rate.

$$q = Q_n \, Cp \, \rho_o \, (T_i - T_o) \qquad (2\text{-}17)$$

When there is no interfacial mixing, the net flow rate Q_n and the immiscible flow rate C_dQ', are equal. As mixing increases, the immiscible flow rate is reduced by an amount Q_m, defined as:

$$Q_m = C_dQ' - Q_n \qquad (2\text{-}18)$$

where

Q_m = the effective interfacial mixing flow rate

Q_m is referred to as an effective rate because it includes incoming air that transfers to the outgoing stream as well as any reduction in the flow rate caused by momentum transfer. The mixing coefficient C_m, is defined as:

$$Q_m = C_m \, Q \qquad (2\text{-}19)$$

If C_m=0 then the two streams are immiscible and the net flow rate is equal to the gross flow rate C_dQ'.

Combining this definition of mixing coefficient with the inviscid expression given by Equation 2-12 results in:

$$Q_n = \frac{C_d \, (1-C_m)}{3} \, W \, (g'H^3)^{0.5} \qquad (2\text{-}20)$$

Molecular diffusivity and thermal conductivity across the interface between the incoming and outgoing flow streams can also reduce the net mass and energy exchange. An analysis was performed to determine the

importance of both molecular diffusivity and thermal conductivity compared to convective exchange. The analysis revealed that convective transport is several orders of magnitude more important than either diffusivity or conductivity and thus their contributions may be neglected.

Asymmetric Interfacial Mixing

Interfacial mixing is further complicated by both indoor and outdoor turbulence levels and physical layout. The presence of indoor ventilation and exterior wind both influence the rate at which mixing occurs, altering the magnitude of C_m. The physical layout will determine the interfacial contact area, relative velocities and probably the layer thicknesses, all of which influence interfacial transport.

For example, the presence of an interior ceiling and floor restrict the interior counterflowing streams, unlike the exterior situation where the buoyant outflow from the top of the door rises upon exit, limiting its contact with the exterior inflow. Figure 2-4 illustrates this situation for a long interior hallway. For simplicity the interior ceiling is shown at the same height as the door. The incoming and outgoing streams will remain in contact down the entire length of the hall with velocity profiles that remain similar except for the momentum transfer caused by mixing. The asymmetric temperature profile at the orifice should be noted. This profile shape will be confirmed by experimental results.

Before considering other factors that influence the mixing and discharge coefficients it is convenient to first define several nondimensional parameters.

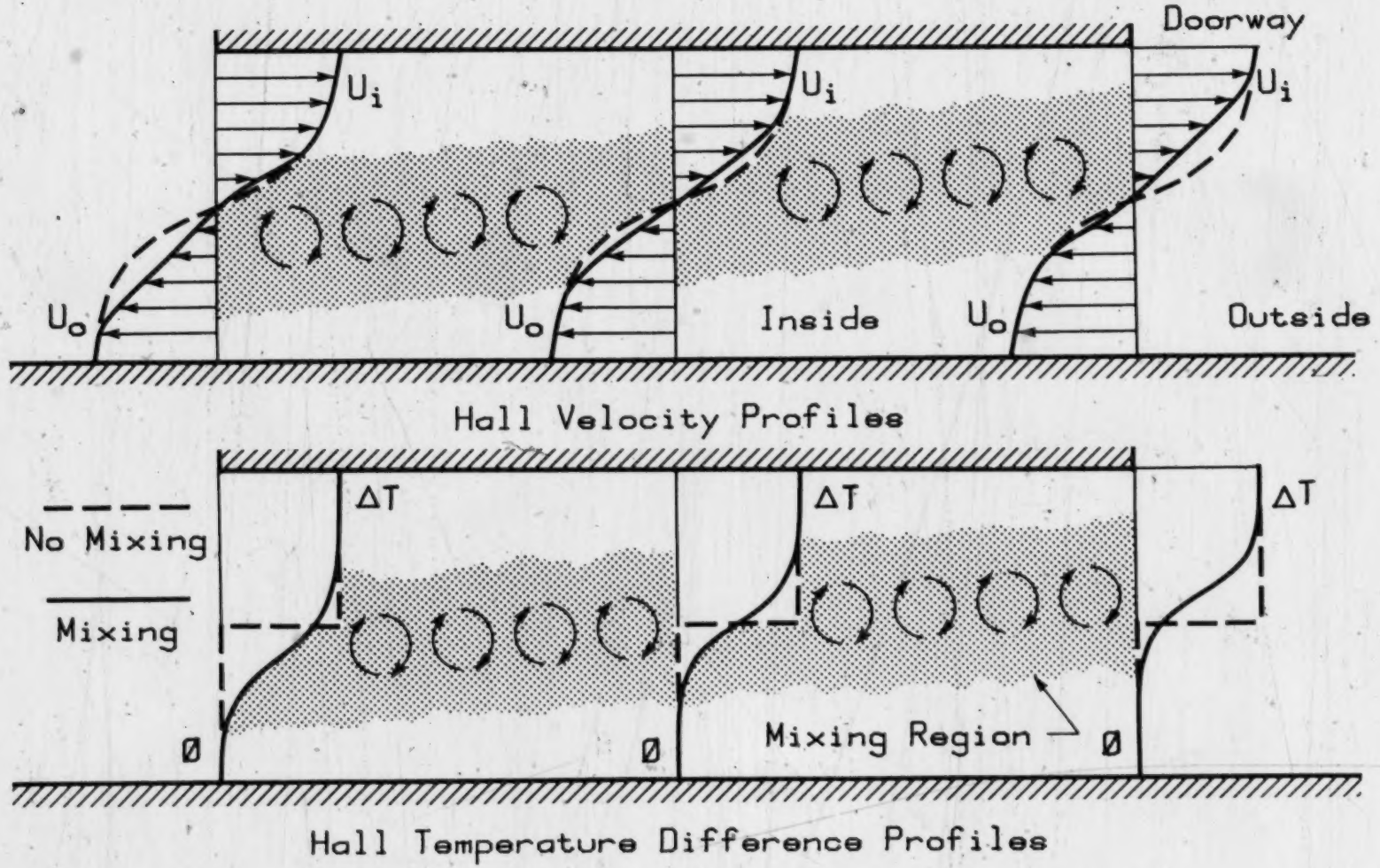

FIGURE 2-4: Velocity and Temperature Difference Profiles for a Long Hall with Interfacial Mixing

Nondimensional Numbers

For the flow problem under consideration, three types of forces need to be considered.

Viscous Forces	$UL\mu$
Inertia Forces	$\rho U^2 L^2$
Buoyancy Forces	$g'\rho L^3$

where

L = characteristic length scale

U = characteristic velocity scale

μ = dynamic viscosity

The following nondimensional numbers can be defined in terms of force ratios:

NUMBER	FORCE RATIO	
Reynolds (Re)	Inertia/Viscous	UL/ν
Froude (Fr)	$(\text{Inertia/Buoyancy})^{0.5}$	$U/(g'L)^{0.5}$
Grashof (Gr)	$(\text{Buoyancy/Viscous})^2$	$(g'L^2/\nu U)^2$

where

ν = kinematic viscosity

When considering gross orifice flow, a length scale based on orifice dimensions is most appropriate. The variations in the flow field for stratified counterflow are most significant in the vertical direction and thus it is reasonable to select a characteristic length which is based on orifice height H, not the orifice width. This is consistent with the convention found throughout lock exchange literature and in other similar applications.

The densimetric velocity scale is given by Equation 2-21 as:

$$U_\Delta = (g'L)^{0.5} \qquad (2\text{-}21)$$

where

U_Δ = densimetric velocity scale

Combining the length scale H, and the densimetric velocity scale U_Δ, with the definitions of Reynolds, Froude and Grashof numbers results in:

$$Re_\Delta = (g'H^3/\nu^2)^{0.5} \qquad (2\text{-}22)$$

$$Gr_\Delta = (g'H^3/\nu^2) \qquad (2\text{-}23)$$

$$Fr_\Delta = (1)^{0.5} = 1 \qquad (2\text{-}24)$$

Comparing these definitions, densimetric Reynolds and Grashof are related directly by:

$$Re_\Delta = Gr_\Delta{}^{0.5} \qquad (2\text{-}25)$$

Another characteristic velocity scale can be defined as the average inflow or outflow velocity. This can be thought of as a uniform velocity over half of the orifice surface WH/2, such that:

$$\overline{U} = \frac{Q}{WH/2} \qquad (2\text{-}26)$$

where

$\overline{U}$ = average inflow or outflow velocity

Using this experimentally determined velocity scale and a characteristic length scale of H, three new nondimensional numbers are defined.

$$Re_H = \frac{2Q}{W\nu} \qquad (2\text{-}27)$$

$$Fr_H = \frac{2Q}{W(g'H^3)^{0.5}} \qquad (2\text{-}28)$$

$$Gr_H = \left[\frac{g'WH^3}{2Q}\right]^2 \qquad (2\text{-}29)$$

where

Re_H = average flow Reynolds number

Fr_H = average flow Froude number

Gr_H = average flow Grashof number

Equation 2-20 may now be written in the following nondimensional form.

$$Re_H = \frac{2}{3} C_d(1-C_m)\, Re_\Delta \qquad (2\text{-}30)$$

Orifice Coefficient

The discharge coefficient C_d, is dependent on the nondimensional flow parameters in Equation 2-30. The value of C_d will depend on the flow rate, fluid viscosity and orifice geometry. It is common practice in the literature to express the discharge coefficient as a function of flow Reynolds number using a family of curves to represent various contraction geometries. For large area contraction ratios, typical of residential and commercial entries, orifice discharge coefficients exhibit only small variations with Reynolds number ASME(1971), and a power law approximation is adequate.

$$C_d = C_1\, Re_H^{\alpha} \qquad (2\text{-}31)$$

where

C_1 = empirical constant

The mixing coefficient C_m, also depends on the flow rate, fluid viscosity and geometry, but may exhibit greater sensitivity to the orifice height compared to the discharge coefficient and thus deserves special attention.

At one extreme, the mixing process may be dependent entirely on the local velocities and gradients near the neutral level, and be independent of the door height. In this case the mixing rate Q_m, is constant and $C_m=C_m(H)$. At the other extreme, if the thickness of the mixing layer and Q_m, scale directly with the height of the door, then C_m is constant and $Q_m=Q_m(H)$.

The following definition proves convenient:

$$C_m = C_{m,ref}\left[\frac{H_{ref}}{H}\right]^n \qquad (2\text{-}32)$$

where the two extremes are given by n=0 and n=1.5:

If n=0 C_m is a constant and Q_m scales with $H^{1.5}$

If n=1.5 C_m scales with $H^{-1.5}$ and Q_m is constant

Complete study of this relationship is beyond the scope of this study, but it is likely that the actual variation of the mixing coefficient lies between the two extremes of n=0 and n=1.5.

In this study all experiments were conducted with a door height of 2.06 m. Selecting this height as the reference height reduces Equation 2-32 to $C_m=C_{m,ref}$, thereby eliminating any functional dependence on n. The mixing coefficient values determined in this study apply only to residential type doors, further experiments are required

to extend these results to taller or shorter openings.

Assuming that the variation of C_m can also be related to the flow Reynolds number by a power law:

$$(1-Cm) = C_2 \, Re_H^{\beta} \qquad (2\text{-}33)$$

where

C_2 = empirical constant

Experimentally it will prove difficult to separate the combined effects of the two coefficients and therefore an orifice coefficient K is used, where:

$$K = C_d(1-C_m) \qquad (2\text{-}34)$$

combining Equations 2-32, 2-33 and 2-34 results in:

$$K = K_1 \, Re_H^{\gamma} \qquad (2\text{-}35)$$

where

$\gamma = \alpha + \beta$

K_1 = empirical constant

Recalling Equation 2-30, it is easy to show that if K is proportional to Re_H to some power γ, then it must also be proportional to Re_Δ to the power ϕ.

$$K = K_2 \, Re_\Delta^{\phi} \qquad (2\text{-}36)$$

where

$\phi = \gamma \; / \; 1-\gamma$

$K_2 = K_1^{1+\phi} \; (2/3)^{\phi}$

The orifice coefficient correlation with densimetric Reynolds number is a more useful relationship for flow prediction purposes because it

depends on the fractional density difference, not the measured flow rate. Equation 2-20 may now be written as:

$$Q_n = \frac{1}{3} K W (g'H^3)^{0.5} \qquad (2\text{-}37)$$

If the variation in K is small, then it is possible to correlate K linearly with temperature difference. This approach was taken by Fritzsche (1968) in his measurements of flow through cold room doors. He proposed the following correlation:

$$K = 0.48 + 0.0043\ \Delta T \qquad (2\text{-}38)$$

An empirical approach was taken toward the same problem by Brown, Wilson and Solvason (1963), and Brown and Solvason (1962) for the range of $0.19 < w/H < 0.75$ and $10^3 < Re_\Delta < 10^4$, resulting in the correlation:

$$Re_H = 2.32(1.0\text{-}0.6w/H)Re_\Delta^{0.846} - 430$$

which may be rewritten in terms of orifice coefficient variation as:

$$K = 3.48(1.0\text{-}0.6w/H)(\bar{\Delta}gH^3/\nu^2)^{-0.77} - 645(\bar{\Delta}gH^3/\nu^2)^{-0.5}$$

One final note concerning interfacial mixing. Research by Rozovsky, Shabrin, and Markov (1972) determined that a critical stability limit exists below which interfacial mixing is strongly suppressed. From their experiments, transition from stable flow to unstable flow with interfacial mixing occurred for densimetric Reynolds numbers in the range of $5 \times 10^4 < Re_\Delta < 10^5$. This will later be significant when comparing full scale and model results.

Buoyancy-Driven Exchange During Door Opening and Closing

An estimate of the buoyancy-driven air exchange that occurs during the door opening and door closing periods can be made by assuming quasi steady flow. Writing Equation 2-37 in integral form for the period when the door is moving from a closed position to 90 degrees open.

$$V_o = \int_{t=0}^{t=t_o} \frac{K\ W'\ (g'H^3)^{0.5}}{3}\ dt \qquad (2\text{-}39)$$

where

W' = orifice width at time t

V_o = volume exchanged during door opening

t_o = door opening time

It is easy to show that the orifice width varies with the angular position of the door as:

$$W' = W \cos(\theta) \qquad (2\text{-}40)$$

Using this relationship and assuming that the orifice coefficient and mixing coefficient both apply during the variable geometry period allows Equation 2-39 to be written as:

$$V_o = \frac{1}{3} K\ W\ (g'H^3)^{0.5} \int_{t=0}^{t=t_o} \cos(\theta)\ dt \qquad (2\text{-}41)$$

It should be kept in mind that this is a simplified analysis and thus the orifice coefficient is taken as constant. Data will be presented in Chapter 4 to support this approximation.

The value of the integral will depend on the variation of angular position with time and can be solved for any particular motion. For many practical applications, the door motion can be approximated by a constant swing speed with rapid initial acceleration and rapid final deceleration. In this case, $d\theta/dt$ = constant = $(2/\pi)/t_o$, and Equation 2-41 reduces to:

$$V_o = \frac{1}{3} K (g'H^3)^{0.5} W (2/\pi) t_o \qquad (2\text{-}42)$$

From Equation 2-42 the exchange that occurs during the variable geometry period can be considered as:

a) Steady state flow through an average orifice of width $(2/\pi)W$ for time t_o.

b) Steady state flow through an orifice of width W for a time $(2/\pi)t_o$.

The second approach with a fixed width of W and modified time will prove to be most convenient. Using this approach Equation 2-42 becomes:

$$V_o = Q_n t_{eq} \qquad (2\text{-}43)$$

where

t_{eq} = equivalent opening time = $t_o(2/\pi)$ for $d\theta/dt$=constant

For most practical applications and in all the experiments discussed in this study the opening and closing motions are nearly identical and thus t_{eq} will be the same for both opening and closing.

If the door closes before a reduction in the steady state flow rate is caused by the presence of interior walls, then the total buoyancy volume exchange for the opening period (t_o), closing period (t_c) and

steady period (t_s=t_h) can be determined using Equation 2-44.

$$V_B = V_o + V_h + V_c$$

$$V_B = Q_n\ (t_h + 2t_{eq}) \qquad (2\text{-}44)$$

where

V_B = Total predicted buoyancy exchange volume

Two factors that influence buoyancy exchange have been neglected in this analysis. First, as the orifice enlarges, some time is required for the flow to accelerate to the increased flow rate associated with the enlarged opening size. Because the opening is continuously enlarging, the real flow rate lags the predicted flow. This results in an overestimation of the exchange during the opening period.

The second factor neglected in this analysis is the variation of the orifice coefficient during opening and closing. The variation in the geometry suggests that the fully open orifice coefficient K, may not apply during the variable period and thus associated errors will result. Examination of experimental results will show that the errors associated with neglecting these factors are small.

Departure From Steady State Flow

For a finite interior volume, steady flow can only exist for a limited period of time before it begins to decrease, ultimately approaching zero flow rate. The time at which departure from steady state flow rate begins is related to the time required for the cold front to advance across the floor to the interior walls, reflect off and return to the entry. Figure 2-5 schematically illustrates the progression of a gravity current as it flows down a long hallway, strikes the end wall and is reflected to the doorway. The wave return

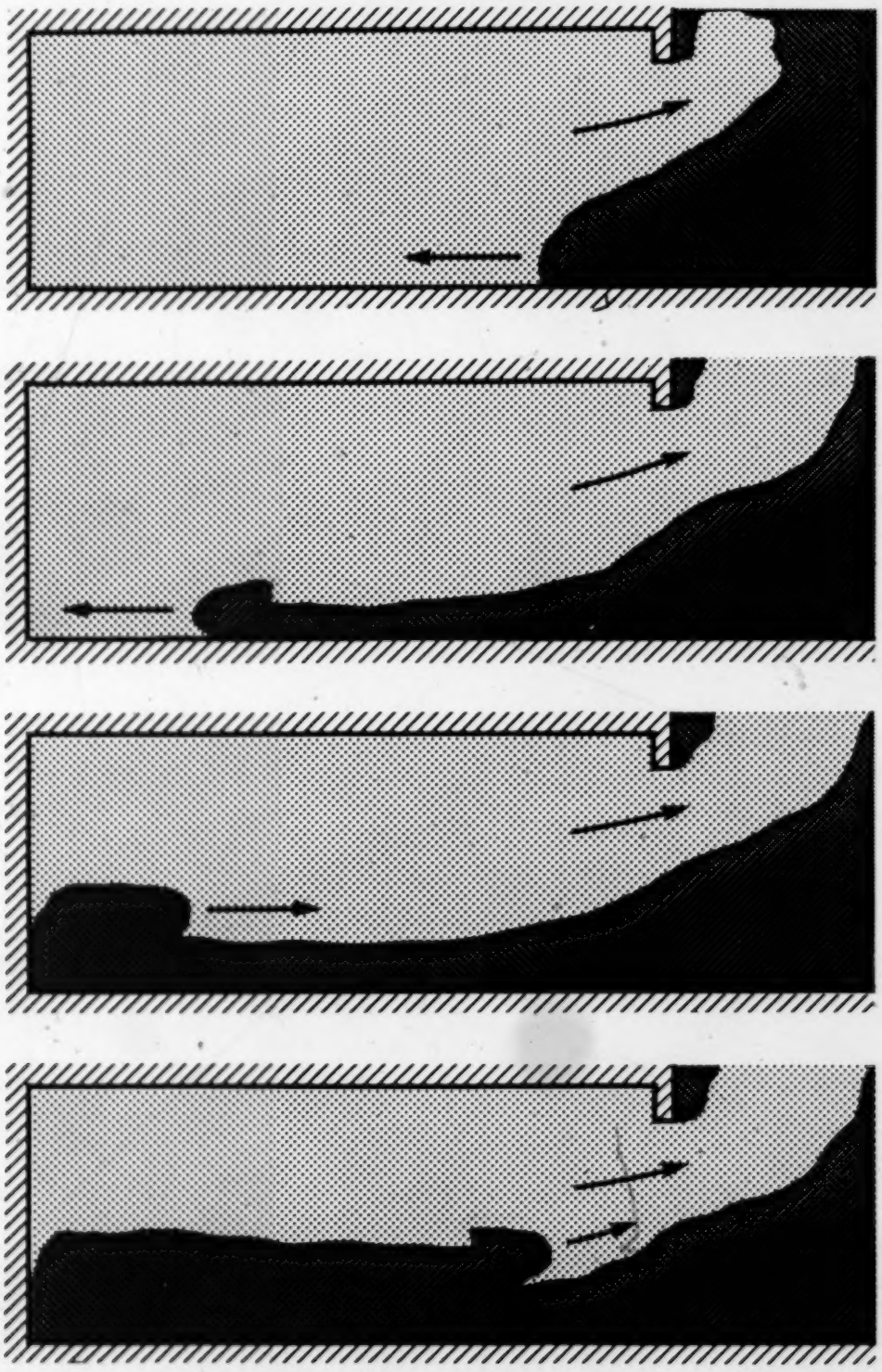

FIGURE 2-5: Gravity Current Flow Down a Long Hall with Reflection and Return Wave

time is very important in the determining of the effectiveness of an entry in limiting energy losses or contaminant transfer. A theoretical approximation for the wave return time will be developed by utilizing existing channel flow equations.

Cold Front Flow Down a Long Hall

From lock exchange studies it has been shown that the frontal velocity of a gravity current may be approximated by Equation 2-45, Benjamin (1968).

$$U_f = Fr_f^{2/3} \left[\frac{g \Delta' Q}{W_f} \right]^{1/3} \qquad (2\text{-}45)$$

$$\Delta' = \frac{\rho_i - \rho_o}{\rho_i} \qquad (2\text{-}46)$$

where

U_f = frontal velocity

Fr_f = frontal Froude number

W_f = flow width

Δ' = fractional density difference based on indoor density

The frontal Froude number Fr_f, depends on the fractional depth of the counterflowing streams. In lock exchange problems the top and bottom flows move in opposite directions approximately symmetrically and Fr_f is found to be $2^{-0.5} \simeq 0.71$. In situations where the free height above the inflow is much greater than the inflow thickness itself, the value of Fr_f approaches $2^{0.5} \simeq 1.4$, Benjamin (1968), and Wilkinson and Wood (1972). In this case, the front is advancing into a stagnant air mass. Flow down a long hall, as illustrated in Figure 2-5, is similar

to pure counterflow. Experimental results will indicate a frontal Froude number near the lower limit of 0.71.

Combining Equations 2-45 and 2-46 with the expression for flow rate given by Equation 2-37 results in:

$$U_f = Fr_f^{2/3} (gH)^{0.5} \left[\frac{K W \Delta' \bar{\Delta}^{0.5}}{3 W_f} \right]^{1/3} \qquad (2\text{-}47)$$

Equation 2-47 can be further simplified by approximating Δ' by $\bar{\Delta}$, so that $\Delta'\bar{\Delta}^{0.5}$ becomes $\bar{\Delta}^{1.5}$, this results in an error of less than 4% in U_f at a temperature difference of 60°C.

A characteristic flow length L_f, is now defined as the distance from the orifice to the reflecting surface. In the case of a long hallway this is simply the total length of the hall. A critical wave return time may now be defined in terms of the frontal velocity and the hallway length as:

$$t_{cr} = 2 L_f / U_f \qquad (2\text{-}48)$$

where

t_{cr} = critical departure time from steady flow

Experimental results will be used to determine the validity of the critical departure time model which is based on reflected gravity wave return time.

Cold Front Flow Into a Complicated Interior Geometry

When cold air flows through a doorway into an interior geometry which is more complicated than the simple hallway discussed above, it is more difficult to develop a simple model for the occurrence of the wave return. Even a simple four sided room with no interior obstacles is

difficult to analyse. Radial spreading causes the frontal velocity and layer thickness to be a function of distance from the orifice. The arrival of various reflected waves from the end and side walls will tend to smear out the distinct departure point typical of one dimensional flow. For these reasons a single characteristic length is difficult to define.

A general model proves more convenient than Equation 2-48 for approximating the critical time at which the flow rate begins to decrease. The basic assumption is that the volume exchanged at the critical time is related to an idealized maximum exchange volume. The ideal volume V_H, is defined as the interior air volume that lies below a horizontal plane level with the top of the door. For a one level interior, this value is simply the floor area times the door height. If some of the air which is buoyantly trapped above this level is entrained by mixing, then the actual exchange volume can slightly exceed V_H. This idea motivates the definition of the exchange ratio, E.

$$E = V / V_H \qquad (2\text{-}49)$$

where

E = exchange ratio

V_H = interior air volume below a horizontal plane at height H.

Two important values of exchange ratio are defined as:

E_{cr} = critical exchange ratio at t_{cr} and V_{cr}

E_{max} = maximum exchange ratio at infinite time, t_∞

Applying this concept to one dimensional hall flow with W_f=W, by combining Equations 2-47, 2-48 and 2-49 results in:

$$E_{cr} = 2\left[\frac{K}{3Fr_f}\right]^{2/3} \qquad (2\text{-}50)$$

For an ideal hall with $K \approx 0.58$ and $Fr_f \approx 0.75$ the value of E_{cr} can be determined as approximately 0.81. Experimental results will be used to determine the actual critical exchange ratios for various geometries including the long hall case. An estimate of the critical departure time can be made using Equation 2-51.

$$t_{cr} = \frac{E_{cr}\, V_H}{Q_n} \qquad (2\text{-}51)$$

Decreasing Flow Rate Caused by a Finite Interior Volume

Once the critical departure time is reached, a decay in the flow rate begins. To gain some insight into the decreasing flow process an idealized case shown in Figures 2-6 and 2-7 can be considered. The exchange is represented by a series of discrete gravity currents of decreasing thickness, proportional to the unexchanged volume below height H. The resulting reduction in flow will be approximated by a purely empirical exponential function of the form shown in Equation 2-52.

$$E = E_{max}\,(\,1-e^{-A(t-B)}) \qquad (2\text{-}52)$$

where

$$t > t_{eq}+t_s$$

Applying the following boundary conditions:

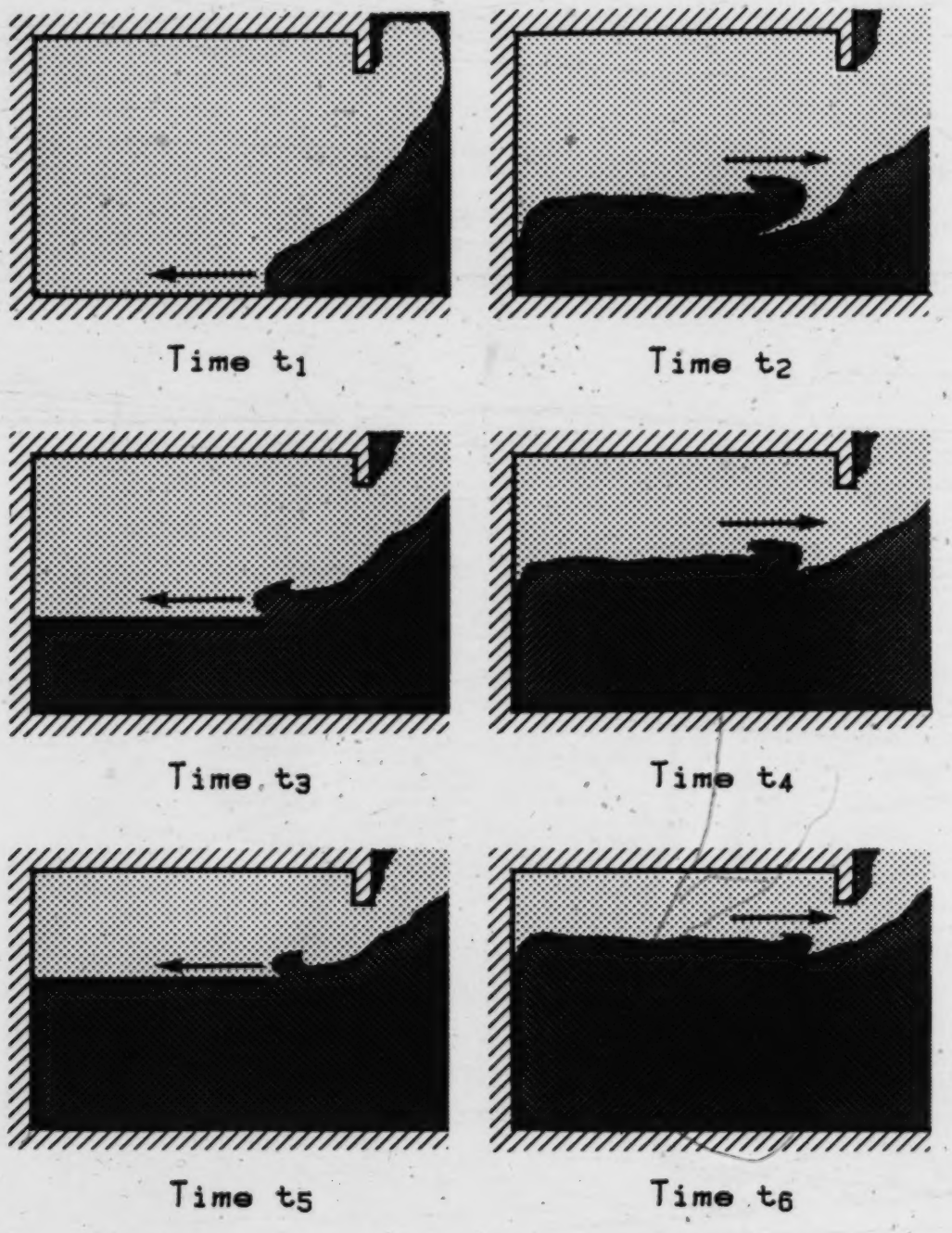

FIGURE 2-6: Idealized Decreasing Flow Assuming a Series of Discrete Gravity Current Inflows; See Figure 2.7 for Time Definitions

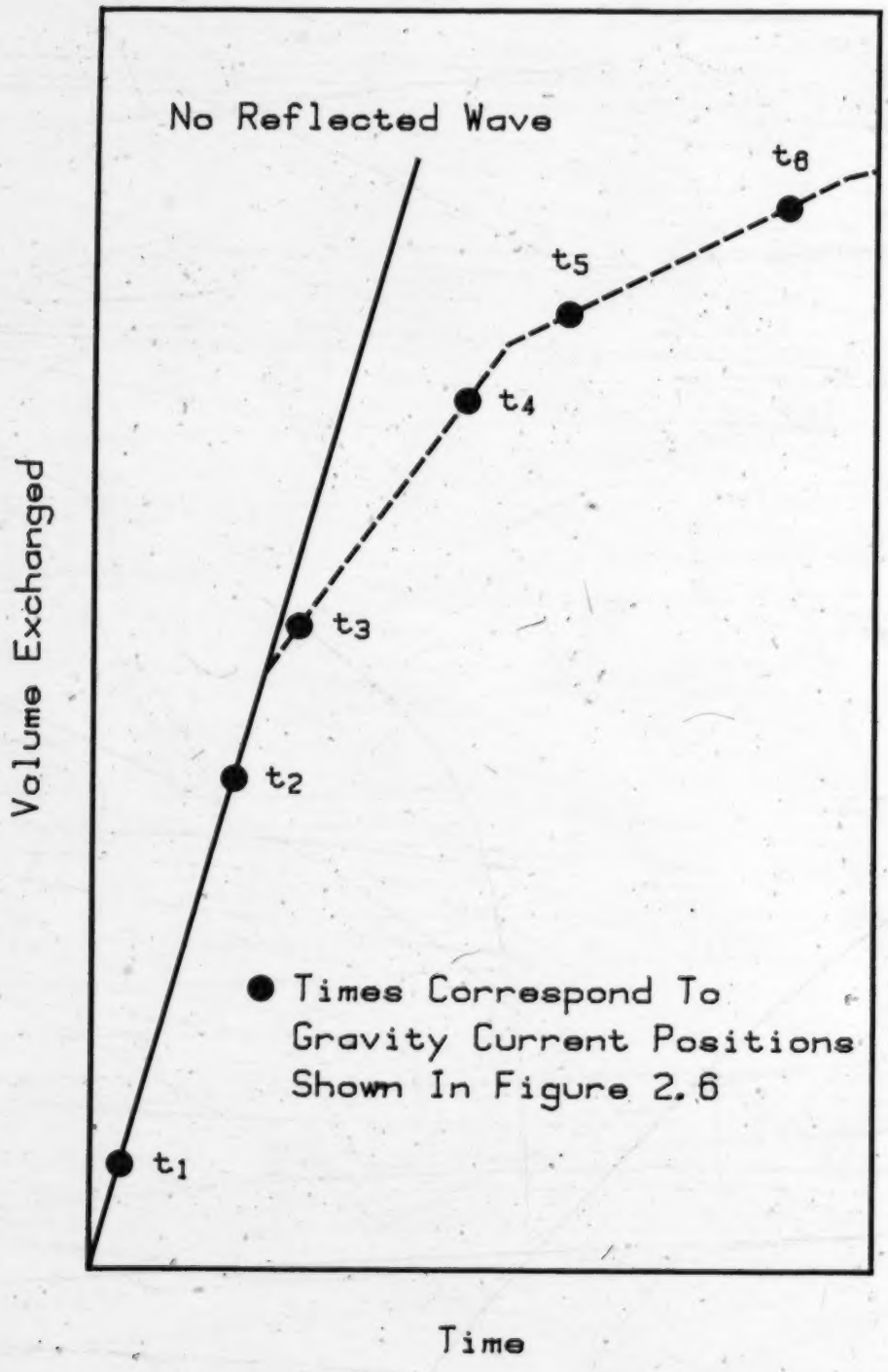

FIGURE 2-7: Volume Exchange as a Function of Time for the Series of Discrete Gravity Current Inflows Shown in Figure 2.6

$$\text{at } t=t_{cr} \qquad \frac{dE}{dt} = \frac{Q_n}{V_H}$$

$$\text{at } t=t_{cr} \qquad E = E_{cr}$$

$$\text{at } t \to t_{\infty} \qquad E \to E_{max}$$

Results in the following values of the constants A and B:

$$A = \frac{Q_n/V_H}{E_{max} - E_{cr}} \tag{2-53}$$

$$B = \frac{E_{cr}}{Q_n/V_H} + \frac{\ln(1 - E_{cr}/E_{max})}{A} \tag{2-54}$$

Experimental data will be used to determine the validity of Equation 2-52 and the values of E_{cr} and E_{max} for various interior geometries.

Interior and Exterior Turbulence

Turbulence is caused by the presence of interior circulation flows or exterior wind. The flow patterns and turbulence levels are strongly dependent on the number, size and position of fans or circulation vents, and the strength, direction and gustiness of the wind.

To gain some insight into the magnitude of air transfer through open doors due to circulation effects, Shaw's (1976) experimental results from tests on operating rooms can be considered. Shaw conducted experiments in a well mixed operating room and found that if the exchange rate was divided by half of the door area, then the orifice face velocity was approximately 0.14 m/s. Based on his literature

survey, this value was typical of well mixed rooms.

Shaw's results indicted that for well mixed conditions, turbulence induced exchange was insignificant above $3^{o}C$. He allowed C_d to absorb the effect of the exchange induced by room turbulence plus the buoyancy exchange. At $\Delta T=0^{o}C$, the value of C_d must go to infinity because Q approaches a constant value. For example at $\Delta T=1^{o}C$, a discharge coefficient of 0.9 was found, compared to 0.6 for $\Delta T>3^{o}C$, indicating that at $\Delta T=1^{o}C$, buoyancy still accounted for 2/3 of the exchange flow.

From Shaw's results, interior circulation flows do not merit intensive investigation in the context of energy losses through doors and thus interior ventilation effects were not studied.

Wind induced turbulence however could not be eliminated and tests revealed the surprising result that exterior wind, while producing negligible exchange at small temperature differences, is responsible for significant reductions in buoyancy-driven exchange flow. It will be shown later that exterior winds cause increased interfacial mixing which in turn results in reduced exchange flows. In this context, future studies may show that strategically placed interior circulation vents may also reduce buoyancy flow rates by increasing interfacial mixing.

Door Pumping Exchange

When a door swings open, air is drawn in behind the door. At the same time, air is forced from behind the opening door, around the leading edge and out of the opening. This generates vorticity and turbulence at the leading edge, inducing air exchange.

The amount of exchange produced depends on the speed at which the door swings, the size of the door and the temperature difference. If

the buoyancy forces produced by the temperature difference are large compared to the inertial forces produced by the swinging door, then the developing counterflow currents rapidly carry away the vorticity and turbulent air from the orifice. This reduces the air exchange that results from the swing effect. At the other extreme, if the buoyancy forces are very small, a standing vortex is generated which will remain intact for some time near the orifice, promoting transfer. In a similar manner, inertial exchange also occurs during the closing period. It is convenient to quantify the net transfer in terms of total exchange for a complete pumping cycle.

The manner in which the buoyancy and pumping contributions combine and the degree to which they influence one another is difficult to determine. The turbulence produced at small temperature differences interferes with the buoyancy exchange process, reducing it below the amount predicted using Equation 2-43. Figure 2-8 illustrates the difference between the predicted and actual buoyancy exchange as well as the difference between the residual pumping exchange and actual pumping contribution. The concept of residual pumping exchange V_P, as the difference between the predicted buoyancy exchange and the actual exchange will be useful.

Two important intercepts are identified on Figure 2-8; $\overline{\Delta}=0$ pumping volume V_{Po}, and critical fractional density difference, $\overline{\Delta}_{cr}$. The residual pumping volume depends on the door height, door width, swing speed and fractional density difference.

Examination of this problem will be limited to the development of an empirical relationship for application to residential doorways where H≈206cm, W≈91cm and $t_o=t_c$. Full scale and model data will be used to

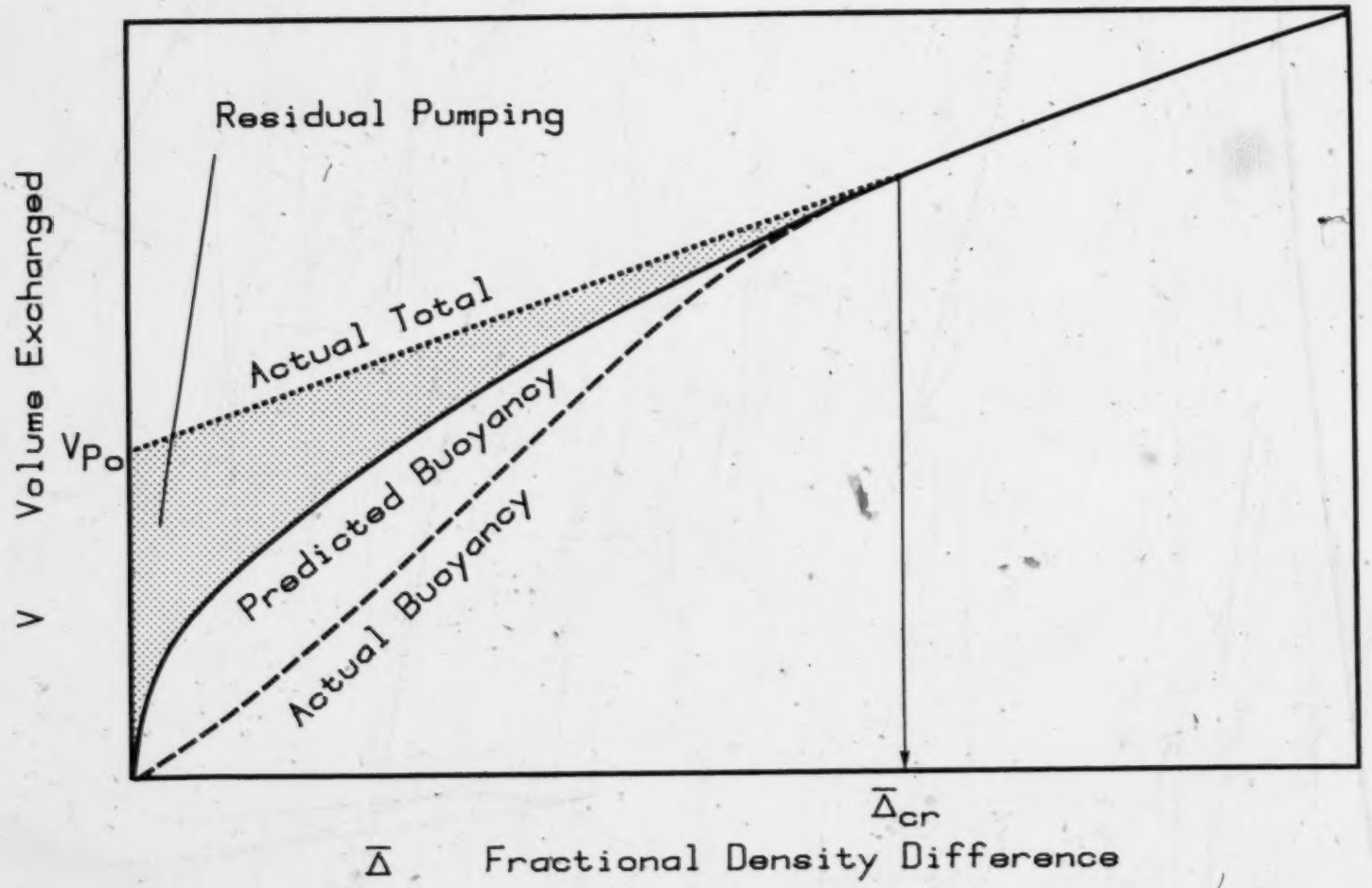

FIGURE 2-8: Idealized Pumping, Buoyancy and Residual Exchange Curves

show that residual volume pumped V_p, can be approximated by a linear variation from a value of V_{Po} at $\overline{\Delta}=0$ to a value of 0 at $\overline{\Delta}_{cr}$. Both V_{Po} and $\overline{\Delta}_{cr}$ will be shown to vary inversely with swing time, with constants of proportionality determined from model and full scale experiments such that:

$$\overline{\Delta}_{cr} = P_1/t_o \qquad (2\text{-}55)$$

$$V_{Po} = P_2/t_o \qquad (2\text{-}56)$$

$$V_P = V_{Po}(1-\overline{\Delta}/\overline{\Delta}_{cr}) \quad \text{for} \quad \overline{\Delta} < \overline{\Delta}_{cr} \qquad (2\text{-}57)$$

where

V_P = residual pumping exchange volume

V_{Po} = residual pumping exchange volume at $\Delta T=0^oC$

P_1, P_2 = empirical constants

Occupant Motion

The movement of a person through the opening causes entrained air to be transfer across the orifice plane. Study of this transfer was conducted by Shaw (1976) using a door 0.90 m wide and 2.05 m high at $\Delta T\approx 0^oC$. The exchanged volume ranged from 0.286 m^3 for a fast walk to 0.0873 m^3 for a slow walk. The size of door that Shaw tested is nearly identical to the entry examined in this study, and his results can be compared to pumping exchange volumes.

The significance of this inertial effect is expected to diminish rapidly as increased temperature differences are considered. Similar to ventilation or pumping exchange it likely has little effect above 4^oC to 5^oC. If larger entries are considered the net effect of occupant motion becomes even less significant.

CHAPTER 3

FULL SCALE EXPERIMENTS

Full scale air exchange experiments were performed to meet the following objectives:

- o Measure the energy losses associated with exterior doors in residential structures over a wide range of temperature differences.
- o Obtain sufficient data to test the validity of the exchange equations.
- o Obtain appropriate data for comparison with 1:20 scale model simulation to determine the degree of similitude and correctness of theoretical time scales and equations.

Experimental Parameters

Numerous factors influence the exchange of air through doorways. These include:

- o door height
- o door width
- o interior floor area and levels
- o door swing characteristics
- o interior turbulence intensity and scale
- o exterior wind speed, angle and turbulence intensity and scale
- o interior partition geometry
- o temperature difference
- o interior and exterior air stratification

The number of factors in this list dictates that only a limited number of parameters be tested in full scale. The focus of this study

is on energy losses through typical entries and thus only the most influential parameters in this context will be varied. Very large and very small H/W aspect ratios fall in the same class of problem but are not typical of residential entries and thus will not be considered experimentally. A review of previous research also assists in reducing the number of varied test parameters. Shaw (1976) showed that for a range of door widths from 0.1 m to 1.4 m, that flow rate was directly proportional to door width W, with negligible effect on the orifice coefficient K.

The following parameters were kept constant, or as close to constant as possible in all tests:

- o door height and aspect ratio
- o door opening and closing swing speeds
- o interior turbulence intensity and scale
- o interior stratification

The following parameters varied between tests:

- o fully open hold time
- o indoor-outdoor temperature difference
- o interior volume and geometry
- o wind speed and direction

Exchange Flow Measurement Techniques

Accurate measurement of exchange rates are not easily achieved. Several techniques are available but each has some disadvantages in terms of accuracy, equipment requirements and measured quantities. Two of these alternatives will be compared.

Velocity Profiles- The measurement of flow velocities and flow directions in doorways was used with some success by Shaw (1976) to determine exchange rates through operating room doorways, and by Fritzsche (1968) in measuring flow through open cold-room doors. The

technique requires the measurement of velocities in the doorway opening as a function of time. Integration of these velocities provides valuable time dependent volume flow information.

Unfortunately this technique has two major drawbacks. First, simultaneous multiple velocity measurements of the necessary accuracy and number are very difficult and expensive to perform. Traversing methods could be employed, but only for steady state flows that last for a sufficiently long duration to allow a complete traverse of the orifice area. Shaw employed 40 hot wire anemometers and smoke generators in his operating room experiments. Even if accurate local velocities can be determined, this information is insufficient to determine net mass transfer if significant mixing between the two air streams occurs. As shown in Chapter 2, it is necessary that the local temperatures or tracer concentration (if one air mass is marked) be measured simultaneously to determine the net mass transfer.

Tracer Gas- Tracer gas is introduced into the interior air volume, mixed thoroughly, and a concentration reading taken before and after the exchange has occurred. The reduction in concentration is proportional to the net mass transfer. The primary advantage of this method is the minimal amount of equipment required, but the method provides no information concerning the time dependent characteristics of the exchange. This problem may be overcome by using a series of experiments, each with the same initial conditions, but varying the door open time in each consecutive test. This allows a correlation between total exchange and open time.

For this study, the tracer gas method was selected as the most

appropriate technique, both in terms of measurement accuracy and equipment availability. To compensate for the lack of flow detail afforded by the tracer gas method, copper-constantan thermocouples were used to provide some insight into the structure of the exchange flow.

Test Facility

Full scale air exchange experiments were conducted at the Alberta Home Heating Research Facility, located south of Edmonton on open agricultural terrain. The facility consists of six unoccupied houses each constructed using different energy conservation strategies. Figure 3-1 illustrates a plan view of the facility including the position of two meteorological stations providing wind speed and wind direction data. Each module has a single room main floor with a small entry and full basement.

Two factors were considered in the selection of the most appropriate module for exchange experiments, natural infiltration and thermal resistance. It was important that natural infiltration be as small as possible to limit its effect on the tracer gas concentration. Selecting the module which had the highest level of thermal resistance reduced the cooling of the house during test periods (during which the furnace and its circulating fan were shut off). Module 3 was selected on the basis of these requirements.

Figure 3-2 illustrates the overall dimensions of module 3. Windbreaks were erected in the locations indicted on Figures 3-1 and 3-2 to reduce the mean wind speed outside the entrance of module 3. They extended from ground level to the roof overhang and were attached between module 3 and the adjacent module. Although the mean wind speed

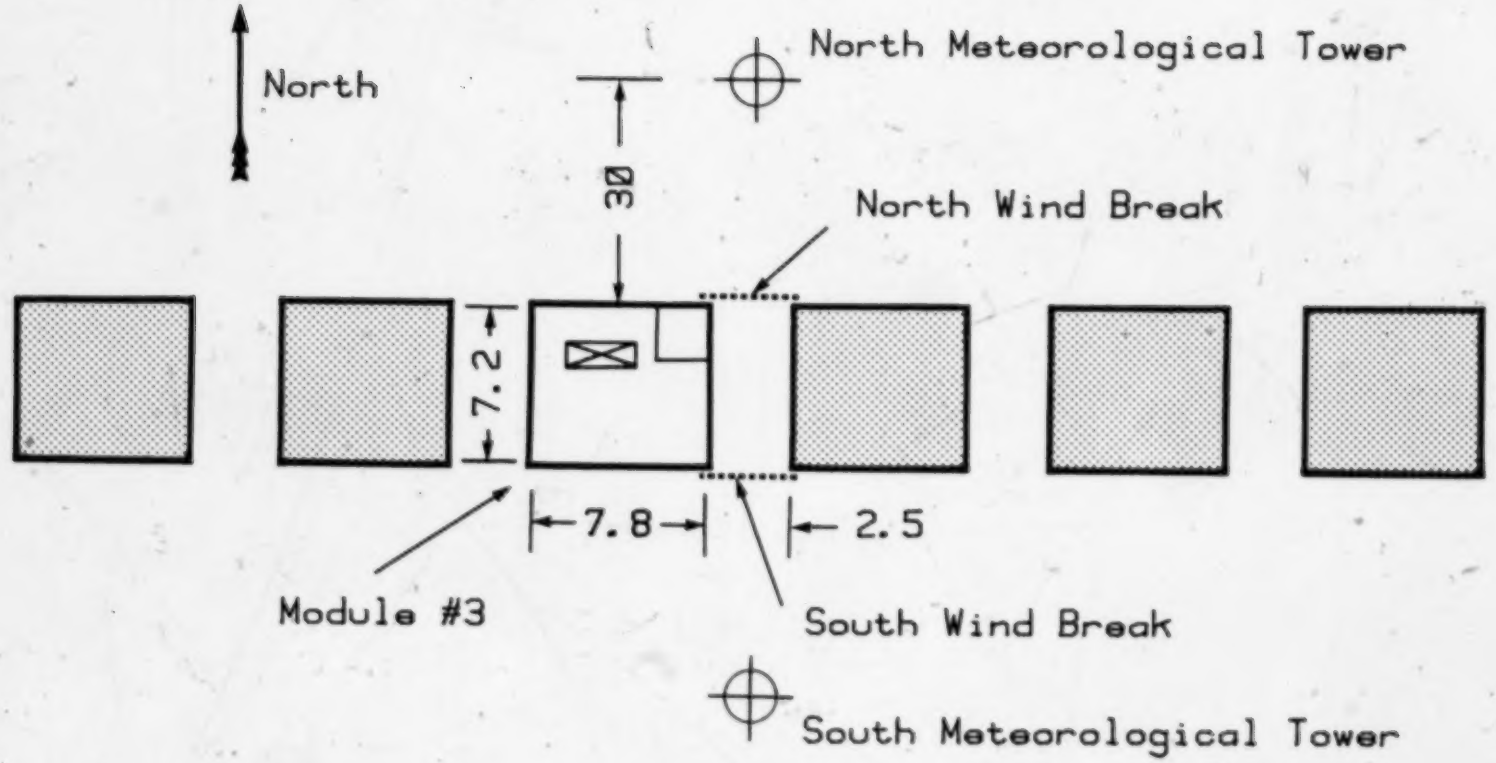

FIGURE 3-1: Physical Layout of the Alberta Home Heating Research Facility, All Dimensions in Meters

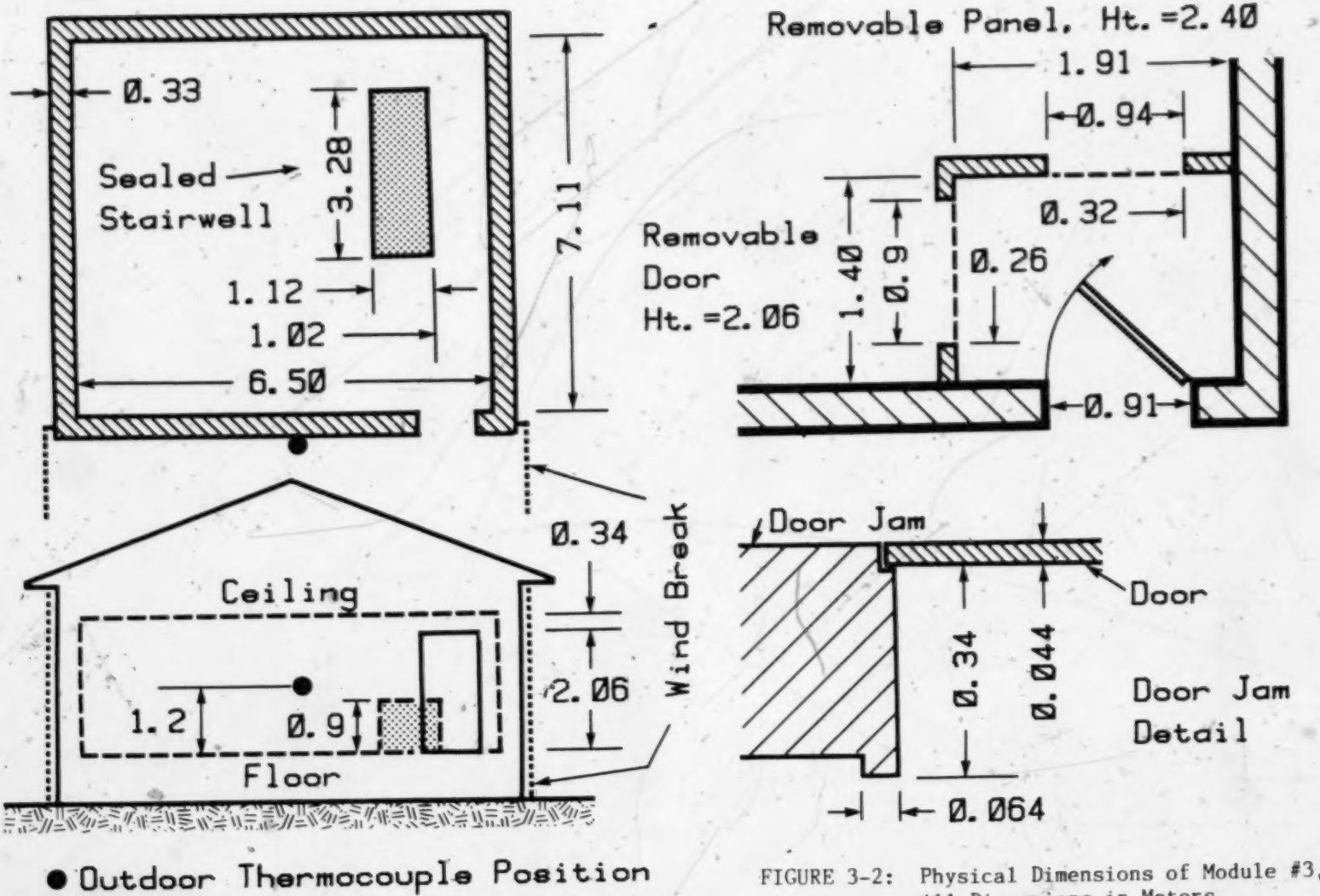

FIGURE 3-2: Physical Dimensions of Module #3, All Dimensions in Meters

was significantly reduced, turbulence was still present outside the entrance due to wind.

Figure 3-3 shows three of the interior geometries tested and Table 3-1 lists the physical volumes and areas associated with each. The three geometries were obtained using tarpaulins, the inner entry door and a removable panel. The tarpaulins were sealed at the floor, ceiling and walls with duct tape. The basement was not included in any of the geometries. This separation was accomplished by sealing both the floor vents and the stairwell opening.

Experimental Equipment

Gas Analyser- A Miran 1A Infrared Absorption Gas Analyser was used with sulphur hexaflouride (SF_6) as the tracer gas. Complete details of calibration and specifications, and a typical calibration curve can be found in Appendix B. Over the six month period of data collection, 14 calibrations were performed, with a calibration preceding each active testing period.

Mixing Fans- Two 19 cm diameter axial fans with 150 watt motors were employed to ensure complete mixing of the tracer gas with room air prior to and following an exchange experiment. Fan positions were selected to provide maximum mixing for each test geometry. The mixing fans were turned off prior to each exchange experiment to allow interior turbulence to dissipate.

Door Control- The physical layout of the experiments required remote control of the exterior door. Both swing time (t_o and t_c) and fully open hold time (t_h) had to be adjustable and the door motion had to be repeatable from test to test. This was accomplished with a simple

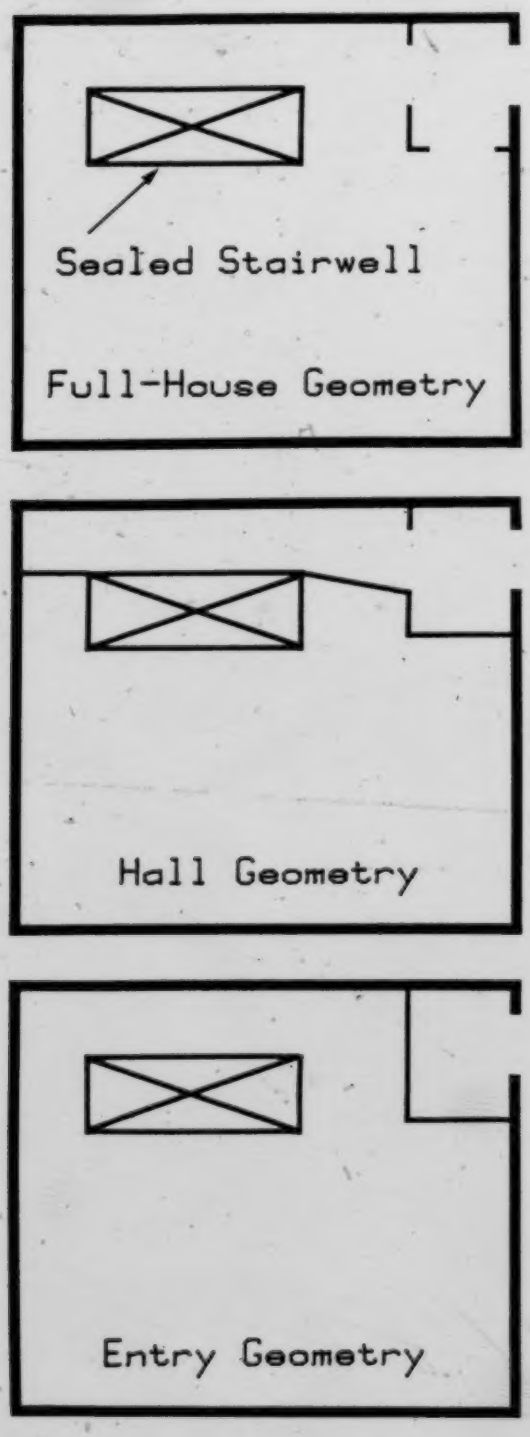

FIGURE 3-3: Interior Test Geometries; Full-House, Hall and Entry

TABLE 3-1: Interior Volumes of Test Geometries

Geometry	A_f m^2	H_cA_f m^3	V_I m^3	V_H m^3
Full-House	46.2	110.9	106.7	91.4
Entry	2.67	6.42	6.42	5.53
Hall	8.63	20.70	20.70	17.85

A_f - Floor area.

H_cA_f - Ceiling height x floor area.

V_I - Gaseous interior volume.

V_H - Interior gaseous volume beneath door height, H.

system consisting of a 3/8 inch electric hand drill mounted on the lower interior door surface. The drill drove a wire brush traction wheel griping the carpeted floor surface. Micro switches were mounted to detect fully open and fully closed positions. Timing and speed were set on the door control unit and the door position was monitored with a potentiometer mounted on one of the door hinge pins. A typical door position curve is shown in Figure 3-4 illustrating the nearly constant opening and closing swing speed.

Wind Speed and Direction- Wind speed and wind direction were determined at the north meteorological station for each exchange experiment. The remote location of the north tower relative to the entrance of module 3 suggests that this information is only useful as a qualitative estimate of the turbulence level outside the entrance. Exchange theories and equations developed in Chapter 2 apply quantitatively to low wind speed conditions and therefore testing was concentrated at low exterior wind speeds. Most tests were conducted for wind speeds less than 15 km/hr.

Temperature Measurements- All temperature measurements were made with copper-constantan thermocouples referenced to an ice point cell. Outdoor temperature was measured at the door midheight 2 m south of the entry door as shown in Figure 3-2. The exterior thermocouple junction was placed in a radiation shield mounted on the exterior wall. Indoor temperature was measured at a central location within the test geometry halfway between the floor and ceiling. It should be noted that due to active air mixing prior to the door opening, stratification was minimized and was less than $0.2^{o}C$ from floor to ceiling, even for large temperature differences.

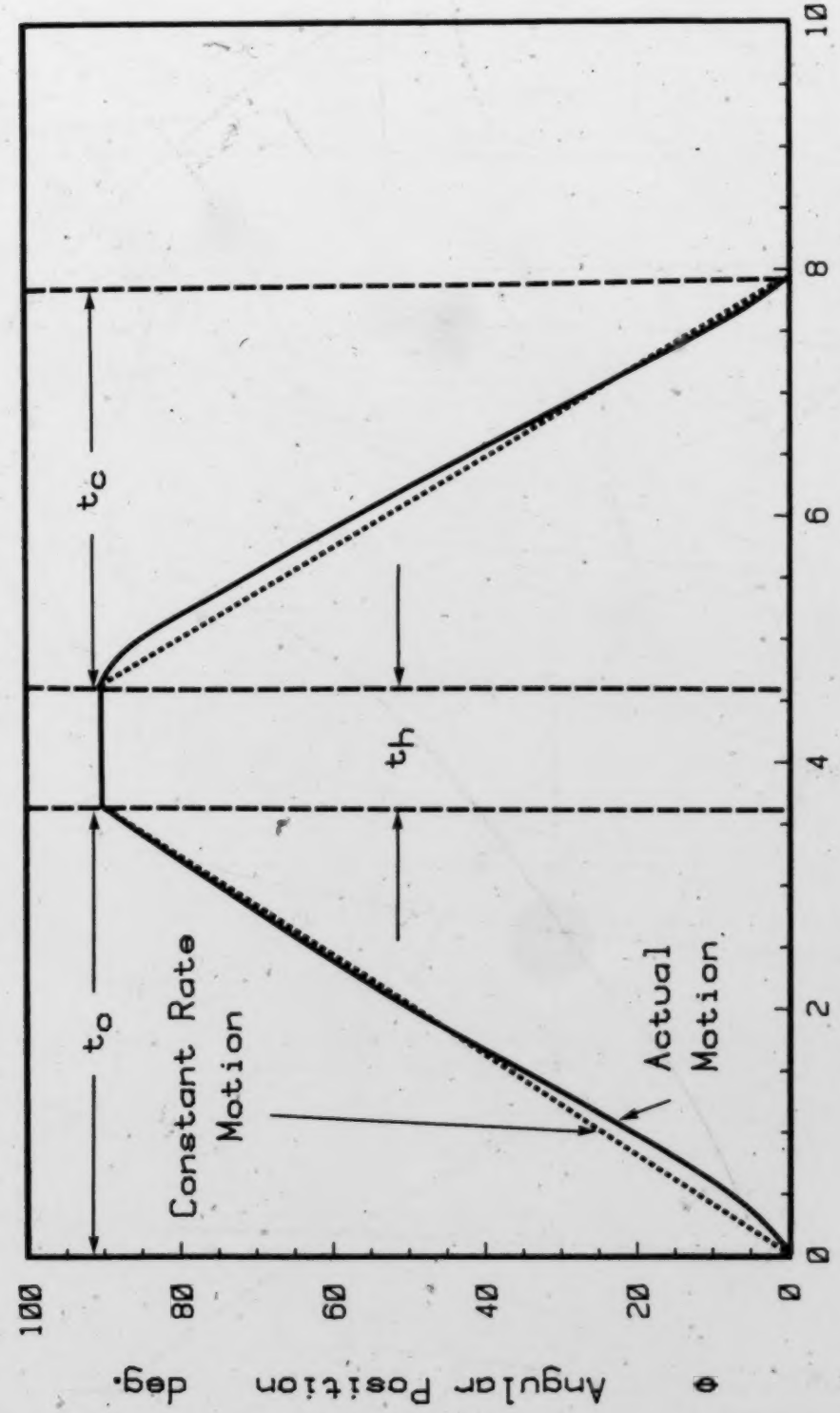

FIGURE 3-4: Typical Door Motion Curve Measured with Position Sensor

In addition to the indoor and outdoor temperature measurements taken before and after exchanges, as many as 21 thermocouples were employed during the exchange process, to measure vertical temperature profiles and record the rate at which the cold air front moved across the floor. These thermocouples were 30 gauge, with a response time constant of approximately 0.5 s.

Data Acquisition and Storage- The collection and storage of data was accomplished using an HP-85 Microcomputer, HP 3050B Multichannel Scanner and HP 3025A Multimeter. Collected data was stored on magnetic tape at the facility and later transferred to 5 1/2 inch floppy disk. Chart recorders were also employed to provide a backup hard copy of door position and tracer gas concentration, and provide operational information during experimentation.

Experimental Procedure

At the start of any exchange test the following descriptive information was recorded: time, date, test #, geometry #, thermocouple layout #, fully open hold time setting and swing speed setting.

With mixing fans operating, tracer gas was then injected into the test volume until a concentration of approximately 5 ppm was achieved. Tracer gas concentration levels and wind information were then sampled over a 3 minute period, followed by indoor and outdoor temperature readings. A 3 minute sample was required to measure the decay in SF_6 concentration caused by natural air infiltration, this information was used to correct the measured exchange volumes for the effect of natural infiltration. The mixing fans were then turned off approximately 45 seconds prior to door opening to allow the small scale turbulence

to dissipate, eliminating its possible effect on interfacial mixing.

Door motion was triggered manually from the door controller. The door then quickly accelerated to the swing speed selected on the controller. After arriving at the fully open position, it remained for the selected duration, and then closed at the same speed as opening. The door position potentiometer voltage and thermocouples were read approximately 13 times per second throughout the door cycle. Often, sampling was continued after the door was closed so that final mixing transients could be determined.

On completion of both the door cycle and the thermocouple sampling, the mixing fans were restarted to ensure complete mixing of the residual interior air (marked with tracer gas) with the unmarked cold air. When mixing was complete and the gas analyser sample chamber fully purged, typically 2 to 4 minutes, another 3 minute sampling identical to the first was started.

ΔT-Sets of Exchange Tests

Characterizing net volume exchanged as a function of time using tracer gas methods required a series of tests with the same geometry, same temperature difference and varying fully open hold time. A ΔT-Set consists of 10 to 12 exchange measurements taken at varying fully open hold times with very similar temperature differences. Table 3-2 indicates the fully open times used for each ΔT-Set, the selected times depended on the geometry type as indicted in Table 3-2.

Extensive use was made of series of tests in which the second decay measurement was used as the first decay of the next test. If the temperature difference was small and the interior volume large, as many

TABLE 3-2: Fully Open Hold Times in Each ΔT-Set

Geometry	# of ΔT's	Hold Times for Each Exchange in a ΔT-Set [s]
Full-House	17	0.5, 2, 3, 5, 10, 20, 34, 50, 67, 120
Entry	9	0.5, 1, 2, 3, 5, 7, 10, 20, 34, 50
Hall	13	0.5, 1, 2, 3, 3.5, 5, 10, 20, 34, 50, 67, 120

as 10 to 15 consecutive tests could be conducted before the SF_6 concentration was to small to be accurately measured. At the other extreme, if the temperature difference was large and the interior volume small, one or two door openings could reduce the SF_6 concentration by 90% and require the addition of SF_6. The stabilization period and initial decay were always required after the addition of SF_6.

The thermal mass of module 3 and the energy from the mixing fans and interior lights warmed the cooled air mixture very quickly. Only for extremely low outdoor temperatures and large percent exchanges was it necessary to halt testing and restore the indoor temperature with the furnace. As will be shown in a later section, it is possible to successfully correct for the small variations in temperature differences between tests in the same series.

Temperature Measurements

Two types of temperature measurements were made. First, a vertical array of 19 thermocouples spaced 10 cm apart on the vertical centerline of the door opening (located 4 cm outside the closed door) were sampled sequentially to measure the inflow and outflow temperature profiles. Second, 21 thermocouples arranged horizontally on the hallway centerline 15 cm above the floor, spaced 25 cm apart, were used to determine the rate of cold front advancement down the length of the hall geometry. The thermocouple closest to the door was was sampled continuously until a $0.5^{o}C$ reduction below indoor temperature was found, the time was recorded and sampling was shifted to the next thermocouple in the line. This procedure allowed the determination of the cold front position as a function of time by comparing the relative response of each thermocouple

to the first. Because each thermocouple was compared to the first thermocouple in line, the thermocouple time response constant was not important in determining an accurate measurement of the gravity front position.

CHAPTER 4

FULL SCALE DATA ANALYSIS AND RESULTS

Approximately five hundred full scale exchange experiments were conducted over a 6 month period providing a temperature difference range from $0^{o}C$ to $45^{o}C$. The method of reducing tracer gas concentration results to determine exchange volumes will be considered first. Experimental results will then be examined in context with the equations and theories presented in the Chapter 2.

Data Reduction

Figure 4-1 shows a typical SF_6 concentration curve for an exchange test on the entry geometry. The rate of exponential decay depends on the wind conditions, temperature differential, interior volume, tracer gas concentration and tightness of the envelope of the volume being tested. The 3 minute measured concentration decay provided sufficient information to establish the constants in an exponential decay caused by natural infiltration as described by Bassett, Shaw and Evans (1981).

$$c(t) = A\, e^{-tB} \qquad (4\text{-}1)$$

where

$c(t)$ = tracer concentration at some time t

A;B = constants

Extrapolation of the initial decay curve from Equation 4-1 to time t_1, established the SF_6 concentration at the instant the door began to open. In a similar manner, extrapolation of the final decay to time t_2,

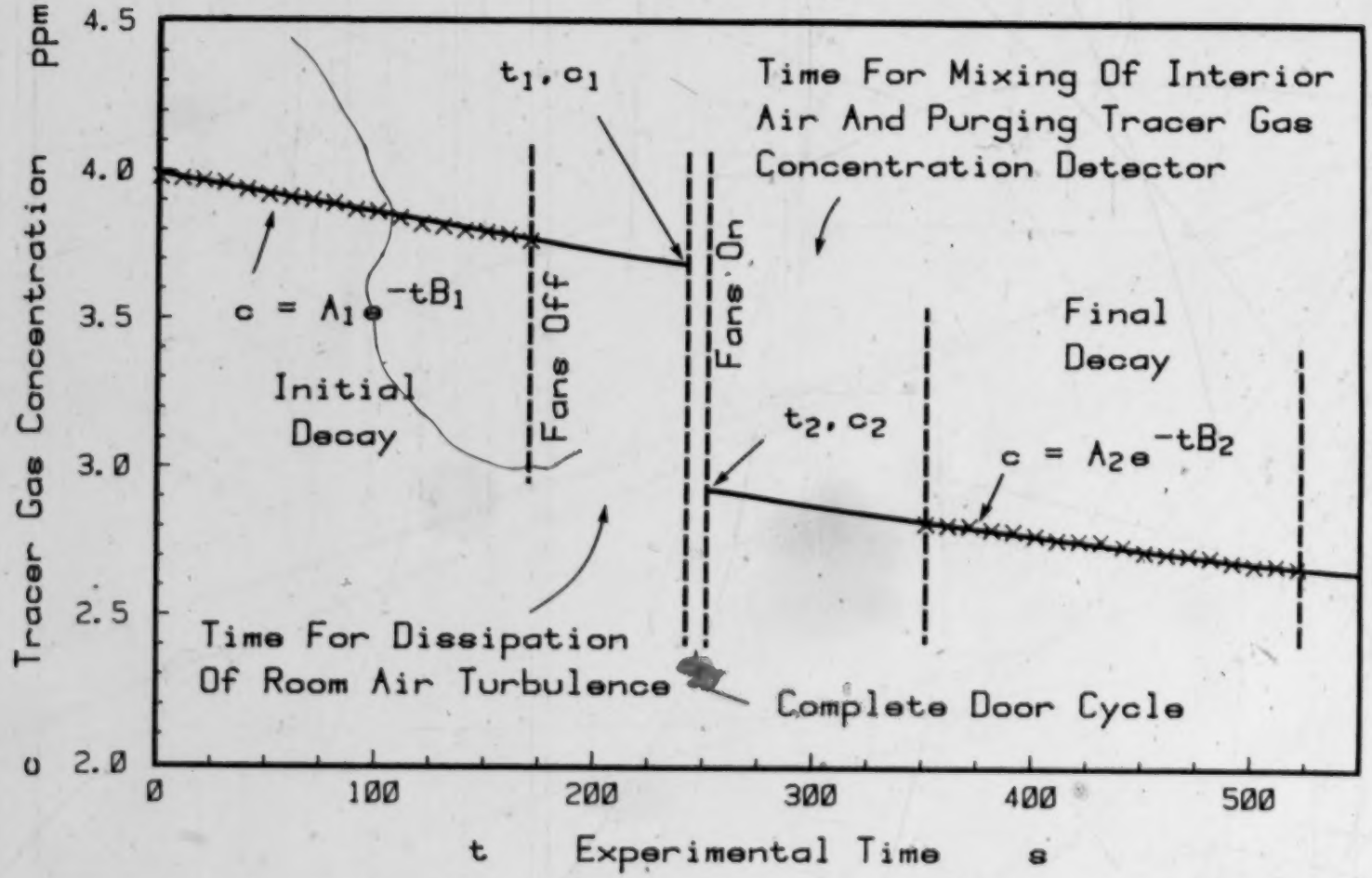

FIGURE 4-1: Measured Tracer Gas Concentration Decays And Exponential Extrapolations for a Typical Exchange Experiment; Entry Geometry, Hold Time=2 s, ΔT=6.5°C, $T_{i,ref}$=22°C

established the effective concentration of SF_6 at the instant the door closed.

The exchange volume was determined from Equation 4-2.

$$V = \frac{c_1 - c_2}{c_1} \quad V_I \qquad (4\text{-}2)$$

$$c_1 = A_1 \, e^{-t_1 B_1} \qquad (4\text{-}3)$$

$$c_2 = A_2 \, e^{-t_2 B_2} \qquad (4\text{-}4)$$

where

t_1; t_2 = time of door opening and closing

c_1; c_2 = concentration of tracer gas at t_1 and t_2

V_I = total interior volume

A_1; B_1 = constants from first decay fit

A_2; B_2 = constants from second decay fit

Thermal Expansion of Incoming Air

Exterior air that is transferred into a house will absorb energy from the interior surfaces, expand and produce exfiltration. The heat transfer process is most significant after the door is closed and the mixing fans are started. The effect of this process on tracer gas concentration is illustrated in Figure 4-2 using a simplified scenario in which the natural infiltration rate is zero. A 50% exchange occurs, indoor air at 20°C and outdoor air at -20°C are adiabatically mixed by the fans soon after the door closes, the resulting indoor temperature is 0°C. The mixture gradually warms back to 20°C resulting in air exfiltration. The actual process in an integral process, whereas the simplified case shown in Figure 4-2 assumes that all exfiltrating air is

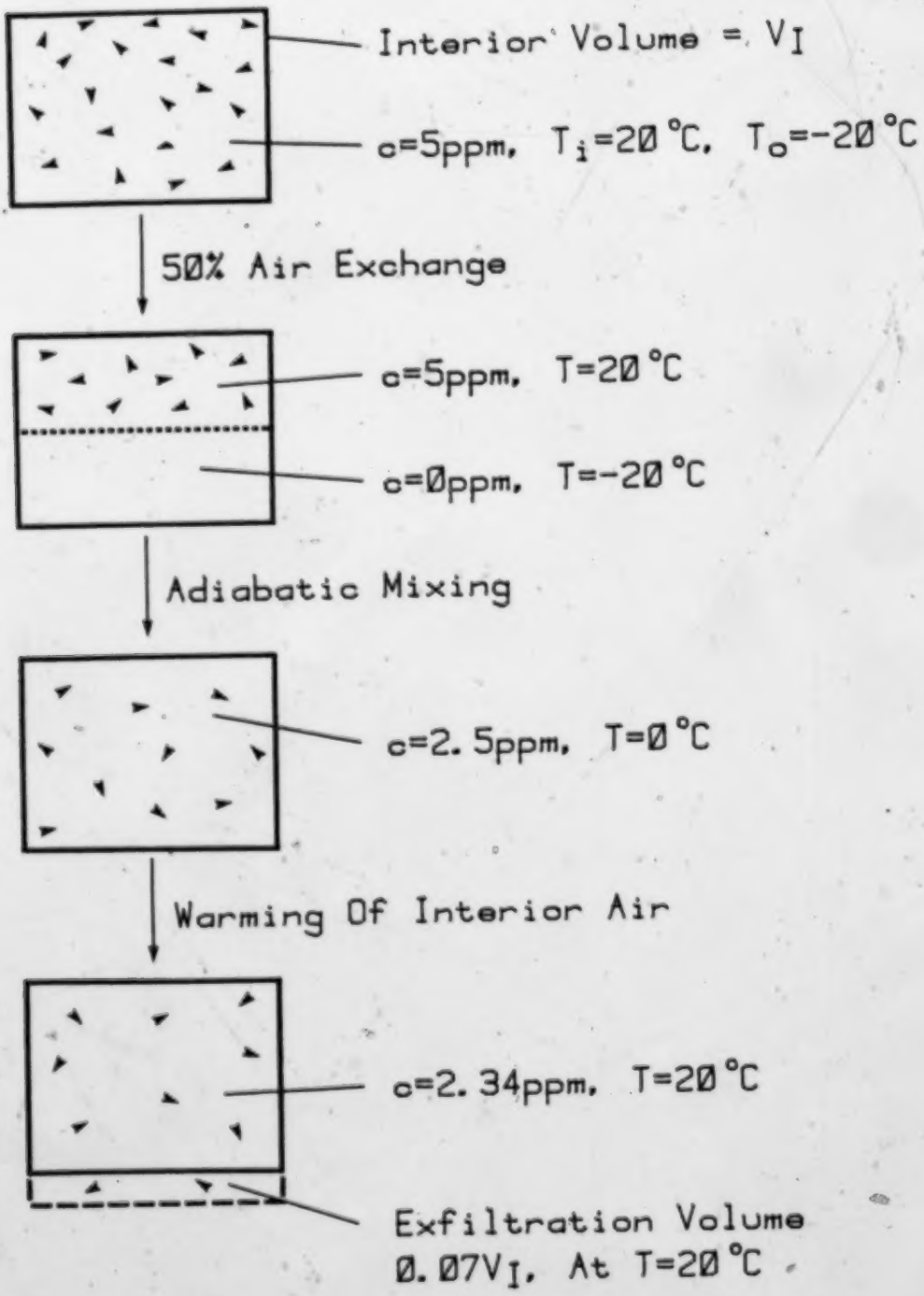

FIGURE 4-2: Effect of Thermal Expansion of Outdoor Air on Tracer Concentration During Final Decay Measurement

at 20°C. This results in a reduced tracer gas concentration which causes an error of 3.2% in the measured volume exchange.

Fortunately, warming effects are measured simultaneously with the natural infiltration effects. Both infiltration and thermal expansion effects are accounted for by the second 3 minute decay measurement.

Steady State Flow for the Fully Open Door Position

As shown in Chapter 2, steady state flow provides the foundation for predicting total buoyancy-driven exchange V_B, and thus represents a logical starting point for data analysis. Recalling Equation 2-44 with t_d=0:

$$V_B = Q_n (t_h + 2t_{eq}) \qquad (2\text{-}44)$$

where

$$Q_n = \frac{K\ W}{3} (g'H^3)^{0.5} \qquad (2\text{-}37)$$

For any ΔT-Set of full scale test data, the fully open hold time t_h, was varied and the associated volume exchange determined. Linearly correlating the measured volume exchange V, with t_h for each set of data allowed the net steady state flow rate Q_n, to be determined for the conditions of each set.

One small complication lies in the fact that the value of g' is not constant between every test in a ΔT-Set. It was possible to adjust the value of V such that each test is corrected to the average value of g' for the set. The correction was made by rewriting Equation 2-44 in terms of $V_{corrected}$ at g'_{avg} and then taking the ratio of the two equations.

$$V_{corrected} = V\,(g'_{avg}/g')^{0.5} \qquad (4\text{-}5)$$

where

$V_{corrected}$ = volume exchanged V, corrected to g'_{avg}

g'_{avg} = average value of g' for the set of tests

For example, if $\Delta T_{avg} = 32^{o}C$ and $\Delta T_{test} = 30^{o}C$, the corrected value of exchanged volume is 1.03V from Equation 4-5. Thus the volume exchanged would have been 3% higher if the temperature difference had been $32^{o}C$ (the set average) rather than $30^{o}C$. In general, corrections were not any larger than shown in this example and most were less than one percent.

Figure 4-3 illustrates 5 ΔT-Sets of data for the full house geometry. Each set has a different average temperature difference and average wind speed. All other parameters were maintained as constant as possible for each test in the set. A least squares linear regression gives the steady state flow rate for the average test conditions of the set. The good quality of fit shown in Figure 4-3 is typical of most test results. Figure 4-4 illustrates the steady state flow rates determined in this manner for the full-house geometry. The average wind speed has been included for each flow rate.

The repeatability of exchange volume measurements was examined using a series of tests with the same door motion and as similar as possible wind speed, wind direction and temperature difference. Maximum variations in measured exchange volumes were found to be approximately 15% of the interior volume with typical variations in the order of 3% to 5%. It should be kept in mind that this represents measurement errors as well as differences in the actual exchange.

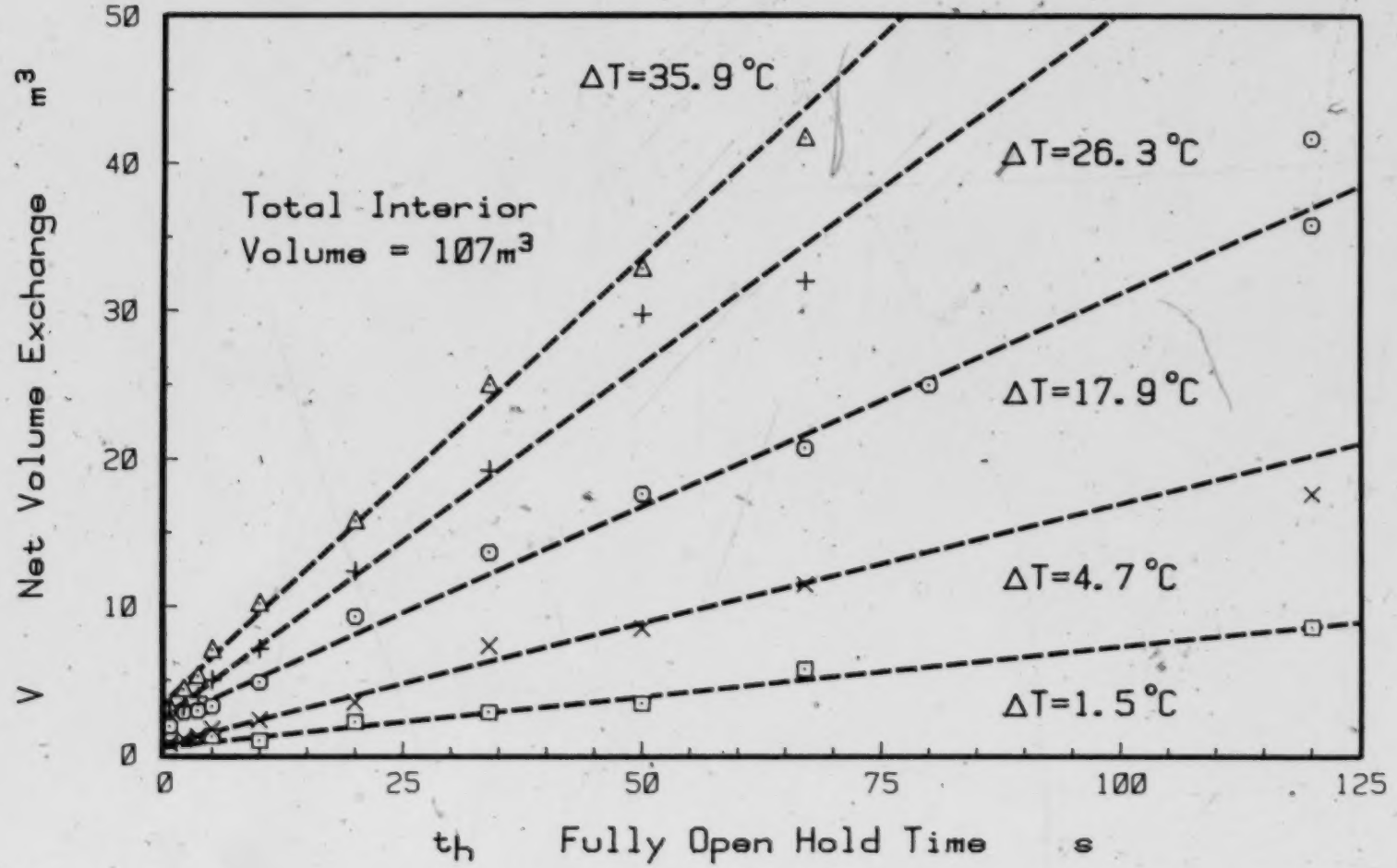

FIGURE 4-3: Typical ΔT-Sets of Exchange Volumes Correlated with Fully Open Hold Time; Full-House Geometry

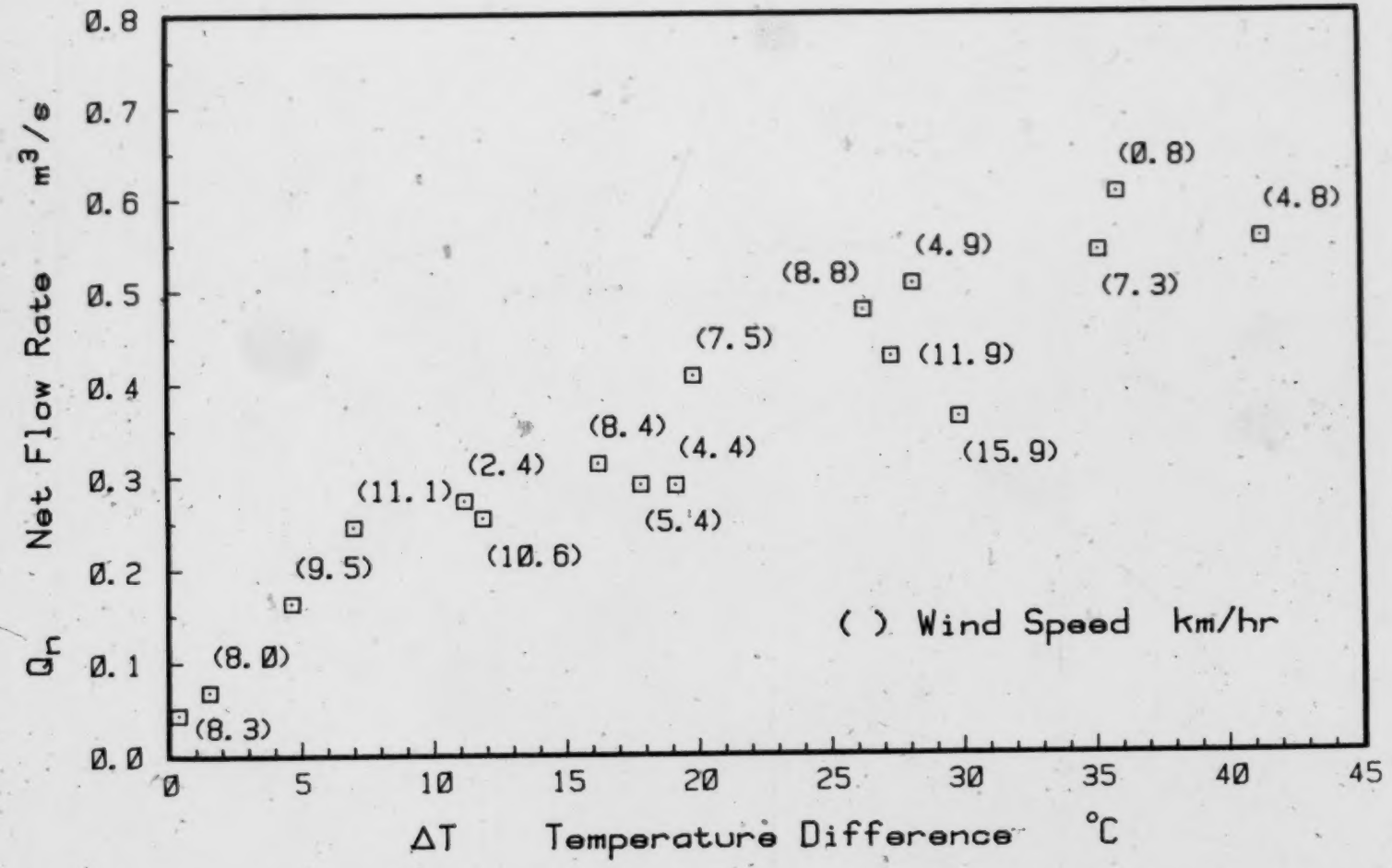

FIGURE 4-4: Variation in the Full-House Steady State Flow Rate with Temperature Difference; $T_{i,ref}=22^{o}C$

Orifice Coefficient Analysis

Having obtained the value of the steady state flow rate for each of the exchange sets, it was a simple matter to determine the orifice coefficient for each. Rearranging Equation 2-37 results in:

$$K = \frac{3\ Q_n}{W(g'H^3)^{0.5}} \qquad (2\text{-}37)$$

The orifice coefficients determined from Equation 2-37 are shown in Figures 4-5, 4-6 and 4-7 for the full-house, hall and entry geometries. Once again, the average wind speeds have been included (bracketed) for each point. There is insufficient data to conclusively comment on the effect of wind speed, but it does appear that smaller orifice coefficients are associated with larger wind speeds. To eliminate this effect, the combined data is shown in Figure 4-8 for wind speeds less than 10 km/hr.

The orifice coefficient decreases from about K=0.6 at the large temperature differences toward K=0.4 at the smaller temperature differences. It is apparent that the entry geometry orifice coefficient lies consistently below both the full-house and the hall geometry. Because of the entries small size the steady flow period was brief and thus significant uncertainty is associated with the linear regressions. For this reason, the entry geometry is not included with the hall and full-house geometries in the correlations that follow.

In Chapter 2 it was proposed that K could be approximated by a power function of either the densimetric Reynolds number or average flow Reynolds number. Using Equation 4-6 to approximate the average indoor-outdoor viscosity, the values of both the densimetric Reynolds

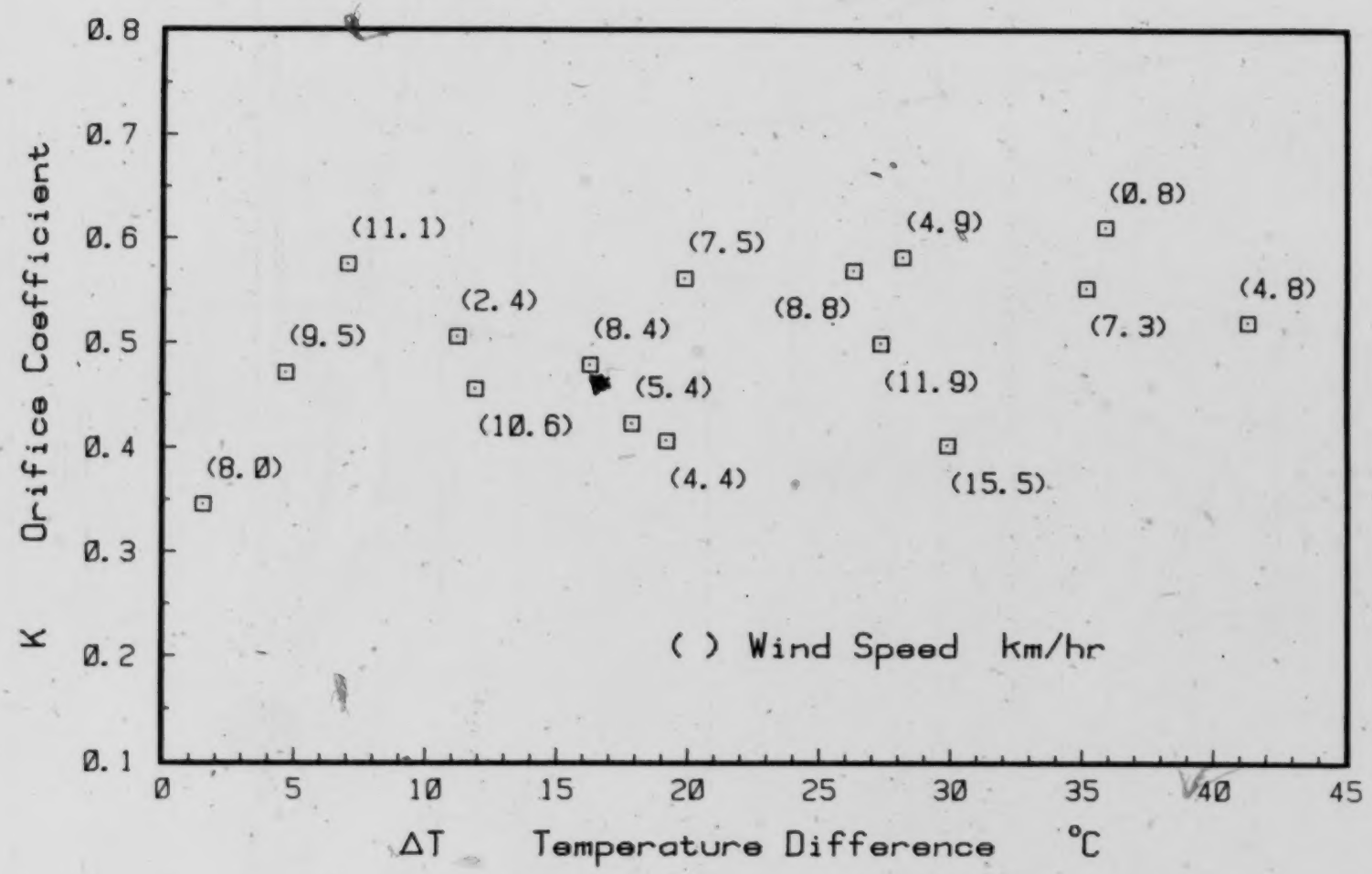

FIGURE 4-5: Variation in the Full-House Orifice Coefficient with Temperature Difference; $^{\circ}T_{i,ref}=22^{o}C$

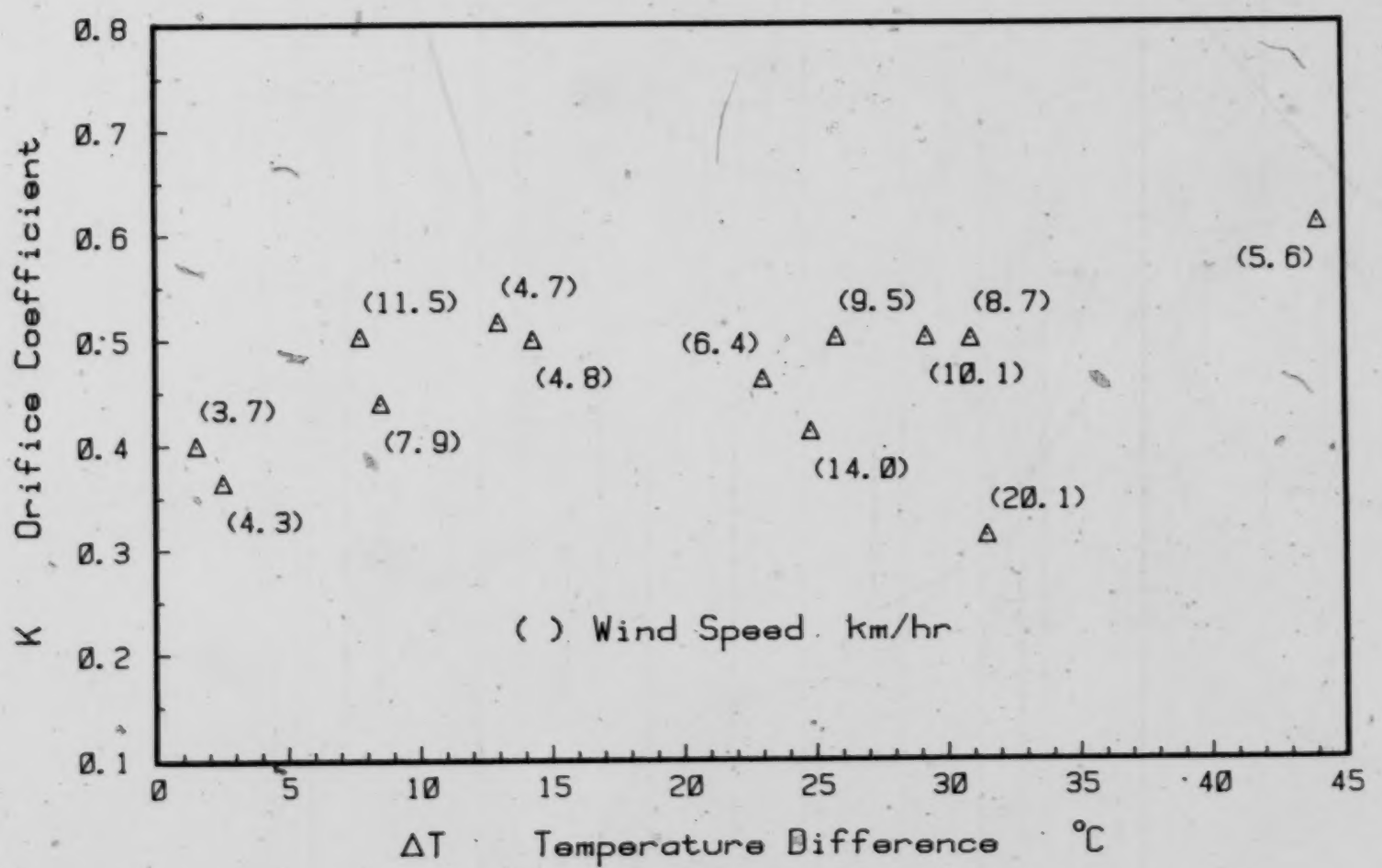

FIGURE 4-6: Variation in the Hall Orifice Coefficient with Temperature Difference; $T_{i,ref}=22^{o}C$

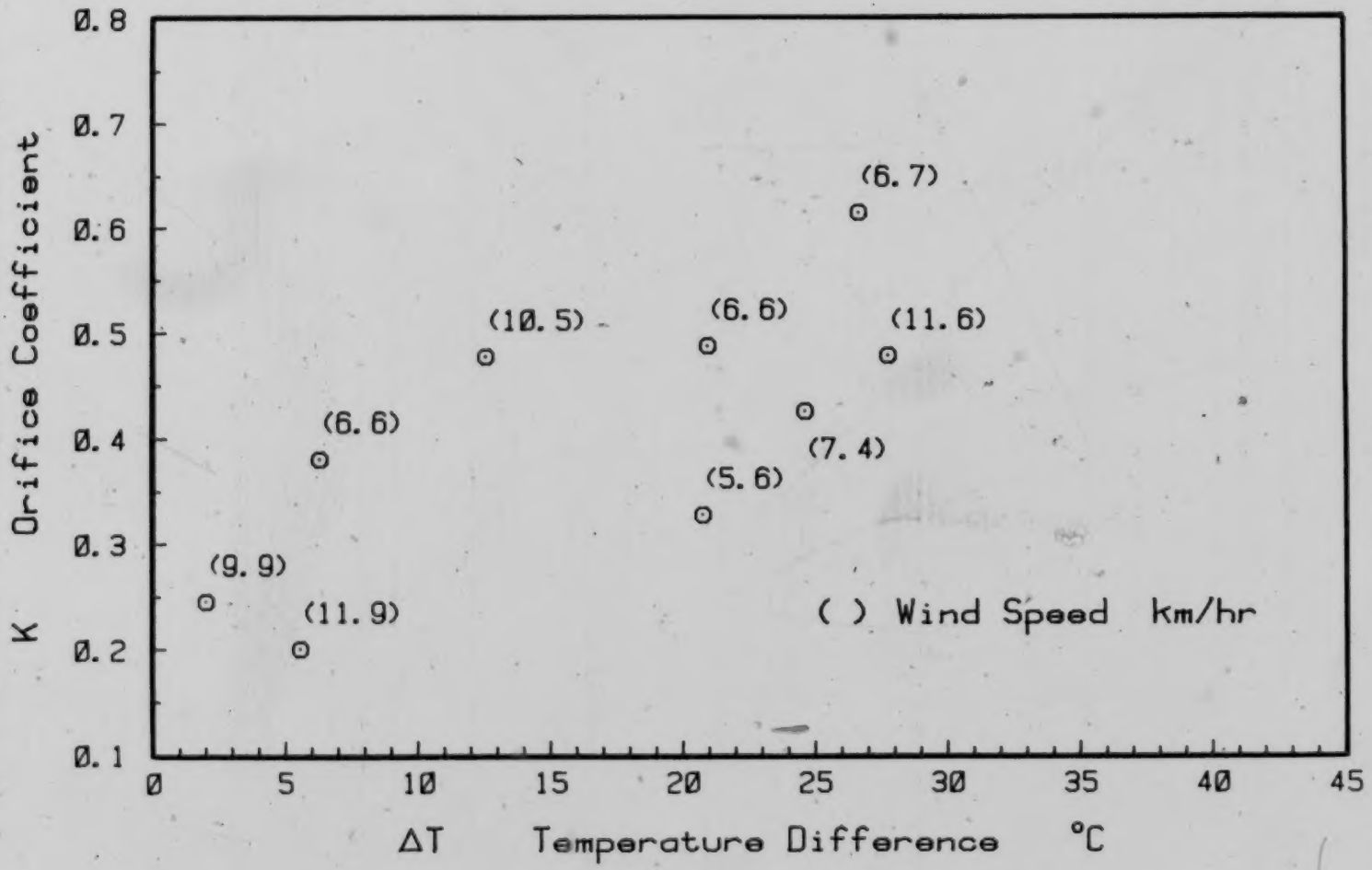

FIGURE 4-7: Variation in the Entry Orifice Coefficient with Temperature Difference; $T_{i,ref}=22^{o}C$

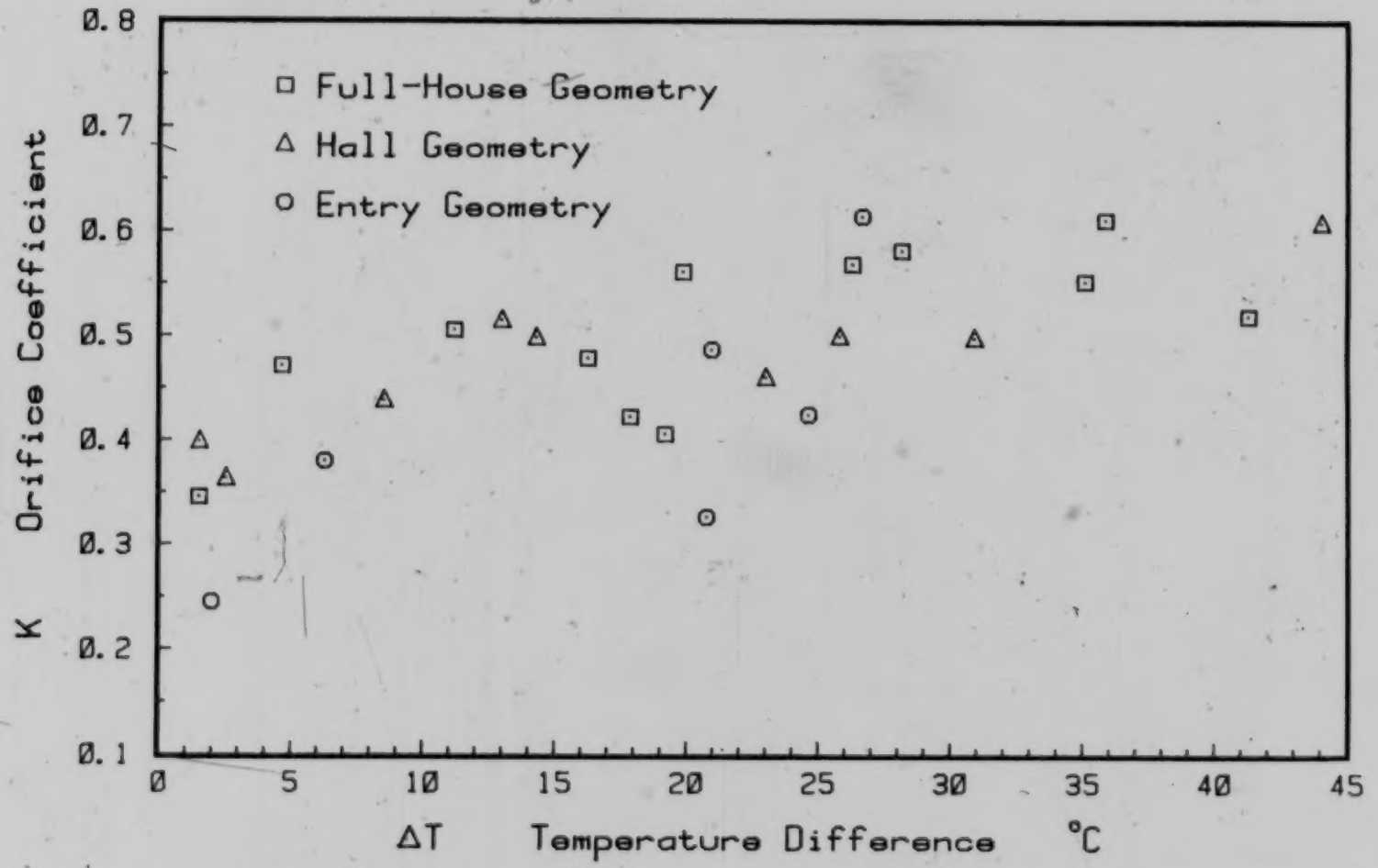

FIGURE 4-8: Orifice Coefficient Variation with Temperature Difference for Full-House, Hall and Entry Geometries, Wind Speeds less than 10 km/hr; $T_{i,ref}=22^{o}C$

number and the average flow Reynolds numbers can be determined.

$$\nu = 1.49\text{x}10^{-5} - 1.8\text{x}10^{-7}\ \Delta T \qquad (4\text{-}6)$$

Figure 4-9 illustrates the orifice coefficient plotted as a function of the flow Reynolds number. A power law relationship appears as a straight line on a log-log plot allowing a linear regression to be applied to determined the constants in the correlation. The data correlates well in this manner with an exponent of 0.17 and constant of proportionality of 0.072. As discussed in Chapter 2, correlations with densimetric Reynolds number (Equation 2-22) or temperature difference, are more useful because they depend on predetermined test conditions and not measured flow rates as with flow Reynolds number (Equation 2-27).

Figure 4-10 illustrates the orifice coefficient plotted as a function of the densimetric Reynolds number and Figure 4-11 shows the same data as a function of temperature difference. The best fit correlations for the full-house and hall data are:

$$K = 0.055\ Re_{\Delta}^{0.18}$$

$$K = 0.40 + 0.0045\ \Delta T$$

Data obtained by Fritzsche (1968) from tests on a 2.5 m high and 1.8 m wide cold room door are also shown for comparison on both figures. His orifice coefficient is also based on the net flow rate Q_n, as determined from integral temperature-velocity measurements. He determined the best fit correlation as:

$$K = 0.48 + 0.0043\ \Delta T \qquad (2.38)$$

Fritzsche's data appears to define an upper bound relative to the

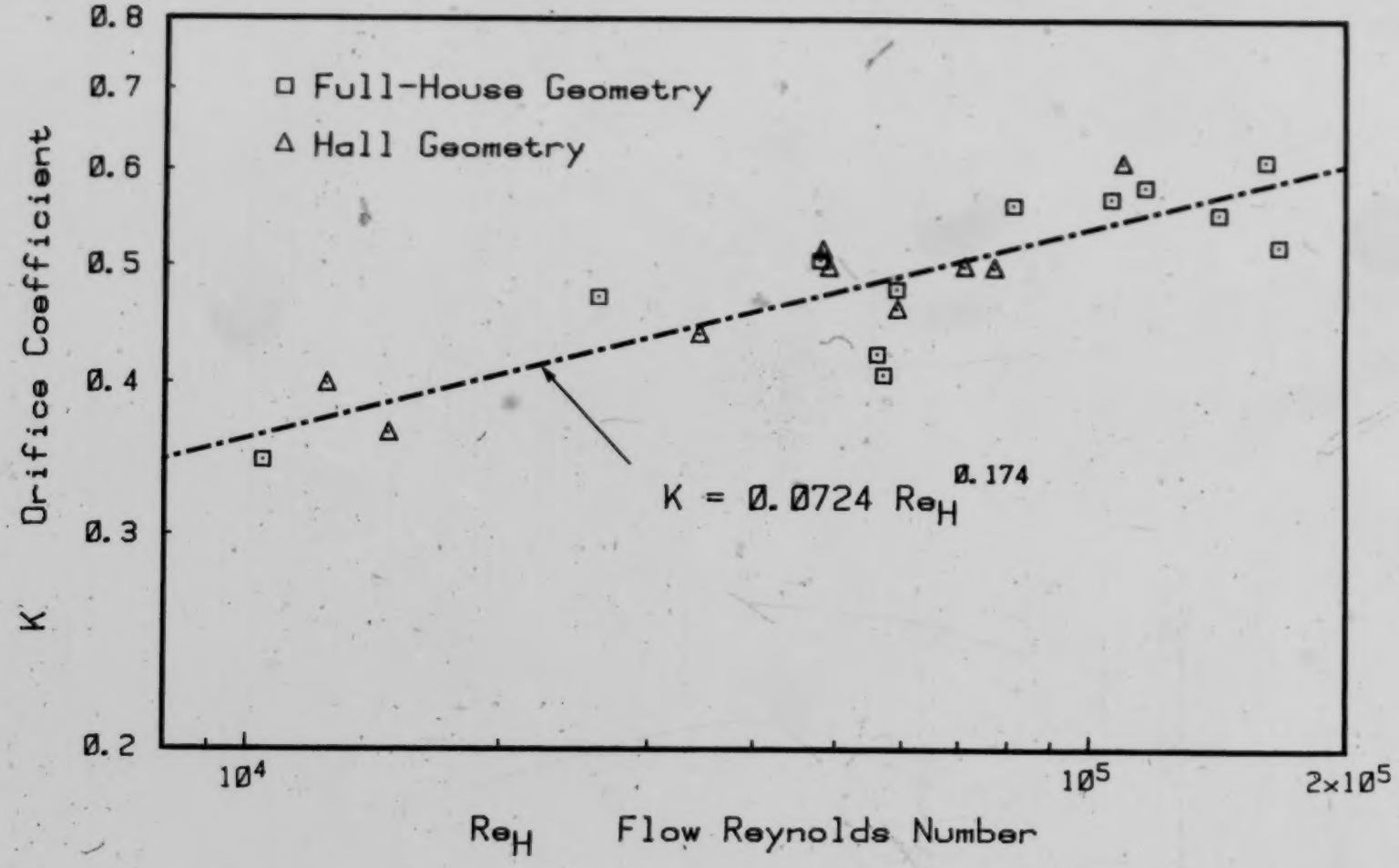

FIGURE 4-9: Orifice Coefficient Correlation with Average Flow Reynolds Number for Full-House and Hall Geometries, Wind Speeds less than 10 km/hr

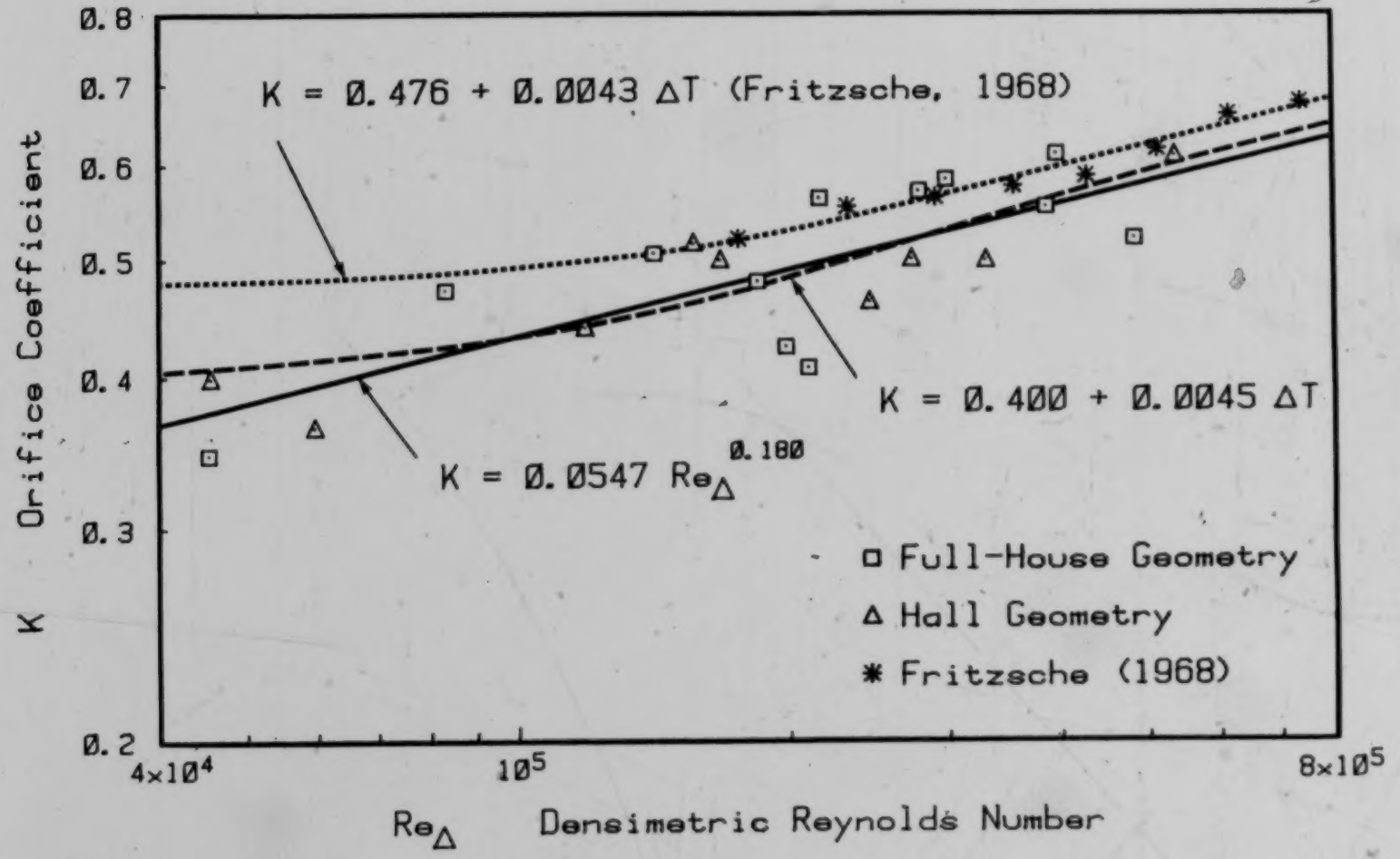

FIGURE 4-10: Orifice Coefficient Correlation with Densimetric Reynolds Number for Full-House and Hall Geometries, Wind Speeds less than 10 km/hr; Cold Room Data by Fritzsche(1968)

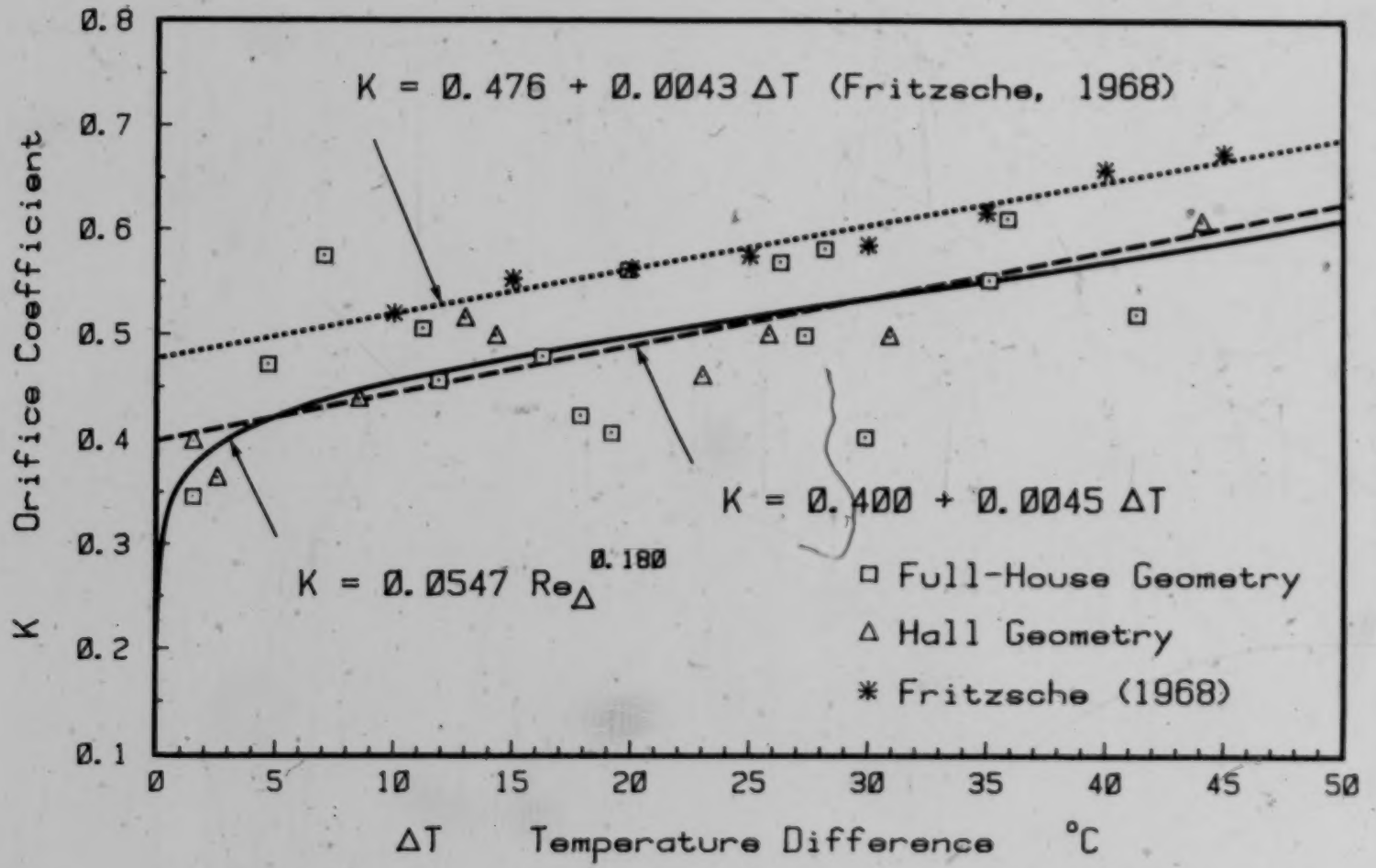

FIGURE 4-11: Orifice Coefficient Correlation with Temperature Difference for Full-House and Hall Geometries, Wind Speeds less than 10 km/hr, $T_{i,ref}$=22°C; Cold Room Data by Fritzsche(1968)

house data, with nearly the same slope. Fritzsche's data may lie higher than the house data because of a higher discharge coefficient arising from geometry differences, or due to a smaller amount of interfacial mixing relative to the gross flow rate. A smaller level of interfacial mixing could result from either lower turbulence levels or from the effects of his 20% higher door as illustrated in Equation 2-32.

It is very important to note that both Fritzsche's data and the data presented here for orifice coefficients are based on the net flow rate Q_n, and thus include the effects of interfacial mixing. Shaw (1976) on the other hand, examined gross flow rates from velocity profiles only and as a result found the discharge coefficient as a constant 0.62 for his test range from 3 to 10°C, (below 3°C circulation effects increased K as discussed in Chapter 2).

These observations lead to the idea that the discharge coefficient is nearly constant at 0.6 and the mixing coefficient varies with temperature difference. The possibility that interfacial mixing is responsible for the overall variation in orifice coefficient will now be examined.

Temperature Profiles and Interfacial Mixing

The orifice coefficient represents the combined effect of the discharge coefficient and the mixing coefficient as $K=C_d(1-C_m)$. The coefficients cannot be determined independently from experimental results, but it is possible to examine the temperature profiles to gain an insight into the variation of the mixing coefficient. As suggested in Chapter 2, the shape of these profiles indicate the amount of interfacial mixing which is taking place.

Figure 4-12 illustrates several normalized temperature profiles obtained from the vertical thermocouple array for varying temperature differences. The 19 thermocouples were monitored sequentially at a rate of 13 samples a second, resulting in each point being read every 1.5 seconds. A 15 second average of these readings will be examined for a period when steady state flow was fully established. Many profiles were obtained, but the three shown in Figure 4-12 are sufficient to illustrate the important points.

Beginning with the profile that is shown for the 28.6°C temperature difference, it is apparent that the incoming air enters in a relatively unmixed condition. This is indicated by the nearly constant normalized temperature ratio across the lower half of the door, $(T(h)-T_o)/(T_i-T_o)=0$. The upper portion of the profile is not symmetric with the lower profile. As discussed in Chapter 2, this skewed profile can only result from interior interfacial mixing as illustrated in Figure 2-4.

Observing the profiles associated with the smaller temperature differences, it is apparent that the mixing region is thicker. In fact, for the $\Delta T=5.8^{o}C$ profile, the entire profile indicates some degree of mixing at all levels within the door opening. It is interesting that the outflow profile does not change substantially (upper half), but the inflow profile becomes much less blunt and is shifted well to the right. This suggests that exterior mixing becomes more important at the smaller temperature differences. The three sample profiles shown were all obtained during tests which had wind speeds of less than 10 km/hr. It is reasonable to suspect that larger wind speeds would further enhanced mixing.

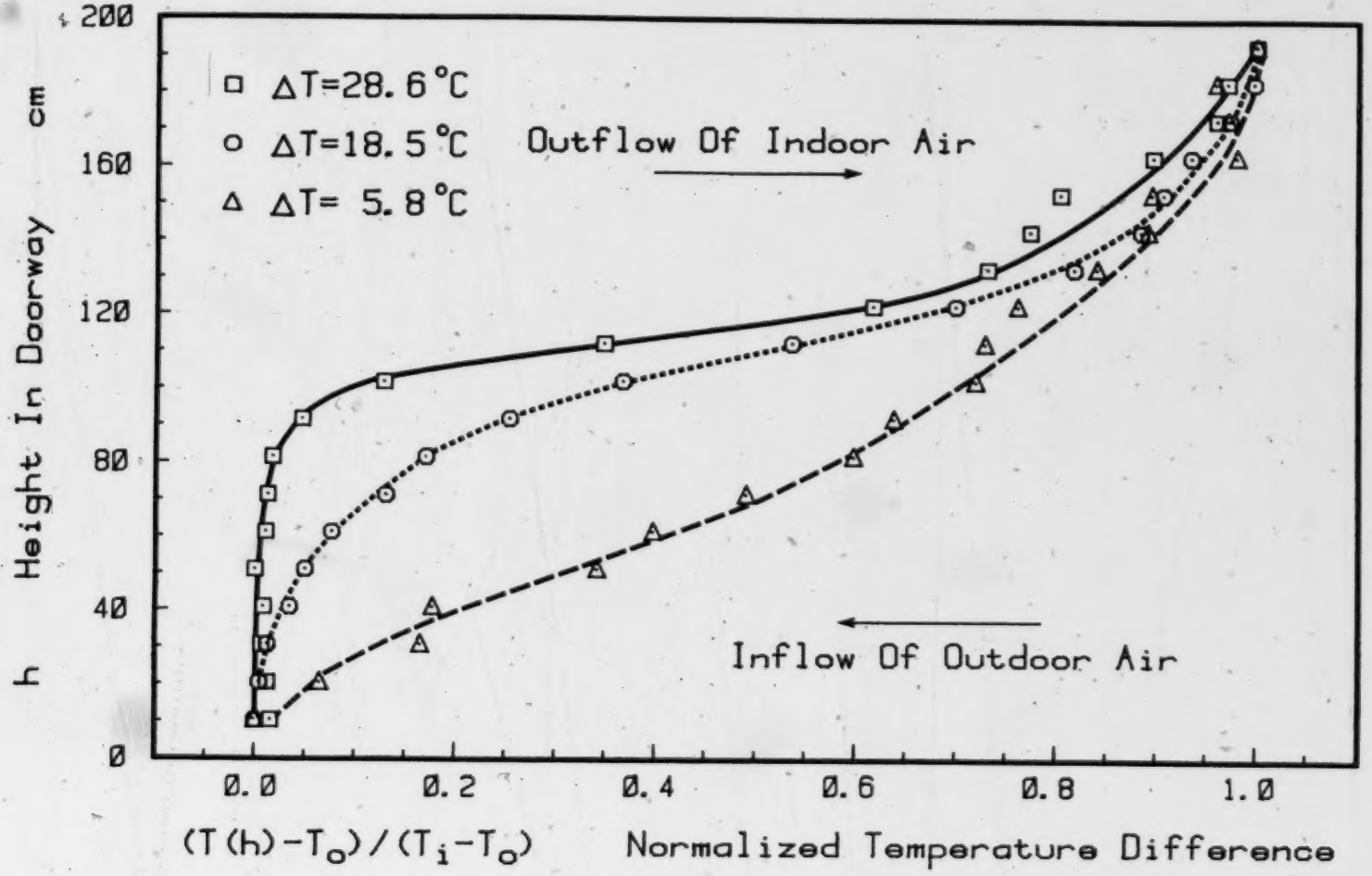

FIGURE 4-12: Normalized Temperature Profiles on the Doorway Vertical Centerline for Full-House Geometry

Based on these observations, it appears that increased interfacial mixing accounts at least in part, for the decreasing orifice coefficient at small temperature differences. If all the variation in K was due to C_m, and if C_m was near zero at the largest temperature differences, that would suggest that C_d=0.6 and that C_m varies from zero at ΔT=40°C to approximately 0.35 at small values of ΔT.

Additional support for this theory will be presented in the small scale model analysis section. It will be shown that the model flow lies below the critical stability value with very little mixing occurring, as supported by profile measurements. The orifice coefficient will be found to be constant at K=0.6 for these conditions, where C_d=0.6 and C_m=0.

Air Exchange During Door Opening and Closing Periods

In Chapter 2 it was proposed that the air exchange during the opening and closing periods could be approximated as the fully open flow rate for a modified period of time t_{eq}, as given in Equation 2-43.

$$V_o = V_c = Q_n \, t_{eq} \qquad (2\text{-}43)$$

Using the tracer gas technique it was not possible to separate the air exchange associate with the opening and closing periods. If the fully open hold time is set to zero, then the expected buoyancy-driven exchange is given by:

$$V_{B,(t_h=0)} = Q_n \, 2t_{eq} \qquad (4\text{-}7)$$

From Figure 4-3 the experimental value of $V_{(t_h=0)}$ can be determined as the intercept on the vertical axis for each ΔT-Set of exchange data.

This method reduces the error associated individual exchange tests. For each ΔT-Set of data then, the fully open flow rate was determined in the last section from the slope of the least squares curve fit and the total zero hold time exchange volume was determined from the intercept. The equivalent time method can now be tested using the ratio of total exchange to predicted exchange as given by Equation 4-8. The full scale opening and closing time varied slightly from 3.5 s to 4.0 s and thus $t_{eq} \simeq 2.4$ s.

$$\frac{\text{Intercept}(=V)}{\text{Slope}(=Q_n) * 2t_{eq}} \qquad (4\text{-}8)$$

Figure 4-13 illustrates the ratio of actual exchange to buoyancy prediction given by Equation 4-8, as a function of temperature difference. Scatter around a ratio of 1.0 indicates that the varying buoyancy flow rate caused by the changing orifice size can be accurately estimated using the equivalent time concept. This also confirms that inertial startup and orifice coefficient variation can be neglected.

Several data points for temperature differences between zero and 5°C lie much higher than all of the others. The source of the extra exchange is the inertial pumping contribution. The important observation is that inertial pumping is not significant above 4 or 5°C for a door swing speed of approximately 3.75 s.

Pumping Exchange

Figure 4-13 demonstrates that inertial pumping is only important for small temperature differences. Figure 4-14 illustrates the total exchange volumes from individual tests as a function of temperature

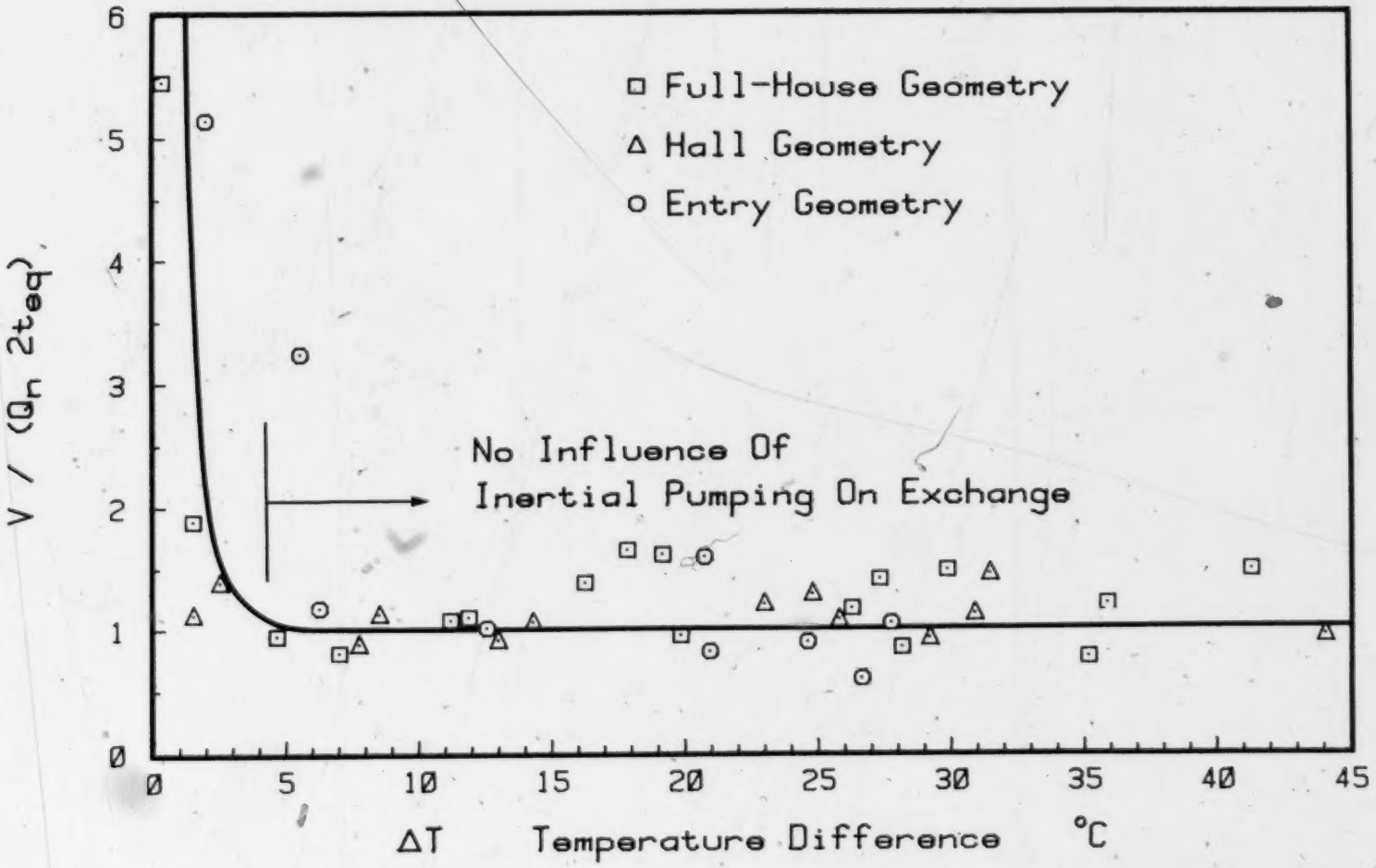

FIGURE 4-13: Ratio of Total Exchange to Buoyancy Predicted Exchange Using Equivalent Time and Zero Hold Time

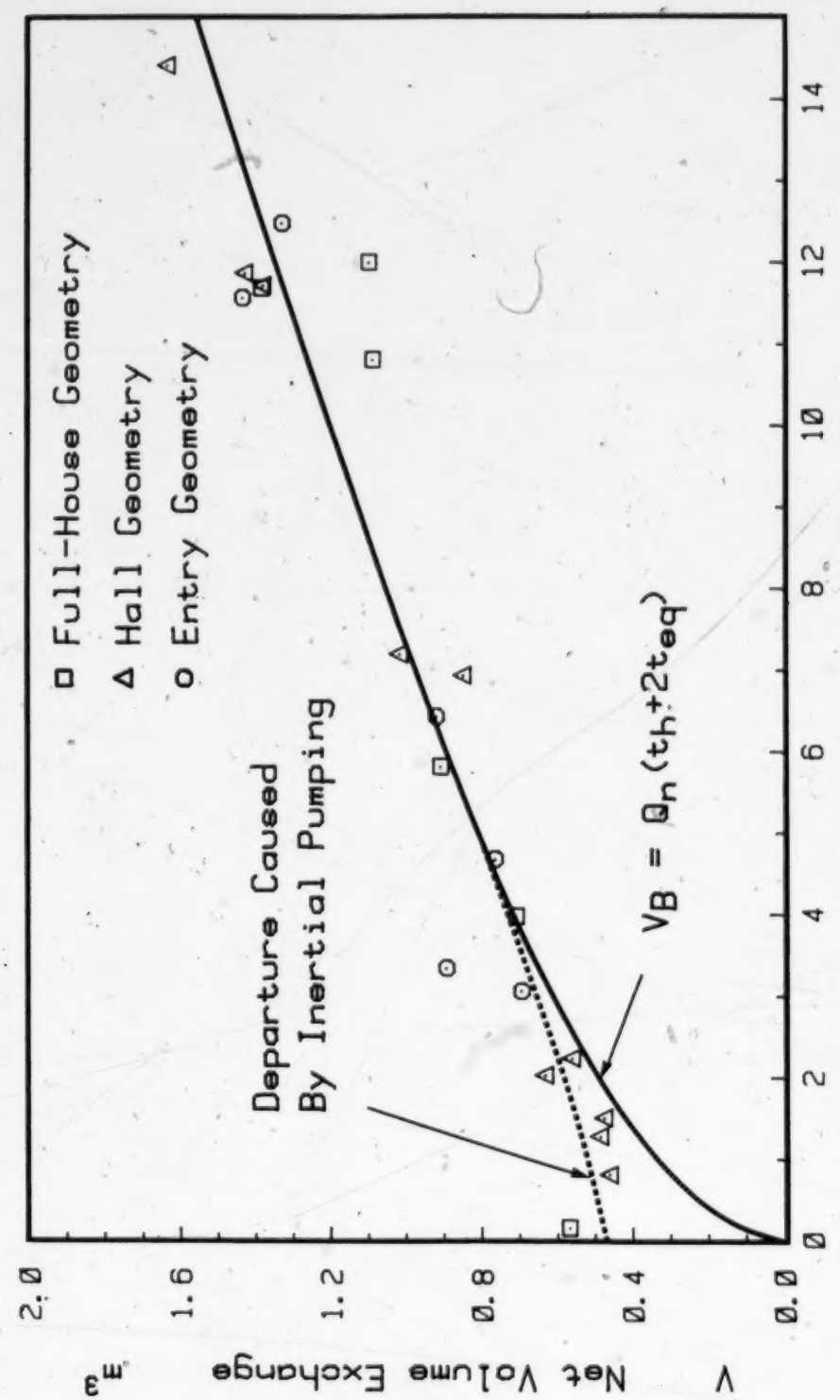

FIGURE 4-14: Correlation of Short Duration Exchanges with Temperature Difference, $T_{i,ref}=22^{o}C$; Swing Time=3.75 s, Hold Time=0.5 s

difference for the shortest hold times tested in full scale, t_h=0.5 s. The predicted buoyancy exchange curve is also shown for this swing speed from Equation 2-44. The buoyancy prediction is accurate to approximately 4^oC, below which, the data and the prediction curve diverge. The difference between the total exchange and the buoyancy predicted exchange was defined in Chapter 2 as the residual exchange, V_P. As the temperature difference approaches zero, the value of V_P approaches $V_{Po} \simeq 0.45\ m^3$.

The critical fractional density difference is easier to identify if the ratio of actual volume exchange to buoyancy prediction V/V_B, is plotted against fractional density difference as shown in Figure 4-15. The critical fractional density difference for this swing time of 3.75 s is identified as approximately 0.012 corresponding to $\Delta T \simeq 4^oC$. This is the temperature at which pumping contribution becomes detectable. From Figure 4-15 it is possible to determine the temperature at which $V_P=V_B$ by noting that $V/V_B=2$, at the same point. This value corresponds to a fractional density difference of approximately 0.002 or a temperature difference of $\Delta T \simeq 0.5^oC$. This clearly illustrates that the contribution of pumping exchange to energy losses is negligible.

There is insufficient full scale data to determine a functional form for V_P between $\bar{\Delta}=0$ and $\bar{\Delta}_{cr}$. Also, because only one swing speed was tested, it is not possible to examine the relationship between the values of V_{Po}, $\bar{\Delta}_{cr}$ and swing speed. These points will be pursued further in the modelling section.

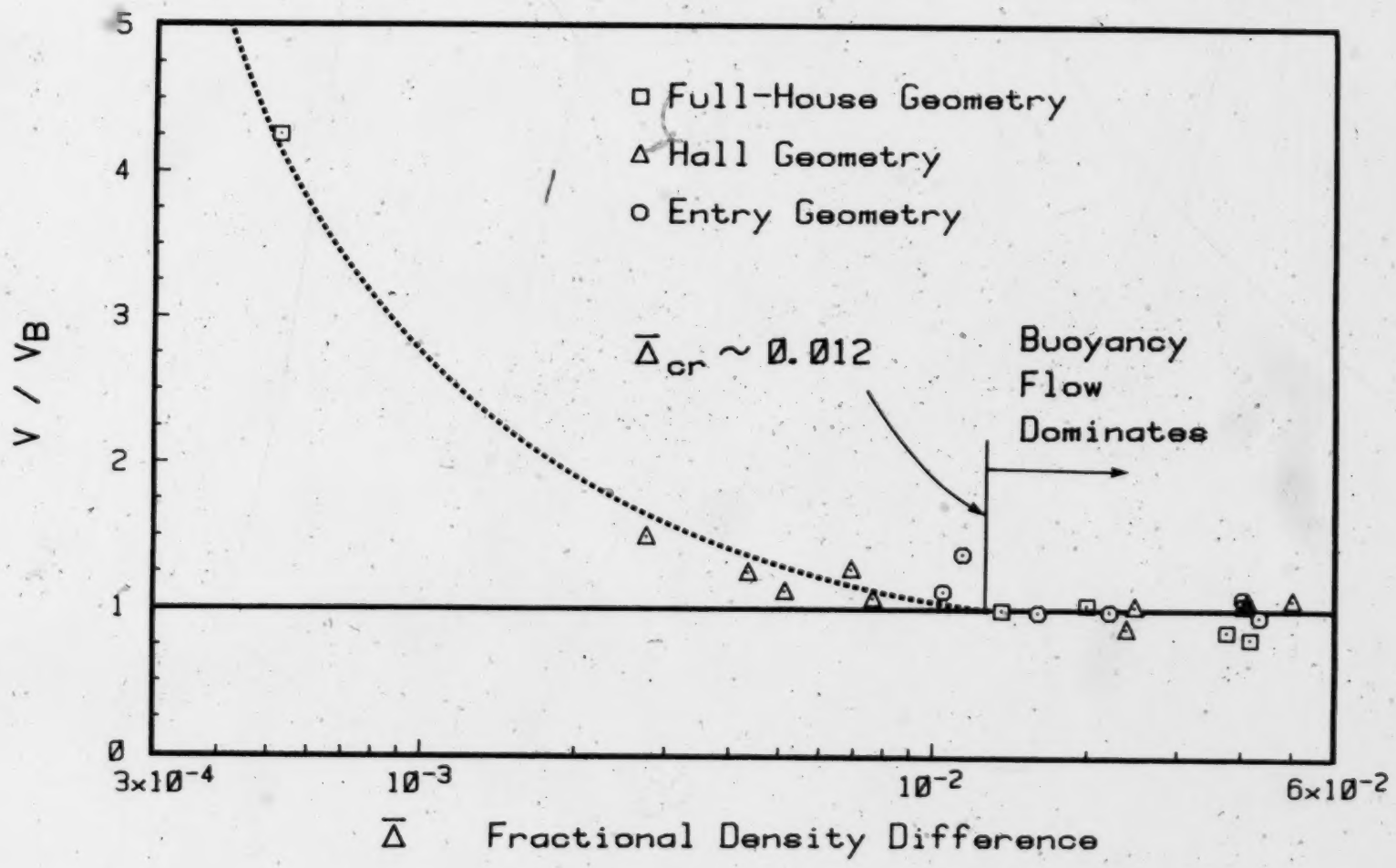

FIGURE 4-15: Critical Fractional Density Difference Determined from the Ratio of Total Exchange to Buoyancy Predicted Exchange; Swing Time=3.75 s, Hold Time=0.5 s

Cold Front Velocity

A theoretical expression was developed in Chapter 2 which allows the calculation of the gravity current frontal velocity for one dimensional flow. It was suggested in Chapter 2 that it is the return of the reflected cold gravity wave to the entry that sets the time at which departure from steady state flow begins. The first step in evaluating these ideas is to compare the experimental velocity results to the theoretical expression for frontal velocity.

The progress of the cold front down the length of the hall was measured using the horizontal thermocouple technique described in Chapter 3. These experiments determined the position of the cold front in the hall as a function of time. Applying a linear regression to the póstion-time data allows the average frontal velocity to be determined. Figure 4-16 shows 5 such sets of experimental results including the best fit linear regressions from which the frontal velocity is determined. A total of 31 such sets of data were taken over the six month experimental period providing a range of temperature differences from 0 to 45°C.

This set of frontal velocities will be compared to the theoretical expression given by:

$$U_f = Fr_f^{2/3} (gH)^{0.5} \left[\frac{K W \bar{\Delta}^{1.5}}{3 W_f} \right]^{1/3} \qquad (2\text{-}47)$$

Substituting the experimental parameters into Equation 2-47 and assuming a value of K=0.6 results in:

$$U_f = Fr_f \; 1.22 \; \bar{\Delta}^{0.5} \qquad (4\text{-}9)$$

Figure 4-17 illustrates the frontal velocity data from the

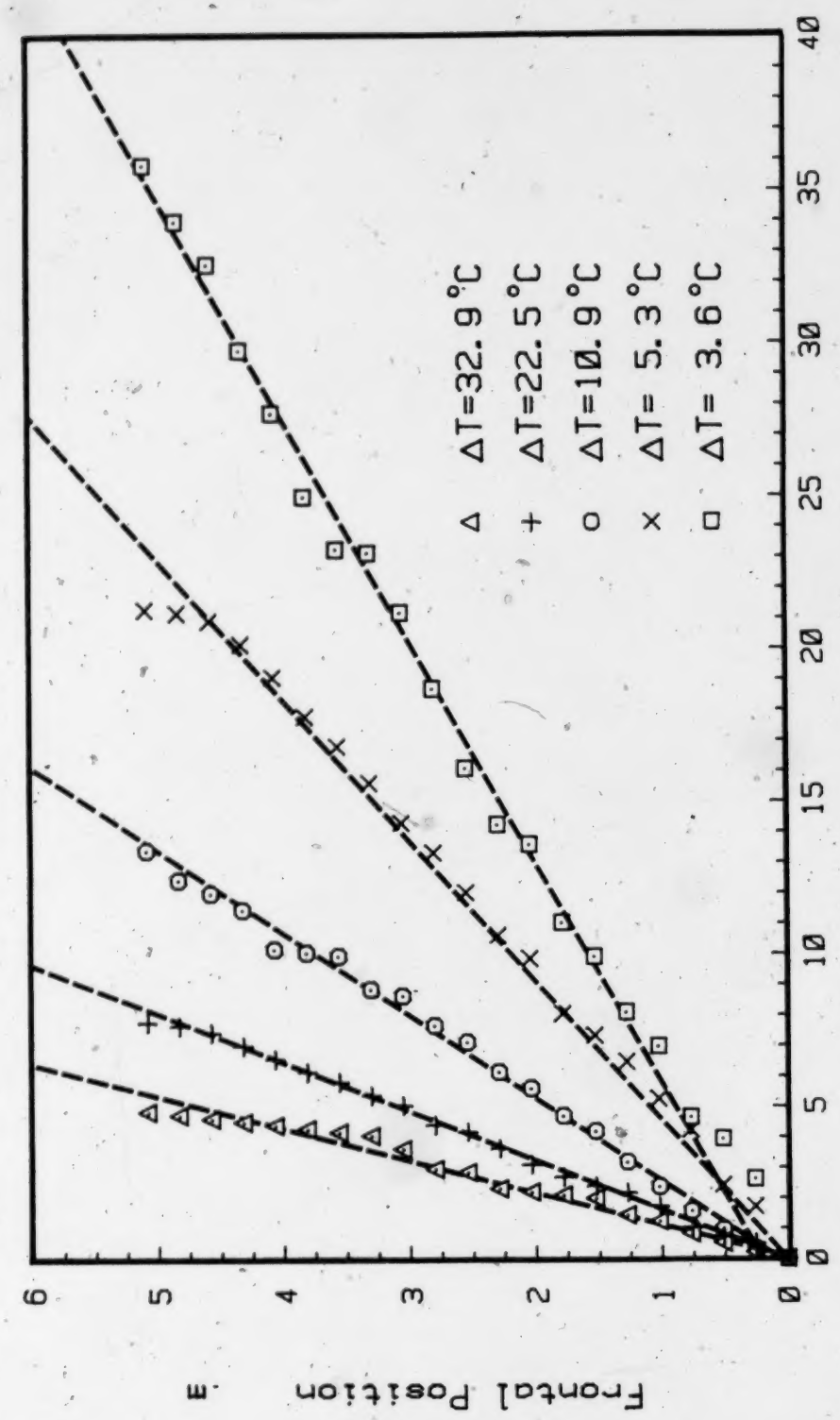

FIGURE 4-16: Typical Frontal Position Curves from Hall Thermocouple Experiments, Time and Position Relative to First Thermocouple

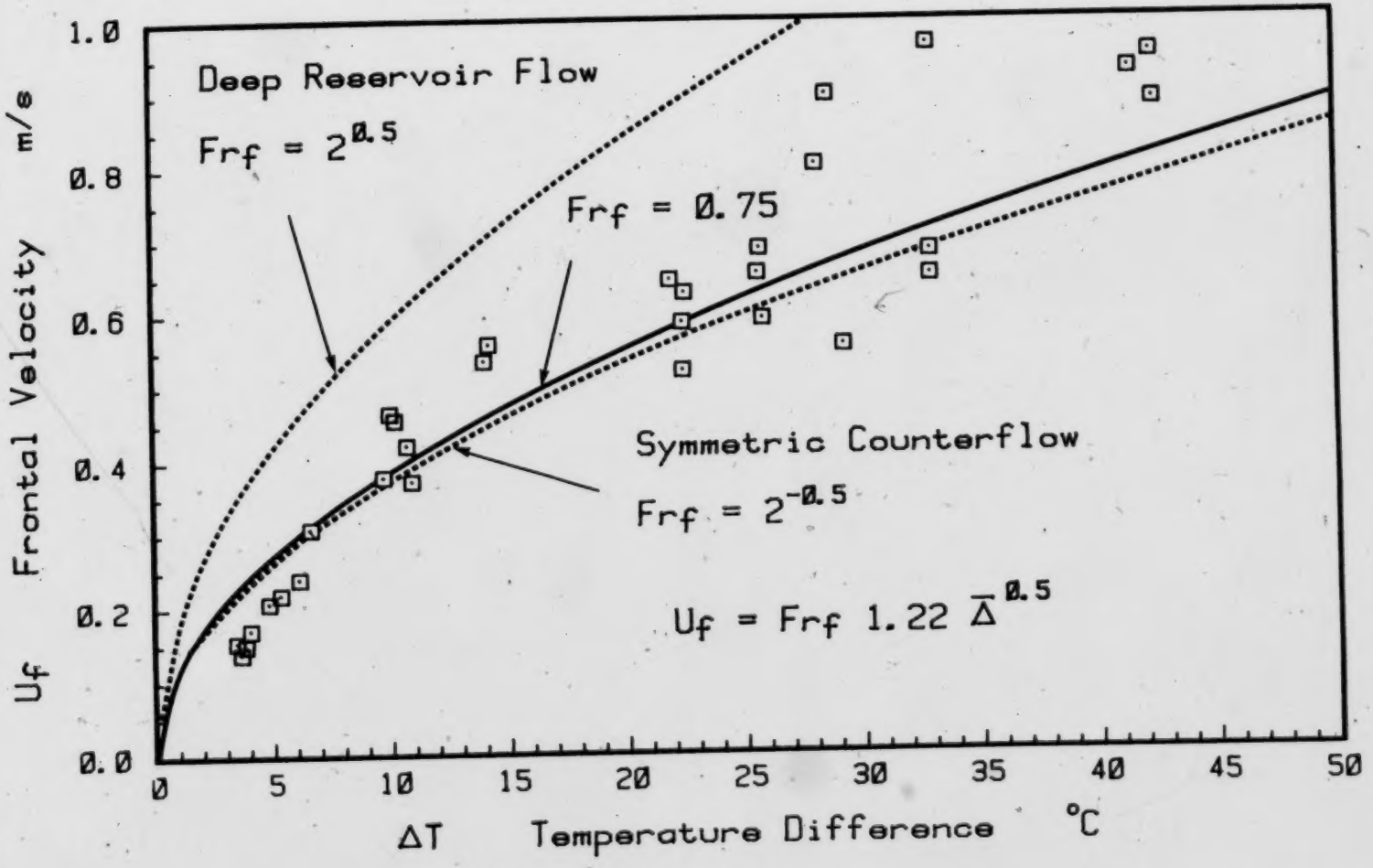

FIGURE 4-17: Hall Frontal Velocity Correlation with Temperature Difference, $T_{i,ref}=22^{o}C$

thermocouple experiments as a function of temperature difference. Equation 4-9 is shown for the theoretical maximum and minimum frontal Froude numbers. A frontal Froude number of $2^{0.5}$ is expected if the gravity current is proceeding beneath a stagnant layer much thicker than itself and a value of $2^{-0.5}$ is expected if symmetric counterflow is occurring. Although the functional form appears to be inaccurate for the very small and the very large temperature differences, in the central region a frontal Froude number of approximately 0.75 provides the best fit. This value is reasonable for hall flow which is expected to be near the extreme of symmetric counterflow. The fact that the ceiling is slightly higher than the door would cause the outflow layer to be a little thicker than the inflow layer, this may account for a Froude number being larger than the counterflow limit of 0.71.

Prediction of Critical Departure Time

Equation 2-48 was developed in Chapter 2 for application in a long hall to predict the departure time on the basis of the time required for the gravity current to travel the length of the hall, reflect off the end wall and return to the opening at frontal velocity U_f.

$$t_{cr} = 2\ L_f\ /\ U_f \qquad (2\text{-}48)$$

Combining Equation 4-9 with 2-48 and setting L_f=7.1 m and Fr_f=0.75 results in the following approximation for the critical time of the hall geometry.

$$t_{cr}\,\bar{\Delta}^{0.5} = 8.7 \qquad (4\text{-}10)$$

This expression indicates that the wave return time is related to the

square root of the fractional density difference.

Critical Departure Time from Experimental Data

The theoretical critical departure time given by Equation 4-10 assumes that the gravity current starts instantaneously at speed U_f, with an orifice width of W. In practice, the opening door will restrict the initial motion of the current, reducing its progress. Comparison with full scale results is further complicated by the fact that only complete door cycle exchanges were measured. For this reason, the critical time in Equation 4-10 will be compared to t_h+2t_{eq}. Noting that $t_h >> t_{eq}$ suggests that opening and closing effects should not be to important for the hall geometry.

Combining Equations 2-37 and 2-44:

$$V_B = K \left[\frac{gW^2H^3}{9}\right]^{0.5} \bar{\Delta}^{-0.5} (t_h+2t_{eq}) \qquad (4\text{-}11)$$

Noting that if the total volume exchanged is plotted against $K\bar{\Delta}^{-0.5}(t_h+2t_{eq})$, then data for all temperature differences will fall on a line of slope $(gW^2H^3/9)^{0.5}$ = constant.

Figure 4-18 shows measured exchange volumes for the hall geometry plotted in this manner for the full range of hold times and fractional density differences. A distinct departure point is clearly discernable. Recalling the theoretical expression for critical departure time, based on frontal velocity, and noting that the average orifice coefficient K, is approximately 0.55 results in:

$$t_{cr}\,\bar{\Delta}^{-0.5}\,K = 8.7 \times 0.55 = 4.8 \text{ s}$$

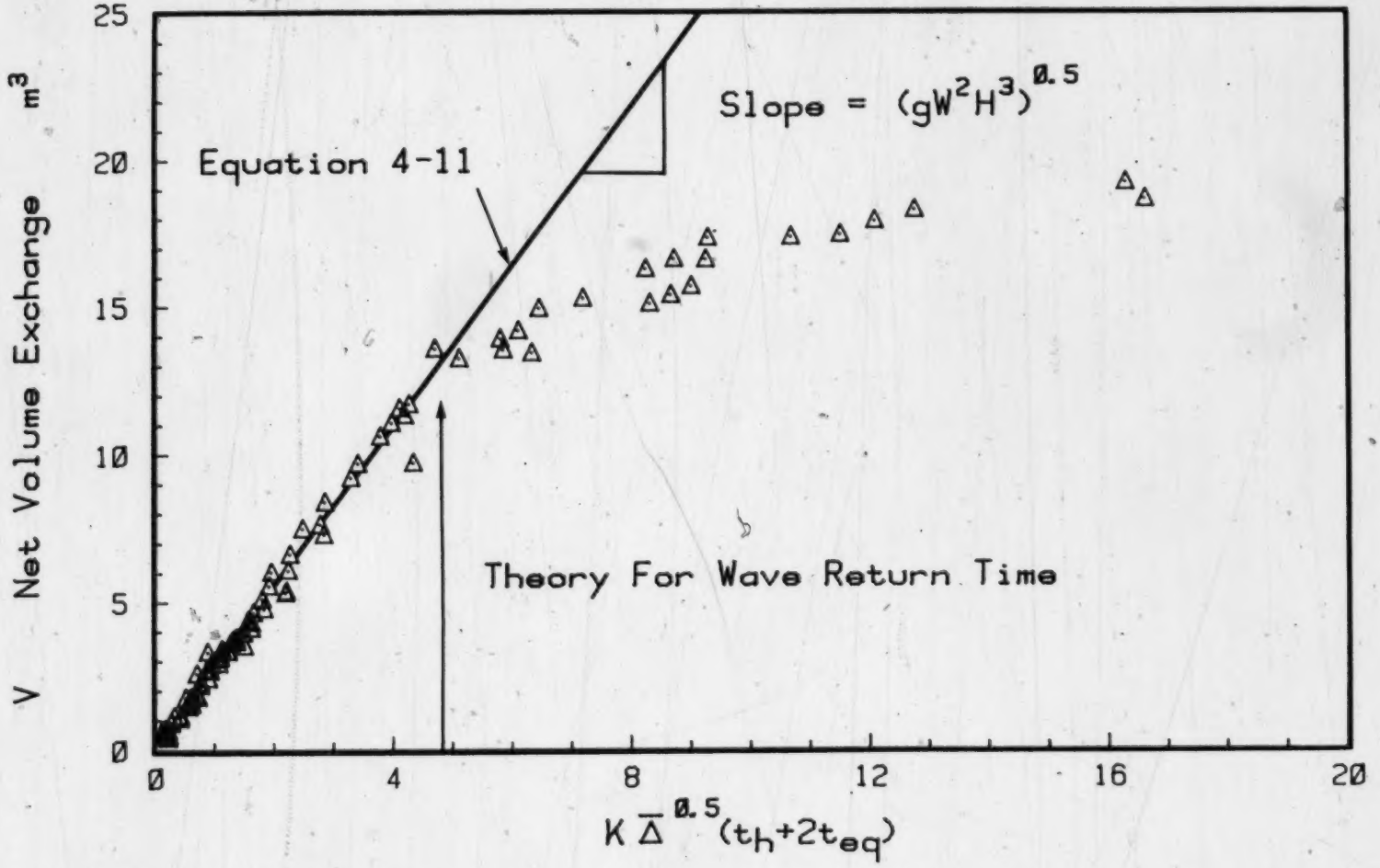

FIGURE 4-18: Critical Departure Time from Steady Flow for the Hall Geometry

This value is shown on Figure 4-18. It accurately defines the experimental departure point, confirming the relationship between wave return time and steady flow departure time.

Extending this approach to more complicated geometries is difficult. For example, if a door enters into the middle of a room, the frontal velocity and the thickness of the radially spreading flow will depend on the distance the front has traveled into the room. As the gravity wave reflects off various interior surfaces, different sections return to the entry at different times, tending to smear out the departure point. For this reason, it is difficult to arrive at an appropriate frontal velocity or characteristic length to use in conjunction with Equation 2-48. Rather than trying to develop a characteristic length based on geometry considerations, it is more convenient and simpler to consider the concept of normalized critical departure volume.

Critical Departure Volume

In Chapter 2 it was suggested that the percentage volume exchanged at the critical departure point is similar for all interiors irrespective of the shape, volume, flow rate, or fractional density difference. If an estimate of the orifice coefficient (and thus the flow rate) can be made, then the departure time can be found. It was proposed that the important characteristic volume is the air volume beneath a horizontal plane level with the top of the door, V_H.

The entry geometry data is plotted in Figure 4-19 in the same manner as the hall data in Figure 4-18. More scatter in the data is apparent for this geometry due to the smaller volumes measured. The departure volume appears to be between 3.5 and 4.0 m^3. Similarly, Figure 4-20

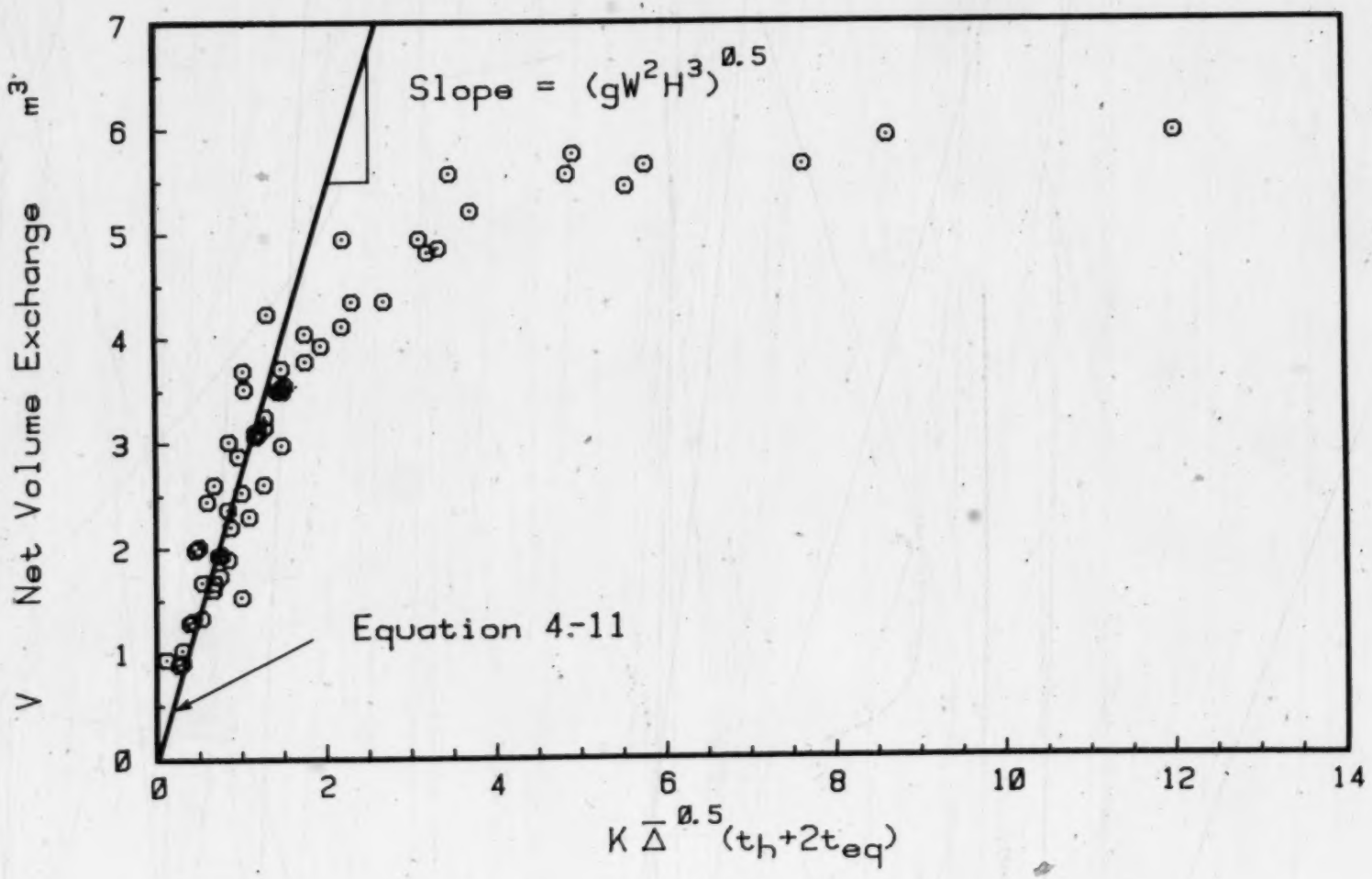

FIGURE 4-19: Critical Departure Time from Steady Flow for the Entry Geometry

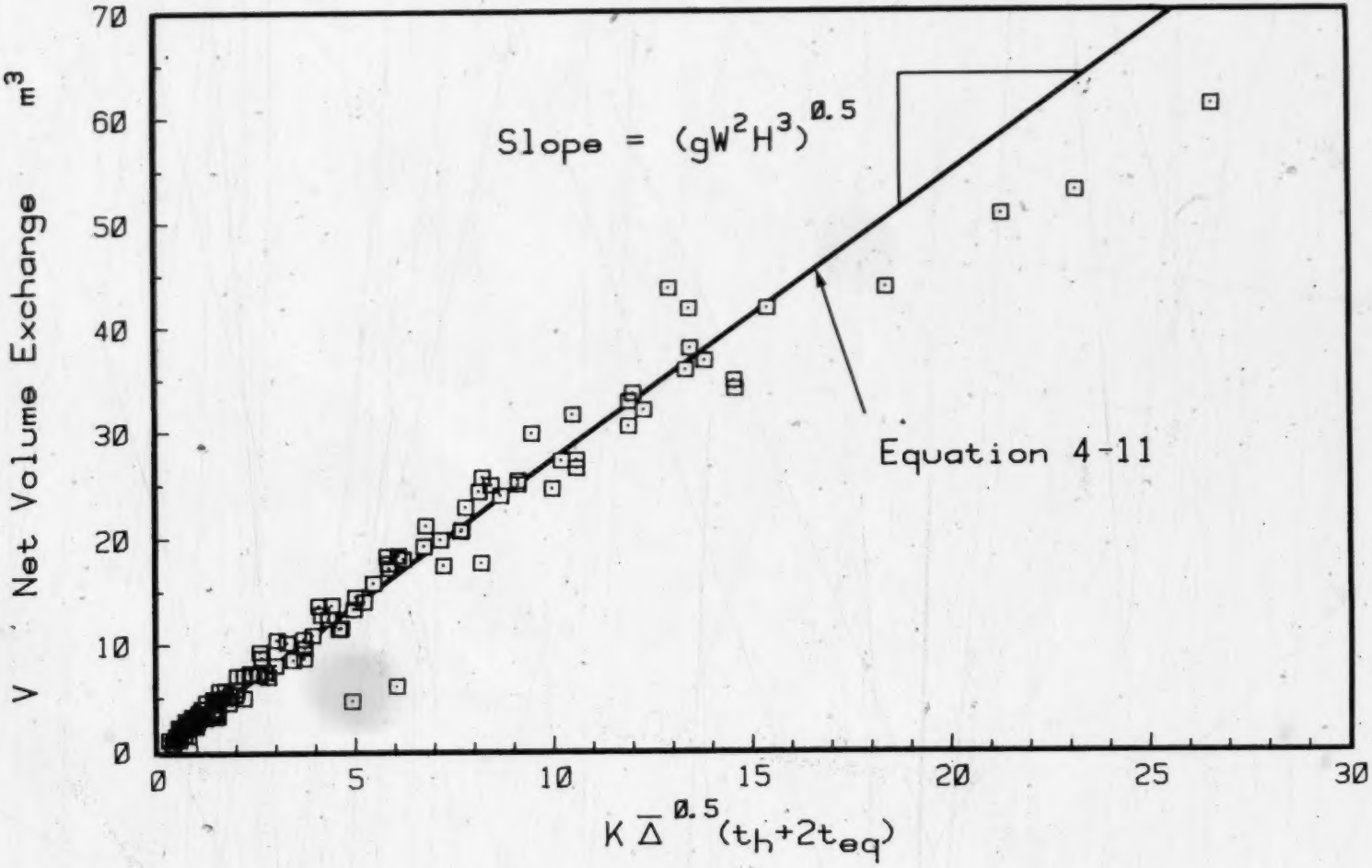

FIGURE 4-20: Critical Departure Time from Steady Flow for the Full-House Geometry

illustrates the full-house results. Unfortunately the exchange experiments were not of sufficient duration to conclusively describe the departure region. Based on the limited number of points present, departure appears to occurs at about 40 to 50 m^3.

Normalizing these volumes with the value of V_H given in Table 3-1 results in the following critical exchange ratios.

Hall	0.67 - 0.73
Entry	0.63 - 0.72
Full-house	0.44 - 0.55

To properly understand the significance of these results it is necessary to consider the effect of interior geometry on the critical departure point. The hall geometry shown in Figure 4-18 exhibits a well defined inflection point with an immediate reduction in flow rate (slope) of 10 to 20%. In this situation, the frontal wave reflects off the end hallway wall and returns uniformly to the entrance causing an abrupt reduction in flow rate. More complicated geometries will send back numerous reflected waves, the strength and frequency of which determine how smooth or how abrupt the flow reduction is. Figure 4-21 illustrates these ideas graphically. Critical departure may begin sooner for the full-house geometry because of the return of an intermediate reflected wave.

Decreasing Exchange Rate

For practical applications, it is reasonable to ignore the abrupt change in slope that occurs for some geometries (like the long hall) and use a general form which smoothly departs from the linear region at a

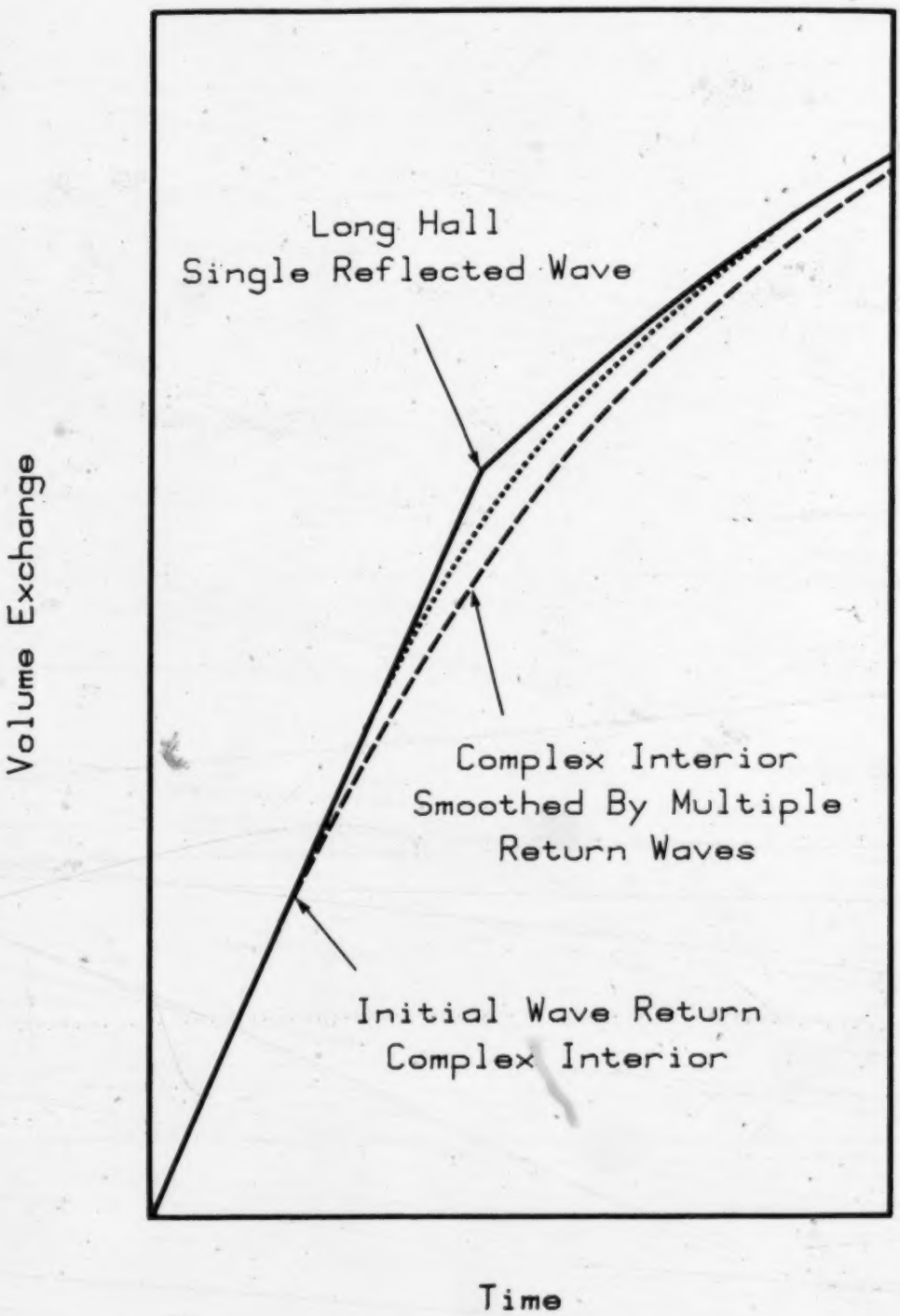

FIGURE 4-21: Single Reflected Wave Departure Compared to Multiple Reflected Wave Departure

lower value. In Chapter 2 an exponential function was proposed that is tangential at E_{cr} and asymptotically approaches E_{max}.

$$E = E_{max}\,(1-e^{-A(t-B)}) \qquad (2\text{-}52)$$

where

$$t > t_{eq}+t_s$$

$$A = \frac{Q_n/V_H}{E_{max} - E_{cr}}$$

$$B = \frac{E_{cr}}{Q_n/V_H} + \frac{\ln(1 - E_{cr}/E_{max})}{A}$$

Plotting E against $K\Delta^{-0.5}(2t_{eq}+t_h)/V_H$ results in the data following a slope of $(gW^2H^3/9)^{0.5}$ until the departure point E_{cr} and then asymptotically approaches E_{max}. The advantage of this approach is that it allows a direct comparison between geometries of decreasing flow rate after departure. Figure 4-22 and 4-23 illustrate the data from the hall and entry geometries in the normalized format.

Equation 2-52 fits the decreasing flow region very well for both geometries. The function does not represent the distinct change in slope characteristic of hall flow but is a good approximation. The curve fit for the hall case could be improved if the exact departure point was used and the function began with a slope about 10 to 20% smaller. The slight improvement that would be provided by this treatment does not justify the loss of generality which would result. The best fit values of E_{cr} and E_{max} are:

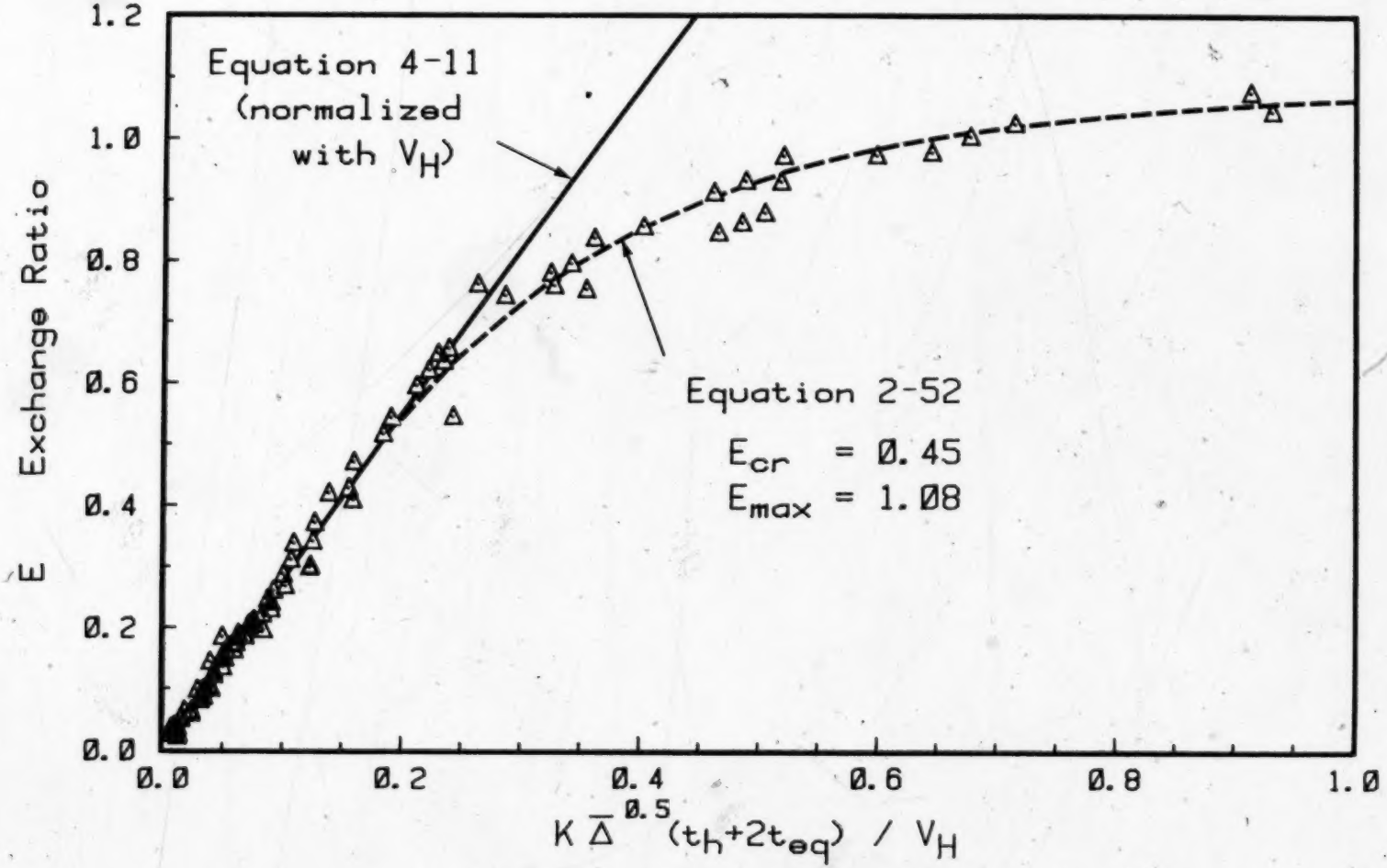

FIGURE 4-22: Normalized Volume Exchange and Decreasing Flow Correlation for the Hall Geometry

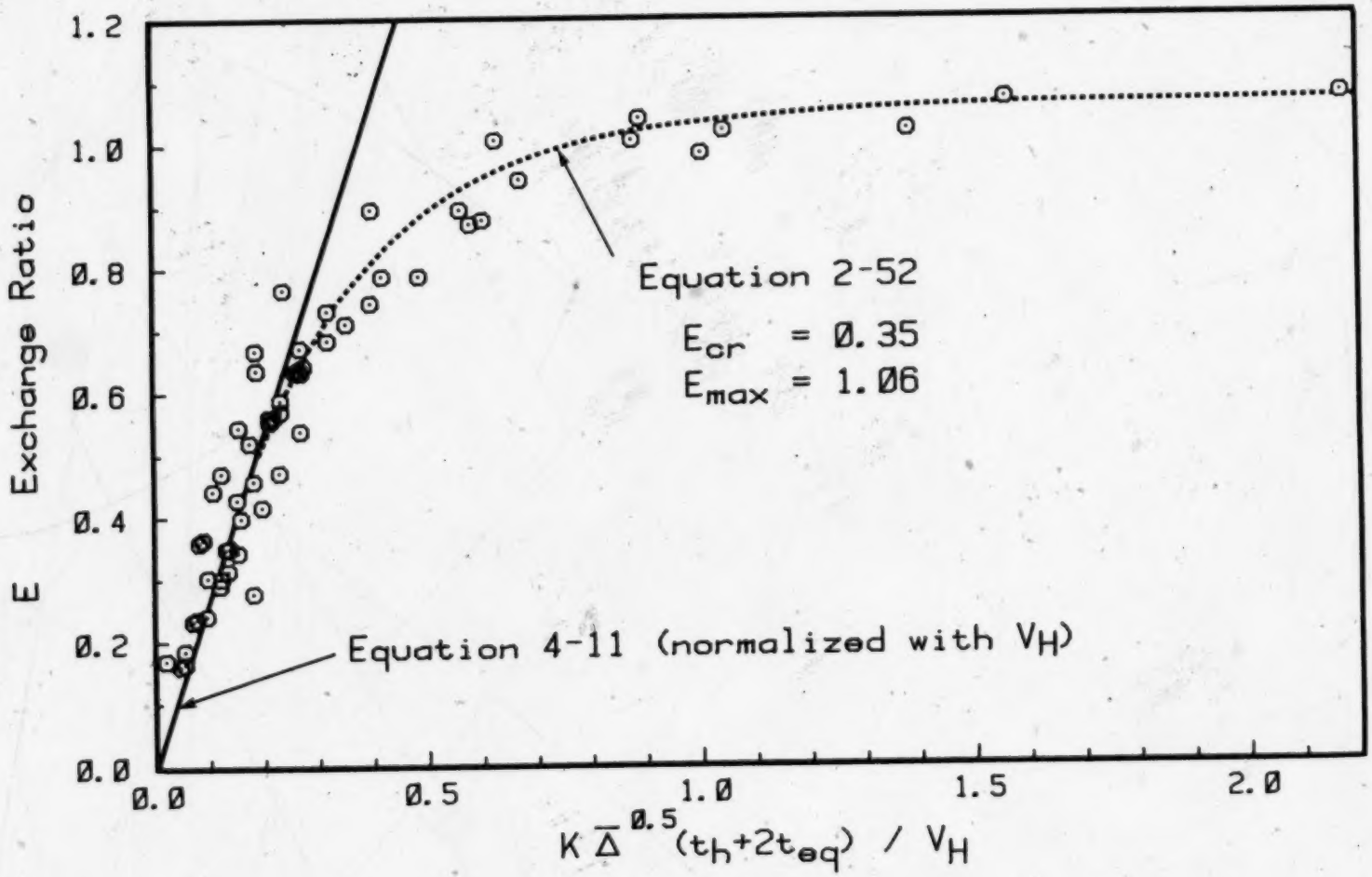

FIGURE 4-23: Normalized Volume Exchange and Decreasing Flow Correlation for the Entry Geometry

Geometry	E_{cr} (fit)	E_{max} (fit)
Hall	0.45	1.08
Entry	0.35	1.06
Full-House	0.34	——

For all the geometries, the function departure point E_{cr} is lower than the value of V_{cr}/V_H determined from the exact inflection point in the previous section. For example, the inflection point for the long hall geometry was between 0.67 and 0.73 compared to the function fit value of E_{cr}=0.45. This lower departure point is necessary so that the function approaches the linear region tangentially.

The exchange ratio at an infinite time approaches a value that is in excess of V_H, by 8% for the hall geometry and 6% for the entry geometry. This is only possible if air above the door height H, is downwardly mixing during the exchange. A value for E_{max} is not given for the full-house geometry because the exchange experiments were not of sufficient duration to provide the necessary decreasing flow data.

For comparison, the hall and entry data, and their respective correlations are shown in Figure 4-24. The similarity between the two sets is strong, considering the differences between the geometries. Based on the limited results available, it appears that the functional form of the decreasing flow period is very similar for different geometries. The form of this decay is well described by Equation 2-52 with constants in the order of $E_{cr} \simeq 0.4$ and $E_{max} \simeq 1.07$.

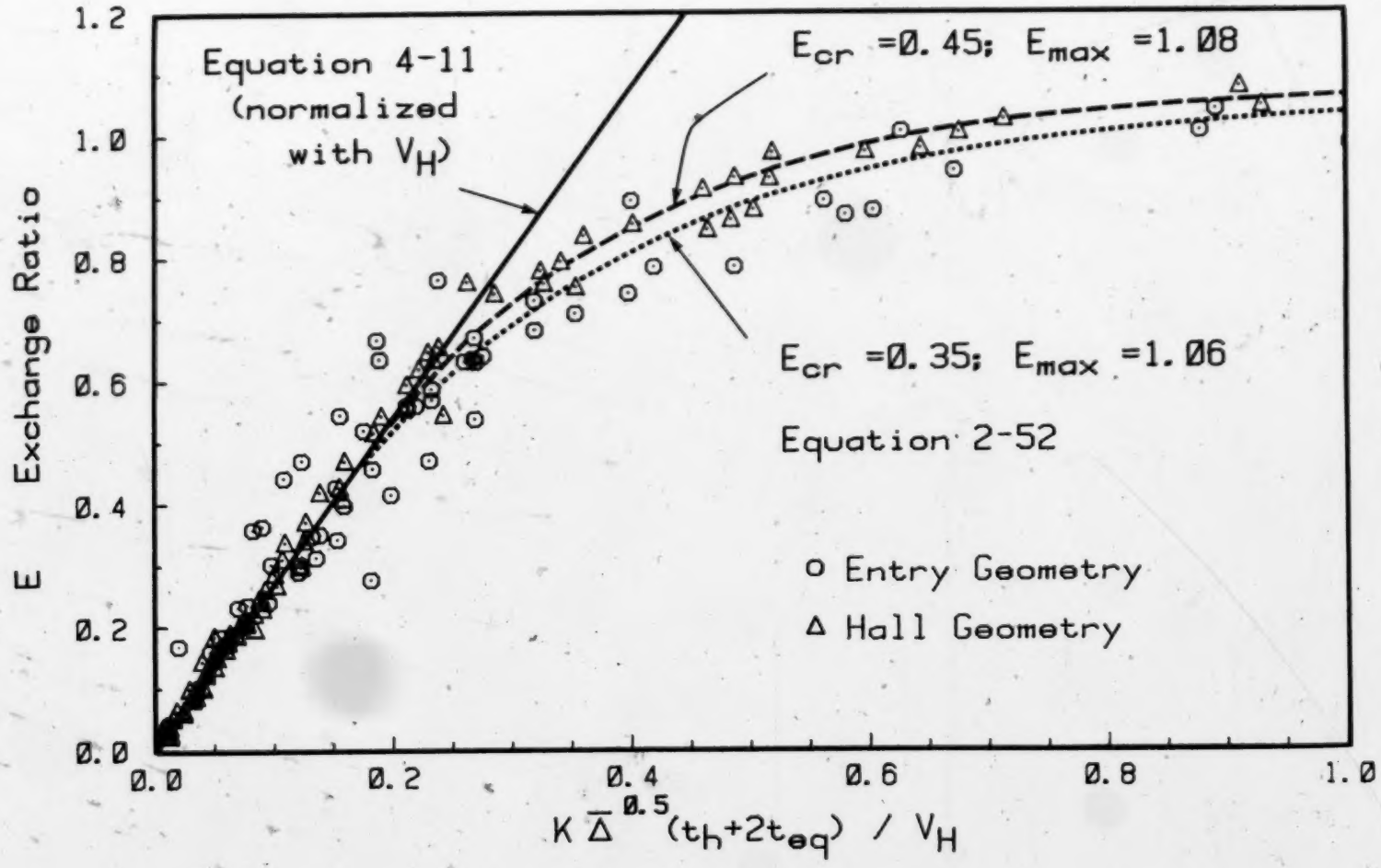

FIGURE 4-24: Normalized Volume Exchange and Decreasing Flow Correlation for the Hall and Entry Geometries

Summary

Combining the information gained in these experiments, the following simplified calculation for determining buoyancy-driven flow through entries is proposed.

For a given problem the following information must be provided

T_i, T_o, W, H, $t_o(=t_c)$, t_h, V_H

Calculate

$\bar{\Delta} = 2(T_i-T_o)/(T_i+T_o)$

$\Delta T = 295\,\bar{\Delta}/(1+\bar{\Delta}/2)$

$K = 0.4 + .0045\,\Delta T$

$t_{eq} = (2/\P)t_o$ (for $d\theta/dt$=constant)

$Q_n = K\,(gW^2H^3/9)^{0.5}\,\bar{\Delta}^{0.5}$

$t = 2t_{eq} + t_h$

Buoyancy Contribution

If $Q_nt/V_H > 0.4$ then $V_B = 1.06\,V_H\,(1-e^{-A(t-B)})$

where $A = 1.5\,Q_n/V_H$

$B = (0.4V_H/Q_n) - 0.474/A$

If $Q_nt/V_H < 0.4$ then $V_B = Q_nt$

CHAPTER 5

SCALE MODELLING THEORY AND EXPERIMENTS

The theoretical equations (with an empirical orifice coefficient K) are satisfactory for predicting the exchange rates for relatively simple geometries and calm ambient conditions. Extending these equations to more specific problems, in terms of gross exchange rates or for local flow characteristics (such as gravity current flow), would require extensive full scale testing. One attractive option is the construction and testing of a small scale model.

Scale modelling of air exchange flows has the following advantages:

- o reduced experimental time and expense
- o complete control over experimental parameters
- o use of alternate measurement techniques not possible in full scale
- o easy and inexpensive modifications

If confidence in the accuracy of the model results can be established, then modelling provides a valuable tool for experimental investigation. The primary objective of this study is to determine the degree of similitude between the full scale and model exchange flows.

Dynamic Similarity

The most important consideration in scale modelling is the question of dynamic similarity between the full scale and prototype. The closer the similarity, the more valid the application of model results to the full scale condition. The fundamental principles of similarity were

first established by Osborne Reynolds and stated as follows by H. Schlichting (1955):

> For two flows about geometrically similar bodies with different fluids , different velocities and different linear dimensions, to be similar, it is evidently necessary that the following conditions should be satisfied : at all geometrically similar points, the forces acting on a fluid particle must bear a fixed ratio at every instant of time.

In Chapter 2 the important forces involved in air flow through doors were identified and two nondimensional parameters based on ratios of these forces defined as the Reynolds number and Froude number. Writing the two parameters with velocity in fundamental units of time t, and length L, yields:

Reynolds number $L^2/t\nu$ (5-1)

Froude number $(L/g't^2)^{0.5}$ (5-2)

where

$$g' = g\,\Delta\rho\,/\,\bar{\rho}$$

Model and full scale parameters will be given subscripts F and M respectively. Having identified the Reynolds number and Froude numbers as the most important parameters, and invoking Reynolds criterion for similarity, requires that $Re_M=Re_F$ and $Fr_M=Fr_F$. Expressing these conditions using Equation 5-1 and 5-2 results in:

$$\frac{L_M^2}{t_M\,\nu_M} = \frac{L_F^2}{t_F\,\nu_F} \qquad (5\text{-}3)$$

$$\frac{L_M^{0.5}}{t_M\,g'_M{}^{0.5}} = \frac{L_F^{0.5}}{t_F\,g'_F{}^{0.5}} \qquad (5\text{-}4)$$

Defining the scale factors as:

$$L_S = L_F / L_M \qquad (5\text{-}5)$$

$$t_S = t_F / t_M \qquad (5\text{-}6)$$

$$\bar{\Delta}_S = \bar{\Delta}_F / \bar{\Delta}_M \qquad (5\text{-}7)$$

$$\nu_S = \nu_F / \nu_M \qquad (5\text{-}8)$$

where

L_S = length scale

t_S = time scale

$\bar{\Delta}_S$ = fractional density difference scale

ν_S = viscosity scale

Using these scale factors, Equation 5-3 and 5-4 can be rewritten as:

$$\frac{L_S^2}{t_S \nu_S} = 1 \qquad (5\text{-}9)$$

$$\frac{L_S^{0.5}}{t_S \bar{\Delta}_S^{0.5}} = 1 \qquad (5\text{-}10)$$

If an appropriate model size and working fluid are selected, then Equations 5-9 and 5-10 can be satisfied, ensuring complete similitude. Unfortunately, physical limitations make this task impossible.

Selection of Model Parameters

The following values are representative of full scale conditions during tests at the Alberta Home Heating Research Facility.

Air viscosity	$\nu_F \approx 1.4 \times 10^{-5}$ m^2/s
Length max. (house length)	$L_F \approx 8$ m
Fractional density difference range	$\bar{\Delta}_F = 0\text{-}0.2$ ($\Delta T_{max} \approx 50^{\circ}$C)
Event time range	$t_F = 1\text{-}100$ s

Physical considerations make it impossible to select a model working fluid, model size and fractional density difference which will satisfy all of the conditions of similarity. Some of the considerations which influence the selection of the model working fluid are density range available, fluid viscosity, expense, diffusivity, measurable characteristics (eg. concentration) and flow visualization potential.

The model fluid selected was water with dissolved sodium chloride to produce the necessary fractional density difference. Although the use of salt water did not allow an exact match of both Froude and Reynolds numbers, it did provide a satisfactory compromise. The viscosity of salt water is approximately 1.1×10^{-6} m^2/s. From Equation 5-8 the viscosity ratio can be determined as approximately $\nu_S = 12.7$. This viscosity scale combined with Equations 5-9 and 5-10 results in the following condition for complete similitude:

$$L_S^{1.5} = 12.7 / \bar{\Delta}_S^{0.5} \qquad (5\text{-}11)$$

Selecting a fractional density difference scale of 1, implies that the same fractional density difference is used in model as exists in the full scale. Based on Equation 5-11, a length scale of 5.5 would be required to insure complete similitude. To model the full scale house, which is approximately 8 m in length, would require a model 1.5 m long. A model of that size is impractical due to both construction expense and limited test facility size.

The opposite approach may be taken by selecting a length scale which is small enough to minimize construction expense and test tank size requirements, but which is large enough to still allow accurate measurements to be made. A length scale of 20 for example, will result

in a model length of about 40 cm and require a fractional density difference scale of $\overline{\Delta}_S$=0.02. To model full scale fractional density differences in the range of zero to 0.15 ($\Delta T \simeq 0\text{-}40^{\circ}C$), would require a model fractional density difference range of zero to 7.4, which is impossible with saltwater solutions. The maximum fractional density difference which can be achieved with saltwater solutions is about 0.2 and therefore the minimum fractional density difference scale is approximately 1, if a full scale range of temperatures is to be modelled. These examples show that avoiding a mismatch of one of the nondimensional parameters is very difficult.

The best alternative is to match the most important parameter and then theoretically and experimentally determine the significance of the mismatch in any other relevant parameters. Full scale results clearly indicated that the exchange process is dominated by buoyancy forces and thus the match of Froude numbers has the highest priority. Using a length scale of 20, a fractional density difference scale of 1 and setting $Fr_F=Fr_M$, as given by Equation 5-10, produces a buoyancy time scale of 4.47. This time scale indicates that inviscid buoyancy flow will occur approximately 4.47 times as fast in the model as in the full scale. A comparison of model and full scale results will allow the accuracy of this time scale to be determined.

Substituting L_S=20, t_S=4.47 and ν_S=12.7 into the LHS of Equation 5-9 results in a ratio of 7 indicting that $7Re_M \simeq Re_F$. It is interesting to note that the mismatch would have been much larger if the viscosity ratio did not help compensate for the large denominator in Equation 5-9. For example, if helium was used rather than water as the model fluid, then the viscosity ratio would be about 1, with a Reynolds number

mismatch of 90 rather than 7.

For very small fractional density differences where buoyancy forces are negligible, an inertial time scale is required which matches Reynolds numbers. Solving for the time scale in Equation 5-9 using the length scale of 20, and the viscosity scale of 12.73, results in an inertial pumping time scale of 31. This suggests that for the inertia dominated pumping exchange, a time scale of 31 will provide complete similitude. This idea will be examined in context with experimental data.

It is interesting to note that the molecular diffusion of sodium and chloride ions from the outgoing flow to the incoming fresh flow reduces the net exchange rate in exactly the same manner as the diffusion of interior air or SF_6 and the conduction of energy across the counterflow boundary. It was noted in Chapter 2 that diffusion and conductivity were negligible in full scale flow. If a similar analysis is performed using the diffusivity of NaCl in water which is approximately 1.5×10^{-9} m^2/s, the resulting ratio of buoyancy driven transfer to molecular diffusion transfer ranges from 6×10^4 to 10^5, for an equivalent temperature difference range of 10 to 30°C. Clearly molecular diffusion in the model can also be neglected.

Model Design

The first important consideration in model development was the question of which solution, the fresh water or the salt solution, should be used to represent indoor air? At first glance this may appear obvious; Should not the dense salt water represent the dense outdoor air? The major problem with this approach is the prohibitive amount of

salt that would have to be added to the test tank to achieve the density difference needed to simulate temperature differences up to 50°C.

Adding the salt solution to the model and using fresh water in the test tank is far more cost effective and convenient, but the densities are reversed. To solve this problem, the model was placed in the tank upside down so that salt solution poured out of the door toward the bottom of the reservoir which will be "up", relative to the inverted model coordinates.

There was a second advantage to placing the salt solution within the model and the fresh water in the reservoir. Because the reservoir volume was large compared to the model volume, repeated addition of salt water from the model into the reservoir that occurred during the exchange experiments did significantly alter the fresh water density from 1.00 and therefore it was not necessary to continually monitor and replace the reservoir contents. This allowed the reservoir density of 1.00 to be used as a reference density in the same manner that the full scale indoor temperature was set to a reference condition of 295 K.

The following design criteria were used in model design development:

- o must allow easy addition of salt solution or salt
- o preferably clear to allow flow visualization
- o access to allow modification of interior geometry
- o geometrically similar to full scale geometry
- o reliable and repeatable scale door operation
- o minimal leakage
- o ability to measure exchange volumes, preferably time dependent
- o must have a mixing device to eliminate stratification

- must fit in water channel of width=0.68 m and depth=0.44 m (total channel volume = 5 m^3)

In light of the various requirements listed above, the model shown in Figure 5-1 was designed and constructed. The extensive use of plexiglas provided visibility of the exchange flows. Access to the interior was afforded either through the opening port in the floor surface or by complete removal of the floor section. With the floor section removed, different interior partitions could be installed. A removable roof section was also constructed which attached independently to the ceiling section.

The door control system components are visible in Figure 5-2, including the vertically mounted D.C. stepping motor, fully open and closed position optical microswitchs, and position rheostat. The speed-duration control unit allowed a wide range of opening speeds and fully open hold times to be selected.

Figure 5-3 illustrates a typical door postion-time curve for the model door. The linear motion should be noted. Comparing Figure 5-3 to Figure 3-4 which illustrated a typical door position curve for the full scale experiments, suggests that the only difference between the full scale and model motion is a slightly slower starting acceleration in the full scale case.

Temperature, Density, Salinity and Mass Relationships

The model was filled with salt solution of density ρ_M and the channel filled with water of density ρ_C. The model fractional density difference for the inverted model may be written as:

COLOURED PICTURES
Images en couleur

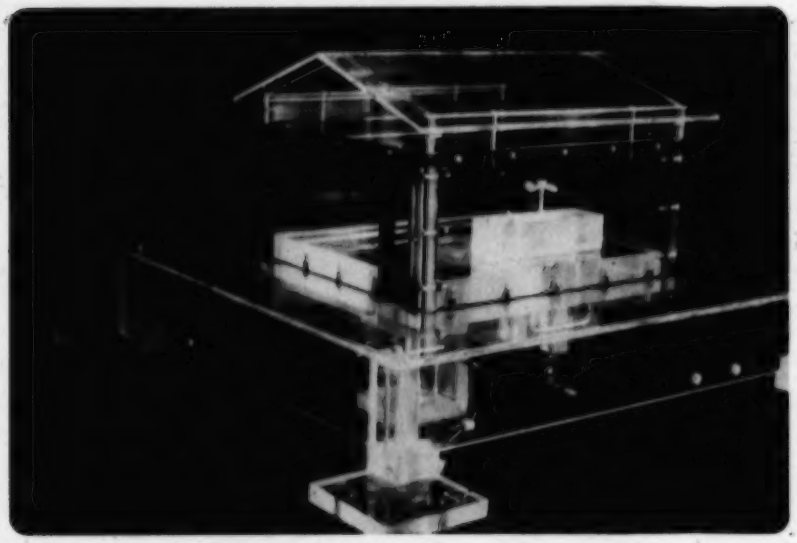

FIGURE 5-1: 1:20 Scale Model House, Interior Dimensions
35.6 cm x 32.5 cm x 12.0 cm

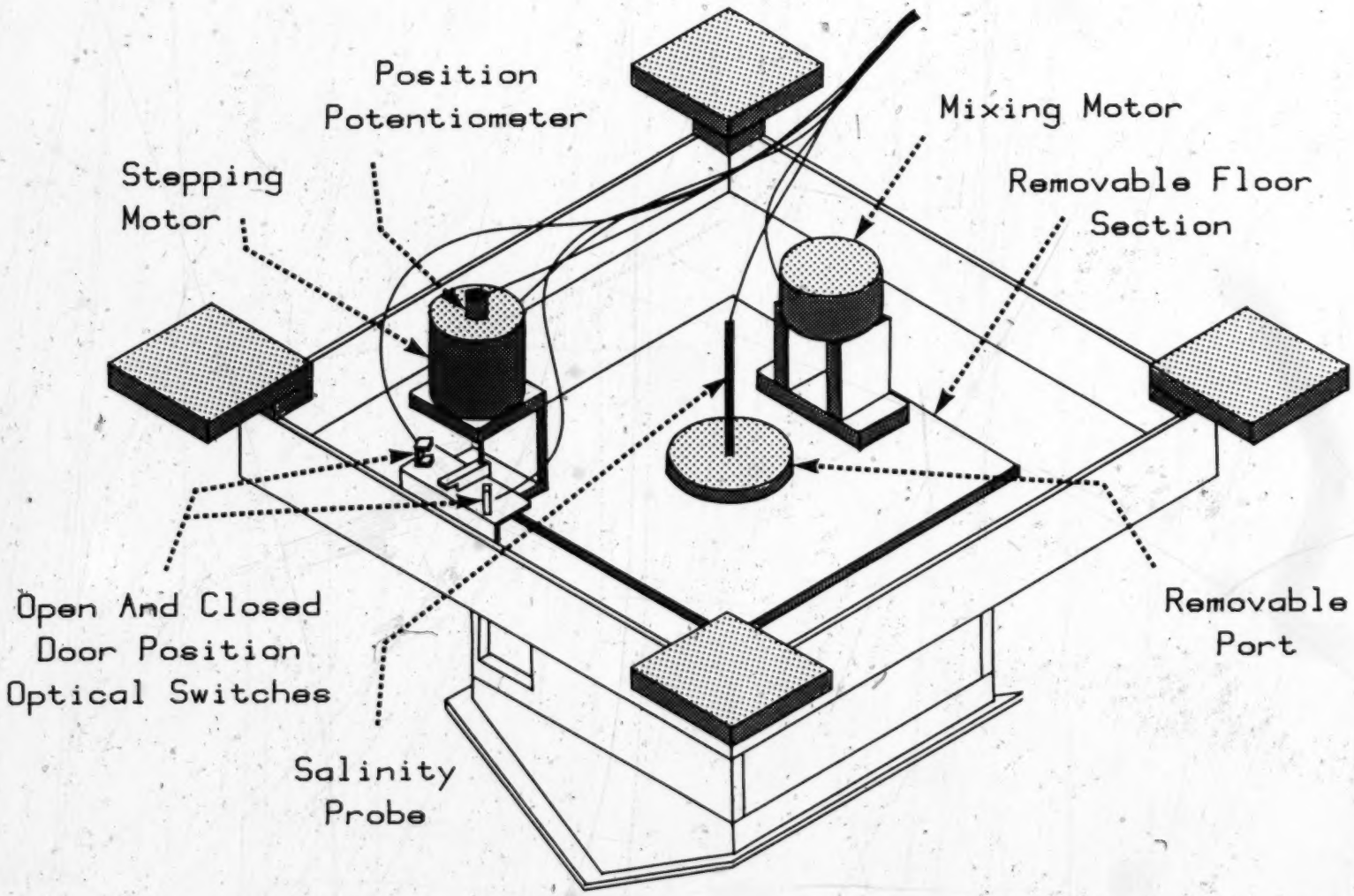

FIGURE 5-2: Illustration of Inverted Scale Model

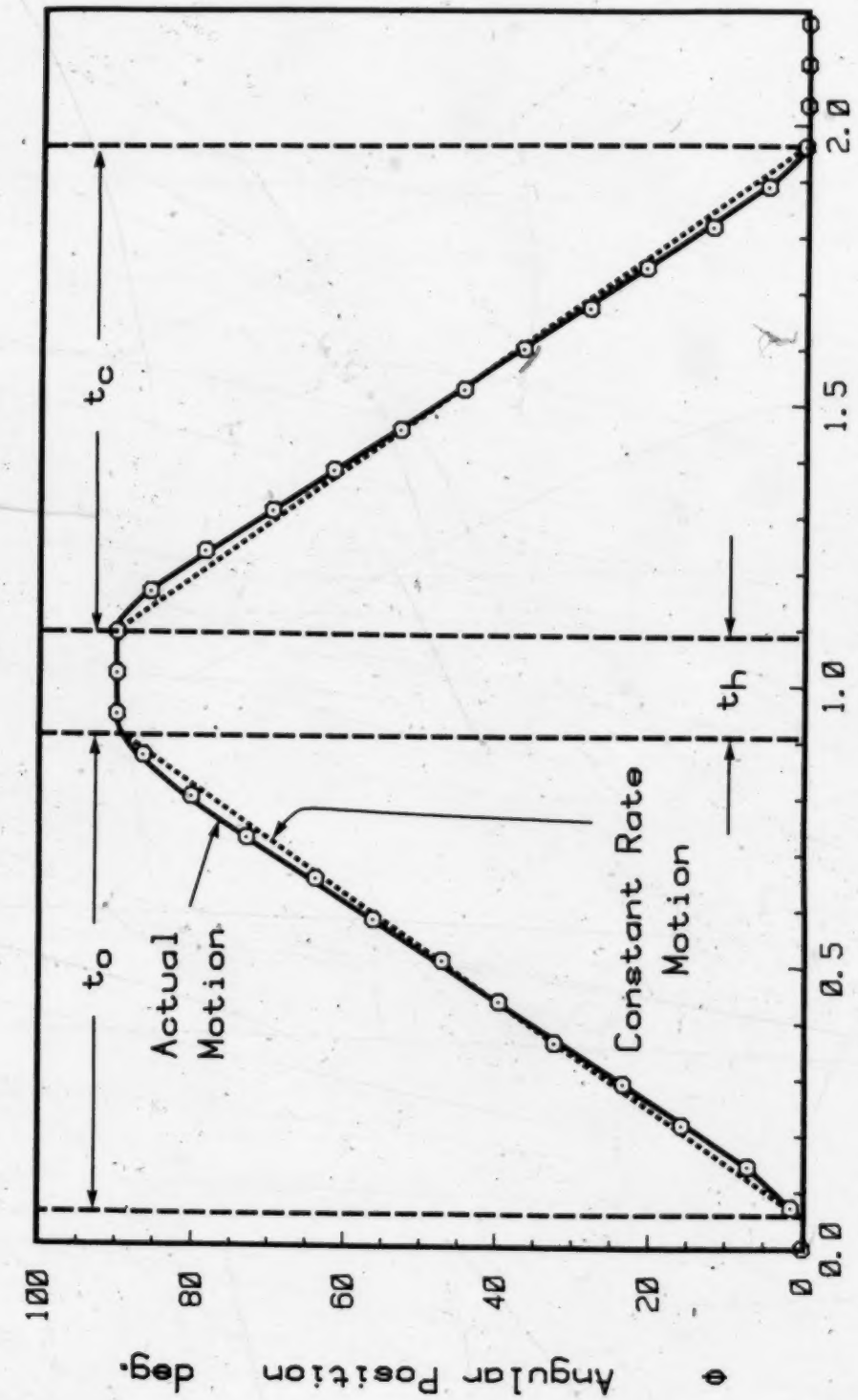

FIGURE 5-3: Typical Door Motion Calibration Curve Measured in the 1:20 Scale Model

$$\bar{\Delta}_M = \frac{2(\rho_M - \rho_C)}{(\rho_M + \rho_C)} \qquad (5\text{-}12)$$

where

ρ_M = the density of the fluid within the model

ρ_C = the channel fluid density

Recalling Equation 2-10:

$$\bar{\Delta}_F = \frac{\Delta T}{295 - \Delta T/2} \qquad (2\text{-}10)$$

and combining with Equation 5-12, results in the following relationship between the model densities and equivalent reference temperature difference.

$$\frac{\Delta T}{295} = 1 - \frac{\rho_C}{\rho_M} \qquad (5\text{-}13)$$

Noting that the channel density is maintained at a density of ρ_C=1.000 allows Equation 5-13 to be written in terms of the specific gravity of the salt solution as:

$$\Delta T = 295(1 - 1/SG_i) \qquad (5\text{-}14)$$

where

SG_i = initial specific gravity of model salt solution

A similar analysis can be done to determine the equivalent local temperature in the model as a function of the local specific gravity as given by Equation 5-15.

$$T_1 = \frac{SG_1}{SG_i} 295 \qquad (5\text{-}15)$$

where

SG_l = local specific gravity

T_l = equivalent local indoor temperature

The total volume exchange can be determined from a mass balance as:

$$V = \frac{SG_i - SG_f}{SG_i - 1} V_M \qquad (5\text{-}16)$$

where

SG_f = final specific gravity after exchange

V_M = model interior volume

The total mass exchange can be expressed as:

$$\Delta m = V (\rho_C - \rho_M) \qquad (5\text{-}17)$$

where

Δm = total mass change

The sign of this result is negative because the model becomes lighter as the salt water is replaced with fresh water.

Exchange Flow Measurements

Several measurement techniques were used in the model exchange experiments. The measurement system employed in any particular test depended on the density difference, the duration of the exchange and the information desired. Each of the measurement techniques will be briefly described with some comment on the advantages and limitations of each.

Weight Measurement System- This system proved to be very effective for those exchanges that had a mass change of greater than 20 g. The outstanding feature of this system is its ability to determine the actual exchange volume as a function of time throughout the experiment.

The apparatus consists of a suspension harness and counterweight system with a 4 element differential strain gauge transducer load cell arranged as shown in Figure 5-4. Most of the submerged model weight is balanced by the counterweight assembly. The remainder of the load is transferred to the load cell via the adjustable lever-arm system. As the salt water pours from the model and is replaced by fresh water, the net model weight decreases and the differential mass change is measured by the load cell. Equation 5-17 allows the calculation of the instantaneous volume exchange from the load cell output.

Problems arose for this system when simulating small temperature differences. Even if the door hold duration was long enough to allow a large percent volume exchange, the absolute weight change was relatively small. The gain of the load cell amplifier could be adjusted to provide sufficient resolution to measure these small changes but the real problem was caused by background noise (weight fluctuations), not measurement sensitivity. These background weight fluctuations resulted from internal channel waves and model vibration caused by door opening and closing. In some experiments the weight fluctuations from these sources were many times larger than the total weight change, obscuring the transient information.

Specific Gravity Measurement- The initial and final specific gravity, and the model volume, is sufficient information to calculate the gross volume exchange according to Equation 5-16. This is analogous to the full scale experiments in which the initial and final tracer gas concentration and the interior volume were use to calculate the total exchange volume. The initial and final specific gravities were determined from hydrometer readings taken in samples drawn from the

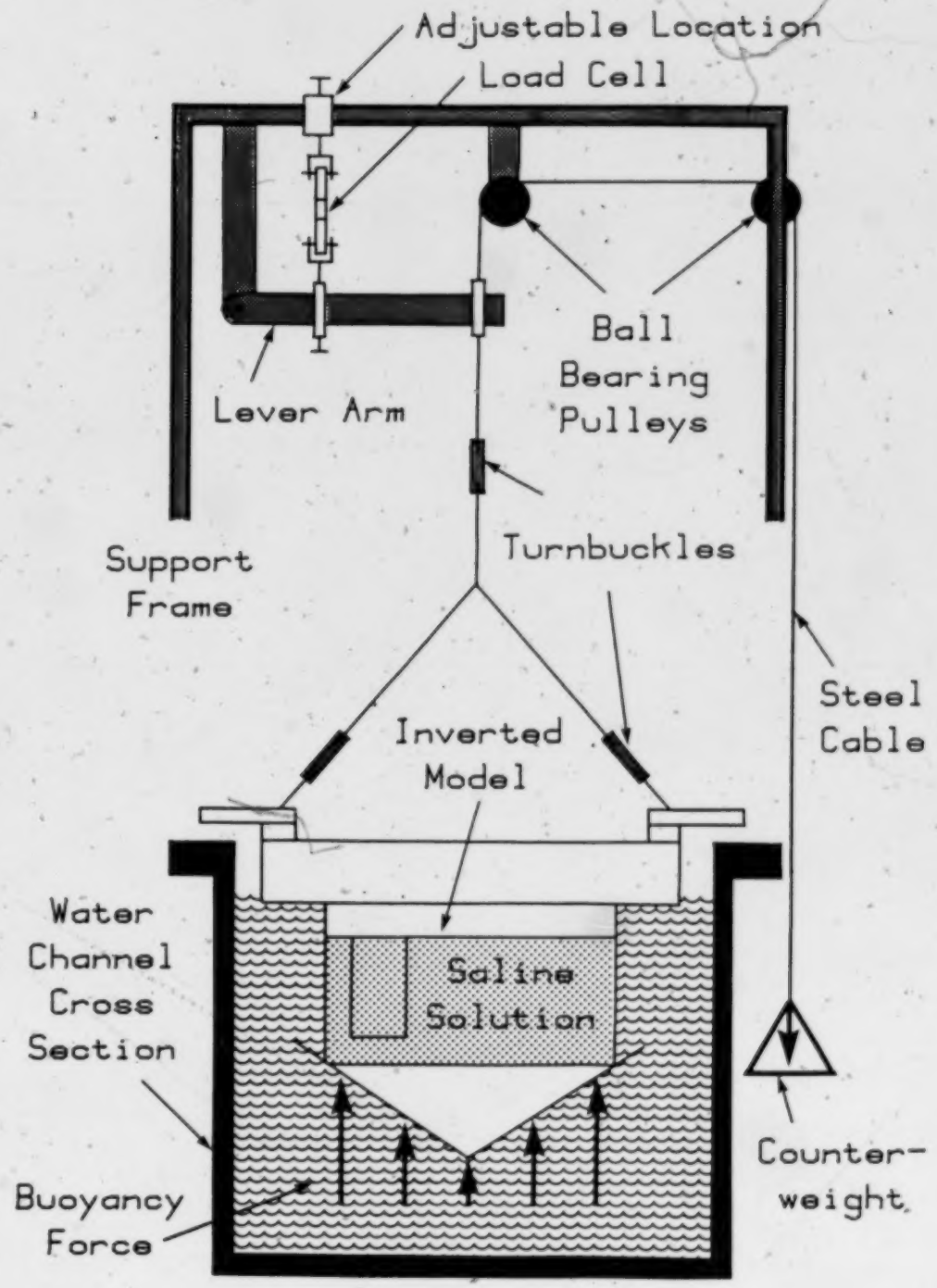

FIGURE 5-4: Counterweight and Differential Load Transducer System

model before and after the exchange.

This method was always used in conjunction with the weight system. The total exchange volume determined by this method was compared directly with the total volume exchange found with the weight system. If a significant difference was found, the constant in the calibration curve was modified such that the difference between the total volume exchange was split. The modified constant was then used to calculate the intermediate exchange volumes from the transducer output. This reduced experimental errors associated with either method independently. In general, the two methods agreed within 3% to 5% of one another.

Similar to the weight system, this method was also unable to accurately determine the exchange volumes associated with small weight and specific gravity changes. Limited accuracy of the hydrometer readings was the major problem. For this reason, an alternate system had to be used, particularly for examination of the short duration door pumping effects.

Salinity Probes- The output voltage of the electrical conductivity probes depended on the concentration of sodium and chloride ions in the salt solution. Once this relationship was established, the salinity probes could be used to determine the local concentration of salt from which the local density (or equivalent temperature) was determined. A complete description of the physical and electronic characteristic of the probes can be found in Bara (1985).

The probes were used for two applications. The first was to determine the total volume exchange. This was accomplished in a manner which is identical to the specific gravity method except that the probes and a predetermined calibration curve were utilized to measure the

specific gravity at the start and end of the test.

In the second application, the probes were used to provide local salinity concentrations within the exchange flow. Two tests of this type were done; one examined the frontal velocity down the hall geometry layout, while the second utilized the probes to determine the salinity profiles on the vertical centerline of the door during exchanges.

For low salt concentrations, a relatively linear calibration curve could be determined from premixed calibration solutions stored in bottles. Unfortunately, for moderate to large salt concentrations, the calibration curves were nonlinear. More importantly, the same voltage could not be expected in both the model (located in the channel) and an isolated bottle of the same concentration solution. The reason for this problem was related to differences in electrical grounding. Although it was not possible to solve this problem, the probes could still be used if the calibration was done directly in the water channel. To do this, specific gravity measurements of the model solution were taken while noting the voltage output from a probe located in the model. This procedure was repeated over a range of specific gravities without the probe gain or span being altered, allowing an in-channel calibration curve to be obtained.

Model Experimental Procedures

The time scale of $20^{0.5}$ indicates that an event in the model will occur 4.5 times faster than in full scale. For example, an eight second door cycle time in full scale, had to be accelerated to 1.77 seconds in the model. To accurately record door position, transducer output and probe output, the assistance of the same computer data acquisition

system employed in the full scale experiments, and described in Chapter 3, was required.

The exchange tests performed on the model fall into several categories. A brief description of the procedure used in each of the categories will now be given.

Long Duration Weight System Experiments- This general group of experiments used the weight system to measure the volume-time relationship for various geometries, over a wide range of fractional density differences. The door hold time was sufficiently long to determine the steady state flow rate and in some cases, the departure time and functional form of the decreasing flow period.

After leveling and aligning the model in the waterchannel, salt was poured into the model through the opening port and the mixing unit turned on. Once the salt was fully dissolved and the desired specific gravity reached (determined by hydrometer readings taken in extracted samples), the port was closed and the initial specific gravity recorded. Any disturbances in the water channel such as internal or surface waves were then allowed to dissipate. When the voltage output from the load cell stabilized, a load cell calibration was performed as follows.

An estimate of model weight reduction was made from the selected door hold duration setting and the fractional density difference, providing some indication of the range over which the transducer was expected to read. Weights were then gently placed on the top surface of the model, in ten increments, each weighing approximately 0.1 of the expected weight change. Measuring the transducer output for each weight added allowed a calibration curve to be determined. The weights were left on the model during the exchange so that as the model weight

decreased during the experiment, the transducer output would lie entirely within the range for which it was calibrated. A typical calibration curve is shown in Figure 5-5; the linearity should be noted.

The mixing motor was restarted after the calibration procedure to remove any stratification which may have developed. Once mixing was complete, the motor was stopped and fluctuations were allowed to dissipate. Door motion was initiated with a manual switch on the control unit, which also triggered the computer to store the start time and begin continuous sampling of the transducer voltage. It was not necessary to sample the door position during the exchange since the repeatability of the door motion was very good and thus could be determined by an independent calibration. This allowed the computer to sample only the transducer output, providing a maximum sampling rate. Figure 5-6 shows the inverted model in the water channel during an exchange experiment.

After the door was firmly closed and the transducer sampling complete, the mixing unit was restarted. The remaining salt water and fresh inflow were throughly mixed and the final specific gravity measured. The final specific gravity was not absolutely necessary for determining the volume exchange. The total volume exchange could be calculated directly from the starting specific gravity, calibration constant and the voltage change. The advantage of taking this last reading, as discussed previously, was that the total exchange could be determined directly from the first and last specific gravity values, thus providing an independent check on the accuracy of the load cell method.

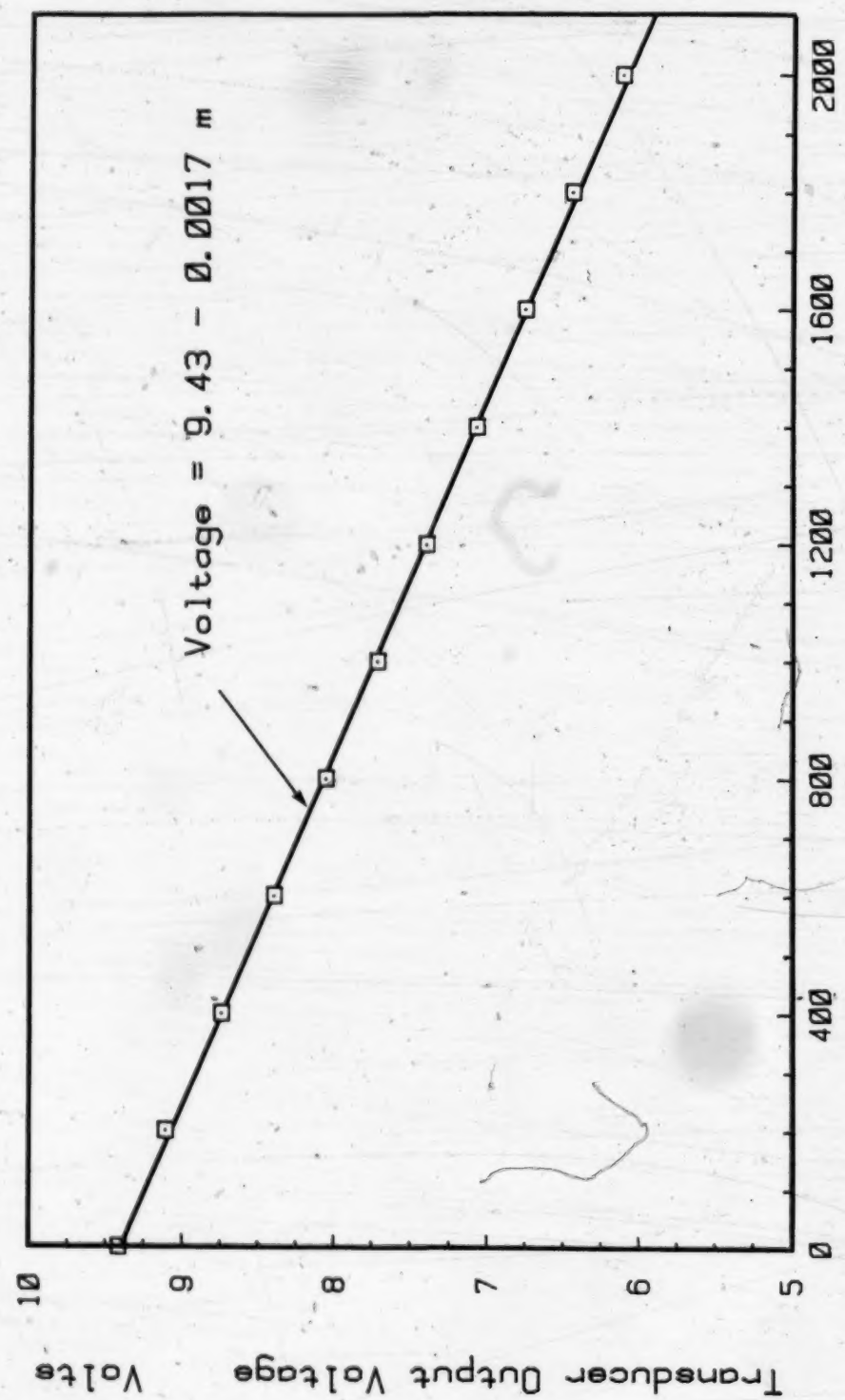

FIGURE 5-5: Typical Load Cell Calibration Curve

COLOURED PICTURES
Images en couleur

FIGURE 5-6: Inverted Model in Channel During Exchange Experiment

Short Duration Weight Measurement Experiments- In addition to the long duration exchanges, the weight system was also used in the pumping exchange measurements. Accurate information could only be determined for the larger density differences. The procedure was similar to the long duration experiments except that a series of openings were performed with complete mixing of exchange fluid and residual fluid after each exchange in the series. This resulted in series of tests in which each consecutive test had a slightly smaller fractional density difference. A single transducer calibration was performed and a specific gravity reading taken at the start and end of the series. This information, plus the transducer readings from each test, made it possible to determine the equivalent temperature difference at the start of each opening cycle, and the volume exchanged for each opening cycle. Four different swing speeds were tested, 0.81, 0.69, 0.56 and 0.43 s, in model time units.

Short Duration Salinity Probe Experiments- The salinity probes functioned poorly in solutions with high salt concentrations due to saturation and drift problems. Fortunately, the weight system was able to obtain reasonably good results for the larger fractional density differences. The probes did function well in the moderate to small fractional density difference range of $\Delta\rho/\bar{\rho} < 0.07$. The same procedure was used with the probes as was employed with the short duration weight system, except that probes were used to determine the concentration after each exchange with frequent specific gravity samples to provide the necessary information to develop calibration curves for the probes.

Very Small and Zero ΔT Exchanges Using Salinity Probes- For very small fractional density differences, the salt concentration became

unmeasurable. This problem was solved by using a model solution which consisted of a mixture of water, salt and alcohol. The proportions of each ingredient were balanced so that any desired buoyancy could be achieved with a measurable salt concentration. This allowed sufficient salt to be added such that it could be used as a tracer in the model in exactly the same manner that the SF_6 was used in the full scale case.

Frontal Velocity Measurements- Determining the frontal velocity of the density current flowing along the hallway floor of the model was important for comparison with the full scale thermocouple results. To achieve these measurements in the model, two probes spaced 92 mm apart were inserted through the floor of the model. The probe tips were positioned such that they were on the same line as the thermocouples located in the full scale house, 15 cm off the floor (full scale units) on the hall center line. As the fresh water inflow passed over the probe tips a discrete drop in the probe voltage would occur. By monitoring the two probe voltages as a function of time and knowing the separation distance, the flow velocity was easily determined.

Salinity Profile Measurements- Temperature profiles in the full scale doorway were measured with a vertical line of thermocouples. The resulting information provided some insight into the effect of downstream and upstream mixing. It has been shown that a local salinity concentration in the model is a direct analogue of the full scale temperature at the geometrically similar location.

The ideal way of determining the salinity profile in the entry of the model would be to employ a vertical line of probes which, when read simultaneously, would provide the average salinity profile. Unfortunately, this was not possible because the probes only provide

correct absolute readings if used individually. The next best alternative consisted of traversing a single probe through a steady flow at a constant traverse speed. This provided useful information concerning the amount of interfacial mixing that was occurring in the model.

CHAPTER 6

SCALE MODEL RESULTS AND ANALYSIS

In this chapter, model results are compared to the full scale results presented in Chapter 4 to determine the accuracy of theoretical time scales and the implications of mismatched Reynolds numbers. The comparison of results will begin with steady state buoyancy-driven flow.

Steady State Buoyancy-Driven Flow

The load transducer system described in Chapter 5 was used to measure the exchange flow in the model for long duration, fully open hold times. Full scale testing required a series of separate measurements to obtain the same time dependent information obtained in a single test using the load cell transducer system. A total of 29 long duration model experiments were conducted for direct comparison with full scale results. In these experiments, the full-house geometry was tested over the same range of fractional density differences experienced during full scale testing. The full-house geometry was selected for the most rigorous comparative testing because it has the largest internal house volume, resulting in the maximum weight change for a long duration experiment, and thus the maximum measurement resolution.

Figures 6-1, and 6-2 illustrate the net volume exchange as a function of time for equivalent temperature differences of 44.4^{o}C and 1.5^{o}C. The model exchange volume was determined by converting the transducer output voltage to a mass change using the load cell calibration curve and then converting this to a volume using

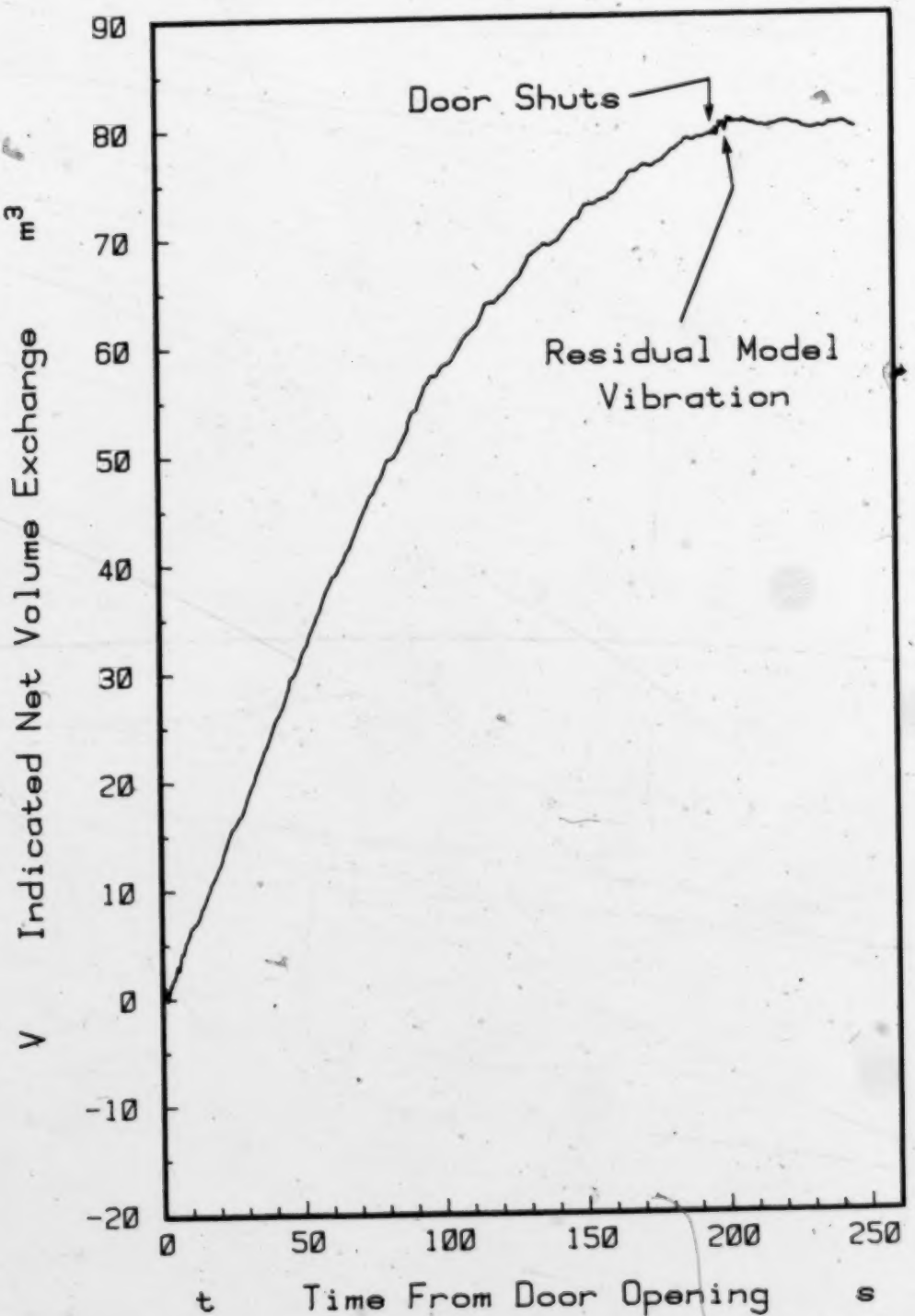

FIGURE 6-1: Indicated Volume Exchange Determined by the Model Load Cell Measurement System, Shown in Full Scale Units; Full-House Geometry, $\Delta T=44.4^{o}C$; $T_{i,ref}=22^{o}C$

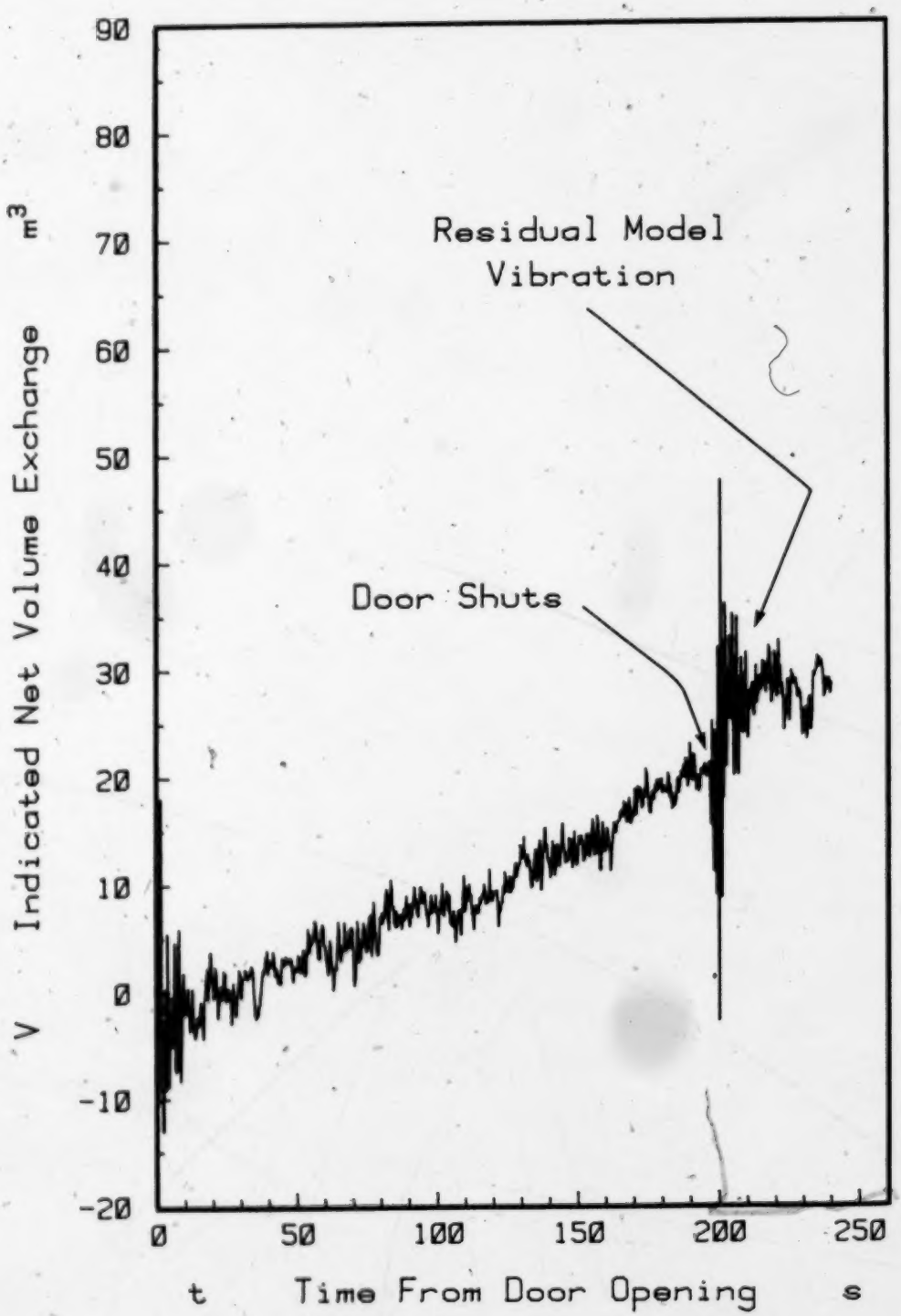

FIGURE 6-2: Indicated Volume Exchange Determined by the Model Load Cell Measurement System, Shown in Full Scale Units; Full-House Geometry; ΔT=1.5°C, $T_{i,ref}$=22°C

Equation 5-17. Throughout this chapter the model data will be converted to full scale units to allow direct comparisons between model and full scale results. For this reason the model exchange volume and time are converted to full scale units using Equation 5-5 and Equation 5-6.

$$L_M^3 * L_S^3 = L_F^3 \qquad (5\text{-}5)$$

$$t_M * t_S = t_F \qquad (5\text{-}6)$$

where

$L_S = 20$ (actual)

$t_S = 20^{0.5}$ (theory)

A mismatch of the model and full scale data will result if the theoretical time scale used to modify the model results is incorrect. It is important to keep in mind that differences between the model and full scale results may not be due exclusively to time scaling errors. In fact it will be shown that the time scale is very accurate and that observed differences are a result of a combination of Reynolds number and outdoor turbulence level mismatches.

One obvious difference between the curves in Figures 6-1 and 6-2, is the increase in signal fluctuations at the smaller equivalent temperature difference. This variation is an inherent characteristic of the weight measurement system as illustrated by the following example. For a volume exchange of 20 m^3, from Figure 6-1 ($\Delta T=44.4^oC$) the net weight change was approximately 440 g, compared to Figure 6-2 ($\Delta T=1,5^oC$) where, for an equivalent volume exchange of 20 m^3, the weight change was only approximately 20g. A typical background weight fluctuation level of 5 g causes a variation of 5 m^3 (25%) for $\Delta T=1.5^oC$, but only a variation of about 0.2 m^3 (1.0%) for $\Delta T=44.4^oC$.

Except for very small density differences, a region of steady state flow is easily distinguishable. This allows the use of simple linear regression to determine the slope and thus the flow rate for each individual experiment. Determining the flow rates and equivalent temperature differences for all 29 model exchange tests allows direct comparison of the model steady state flow rates with the full scale flow rates first shown in Figure 4-4.

A comparison of full scale and model flow rates as a function of temperature difference is shown in Figure 6-3. The model results appear to lie on the upper bound of the full scale results with significantly less scatter present in the model results compared to the full scale data. To gain a better perspective of the differences between the full scale and model results, it proves convenient to compare the steady state orifice coefficients. The orifice coefficients for the model experiments are determined in exactly the same manner as the full scale results using Equation 2-37.

$$K = \frac{3\,Q_n}{W(g'H^3)^{0.5}} \qquad (2\text{-}37)$$

Figure 6-4 illustrates the model orifice coefficient for the full-house geometry as a function of temperature difference. An orifice coefficient of 0.6 appears to represent the model data well for the entire range of temperature differences. The increased scatter in the model orifice coefficient at small temperature differences is the result of a decrease in accuracy of the load cell system at small density differences. The full scale orifice coefficients for both the full-house and hall geometries are also shown, plus the correlation with

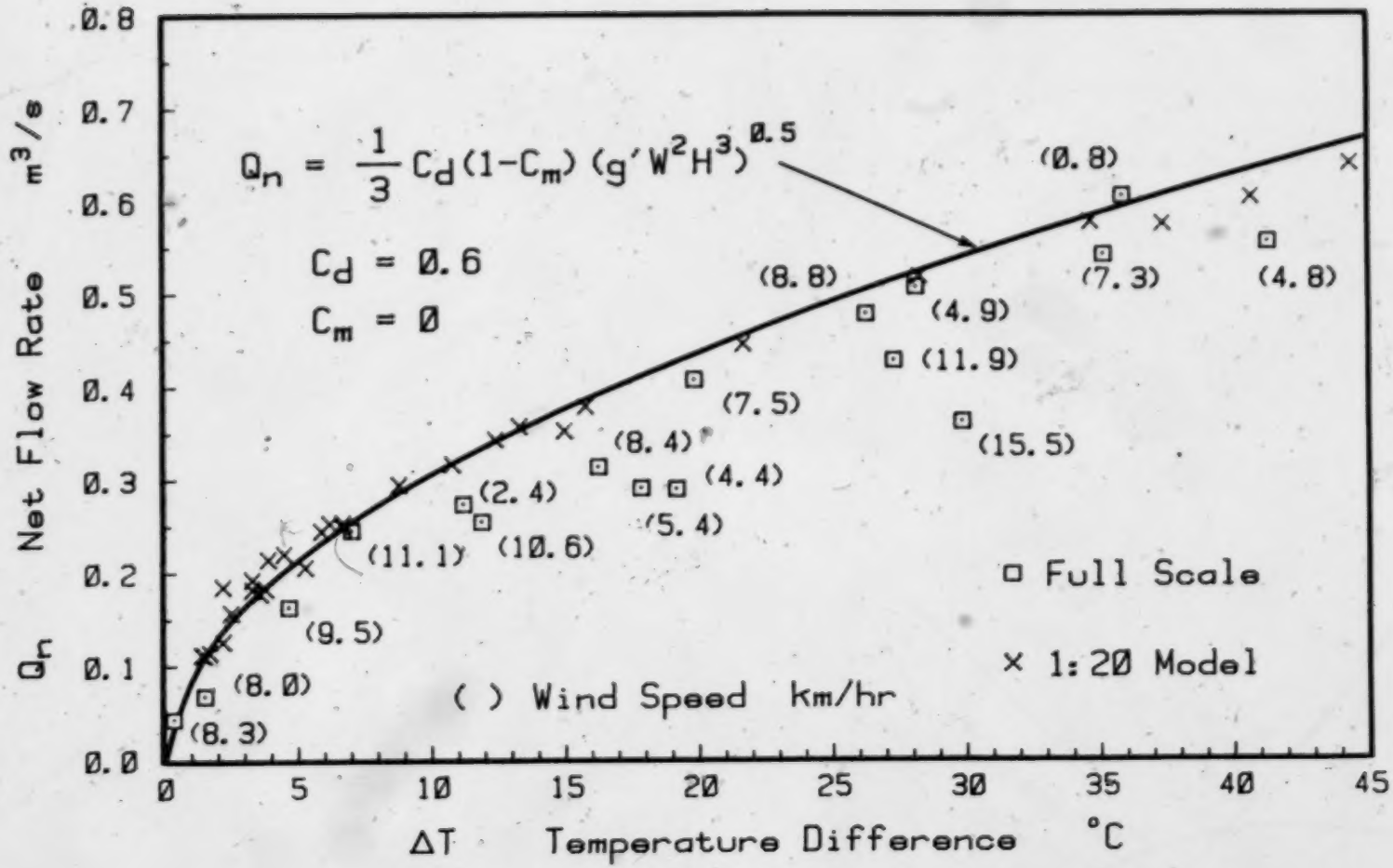

FIGURE 6-3: Comparison of Model and Full Scale Steady State Flow Rate Variation with Temperature Difference, Full-House Geometry; $T_{i,ref}=22^{o}C$

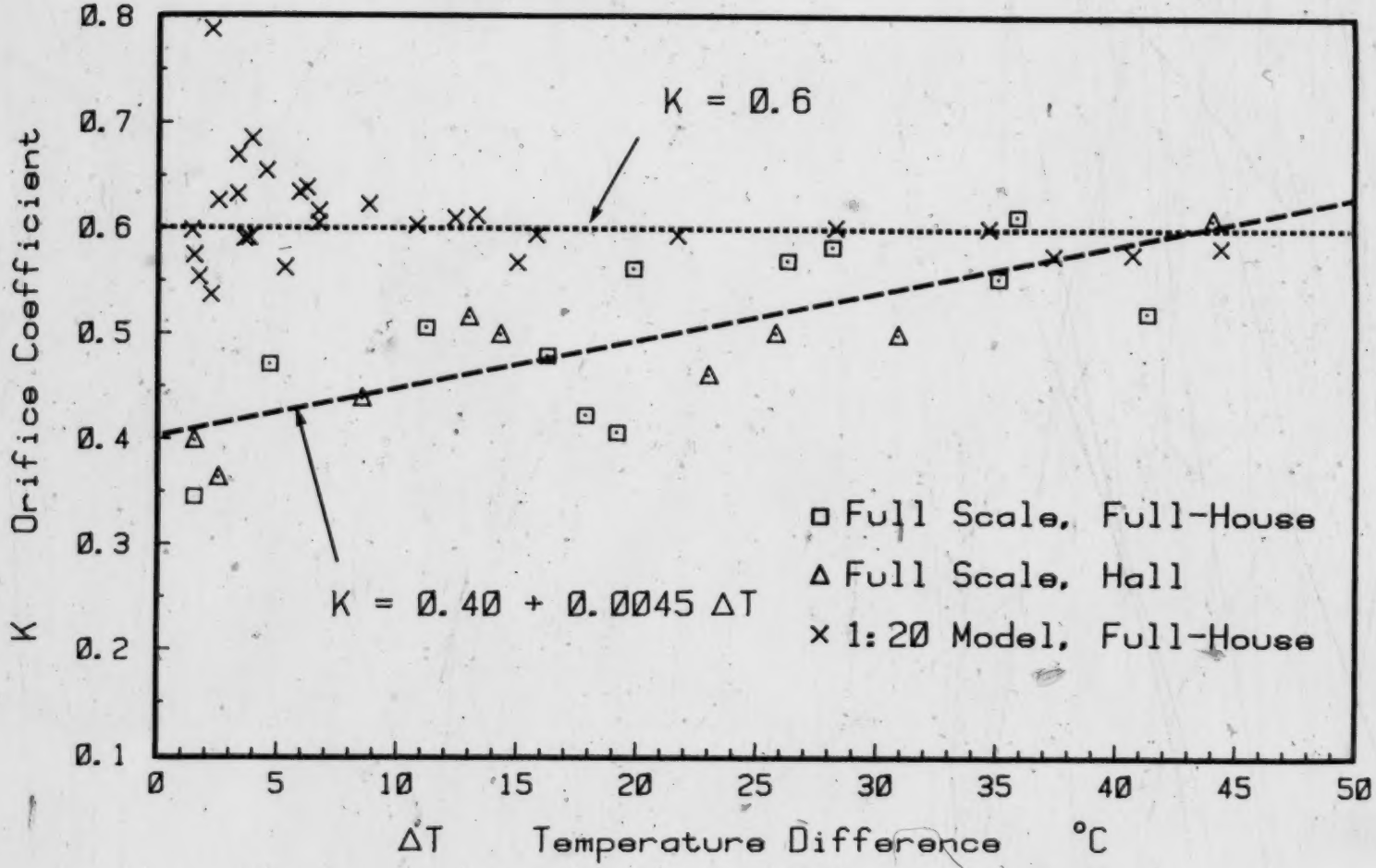

FIGURE 6-4: Comparison of Model and Full Scale Orifice Coefficient Variation with Temperature Difference, Full-House Geometry; Full Scale Wind Speeds less than 10 km/hr; $T_{i,ref}=22^{o}C$

temperature difference from Chapter 4. The model and full scale results have similar orifice coefficients of K=0.6 for large temperature differences. However, the full scale coefficients diminish toward 0.4 at small temperature differences with the model coefficients remaining constant at 0.6.

Time scale errors could be responsible for a constant difference between the full scale and model orifice coefficients but not for the variable difference. In Chapter 4 interfacial mixing was identified as the primary cause for orifice coefficient reduction at small temperature differences, based on the examination of temperature profiles. To further assess the cause of the orifice coefficient mismatch, model salinity profiles will be examined.

Interfacial Mixing

Recalling the discussion of orifice coefficient variation in Chapter 4, it was suggested that the full scale discharge coefficient was approximately 0.6 and that the mixing coefficient varied from about C_m=0 at large temperature differences, to about C_m=0.35 at smaller temperature differences. It was proposed that the variation in the mixing coefficient was caused largely, if not entirely, by increased interfacial mixing at the lower fractional density differences. This idea was strongly supported by temperature profiles measured on the vertical centerline of the door opening. The correlations shown in Figure 6-4 can be explained if the model discharge coefficient is 0.6 and if little or no interfacial mixing was occurring, such that C_m=0.

To examine this theory, the analogy between local salt concentrations in the model and local temperatures in the full scale

will be utilized. This analogy allowed salinity profiles on the centerline of the model orifice to be compared directly to full scale temperature profiles, providing an insight into the question of relative interfacial mixing.

Measurements of the salinity profiles were accomplished using the traverse technique outlined in Chapter 5. Salinity data was then converted into local equivalent temperature differences using Equation 5-15. Despite the fact that local averages could not be determined by traversing through the steady counterflow streams, the results are still very illuminating.

It was important that the traverse speed be fast enough to measure the entire profile before the reflected wave returned to the door, but slow enough to allow the probe time to respond to local concentrations. For these reasons, the shorter the required traverse distance the better. Numerous preliminary tests showed that the upper portion of the orifice (bottom of the doorway due to inversion) through which the fresh water was flowing into the model, contained absolutely no trace salt. Traversing the region of constant composition in every test was redundant, so traverses were started at about 0.3H from the floor surface. This still allowed a small portion of the nonmixing region to be measured.

Twenty three vertical profiles were measured over a full range of density difference ratios. Of these profiles, three were selected which best matched the temperature differences of the full scale measurements presented in Figure 4-12. Each matched pair of model and full scale profiles are shown in Figures 6-5 to 6-7, representing average temperature differences 26.5, 18.7, and 5.7^{o}C respectively.

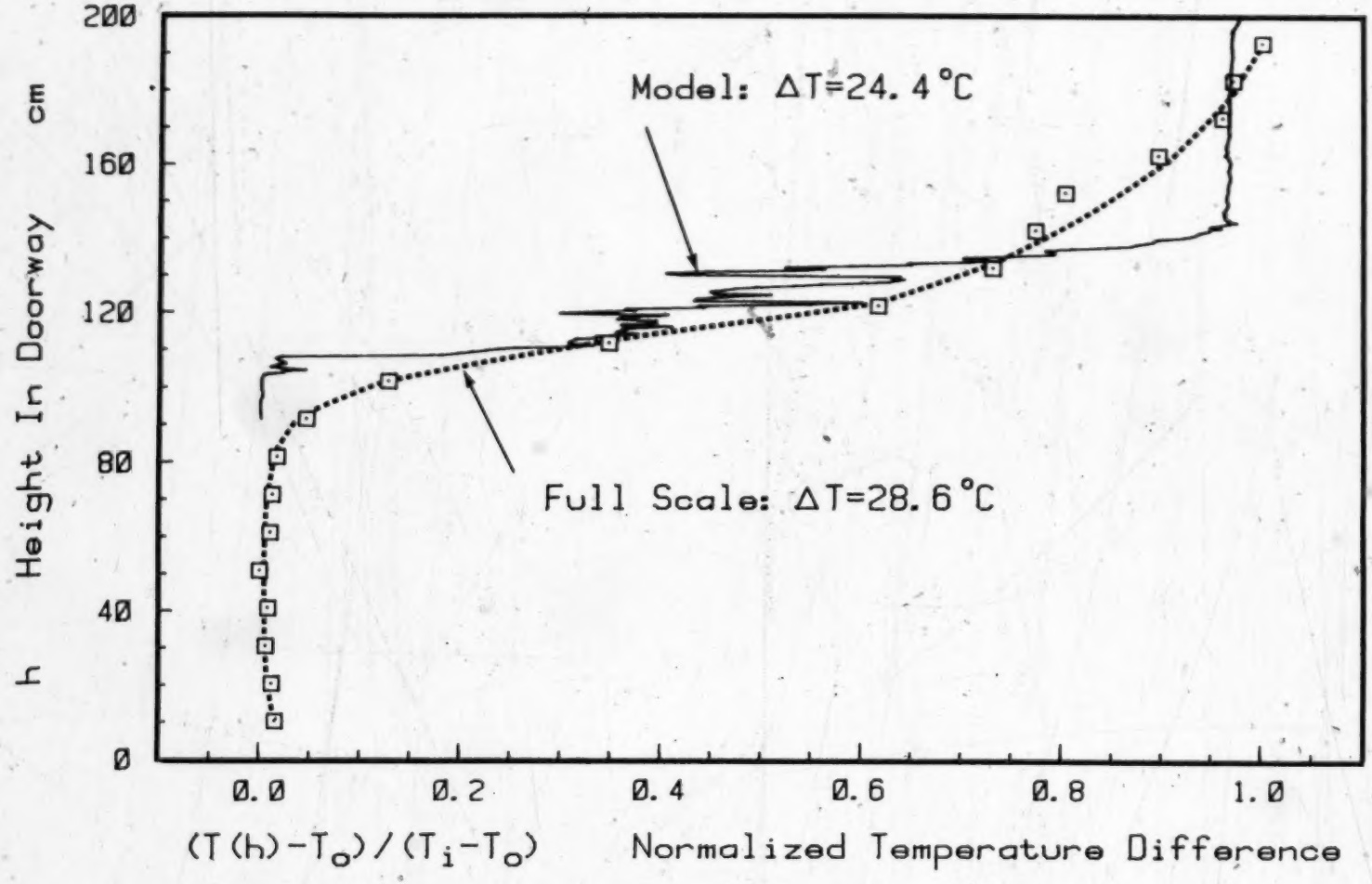

FIGURE 6-5: Comparison of a Model Salinity Profile with a Full Scale Temperature Profile Measured on the Doorway Vertical Centerline at an Equivalent Full Scale ΔT Model =24.4°C and ΔT Full Scale =28.6°C

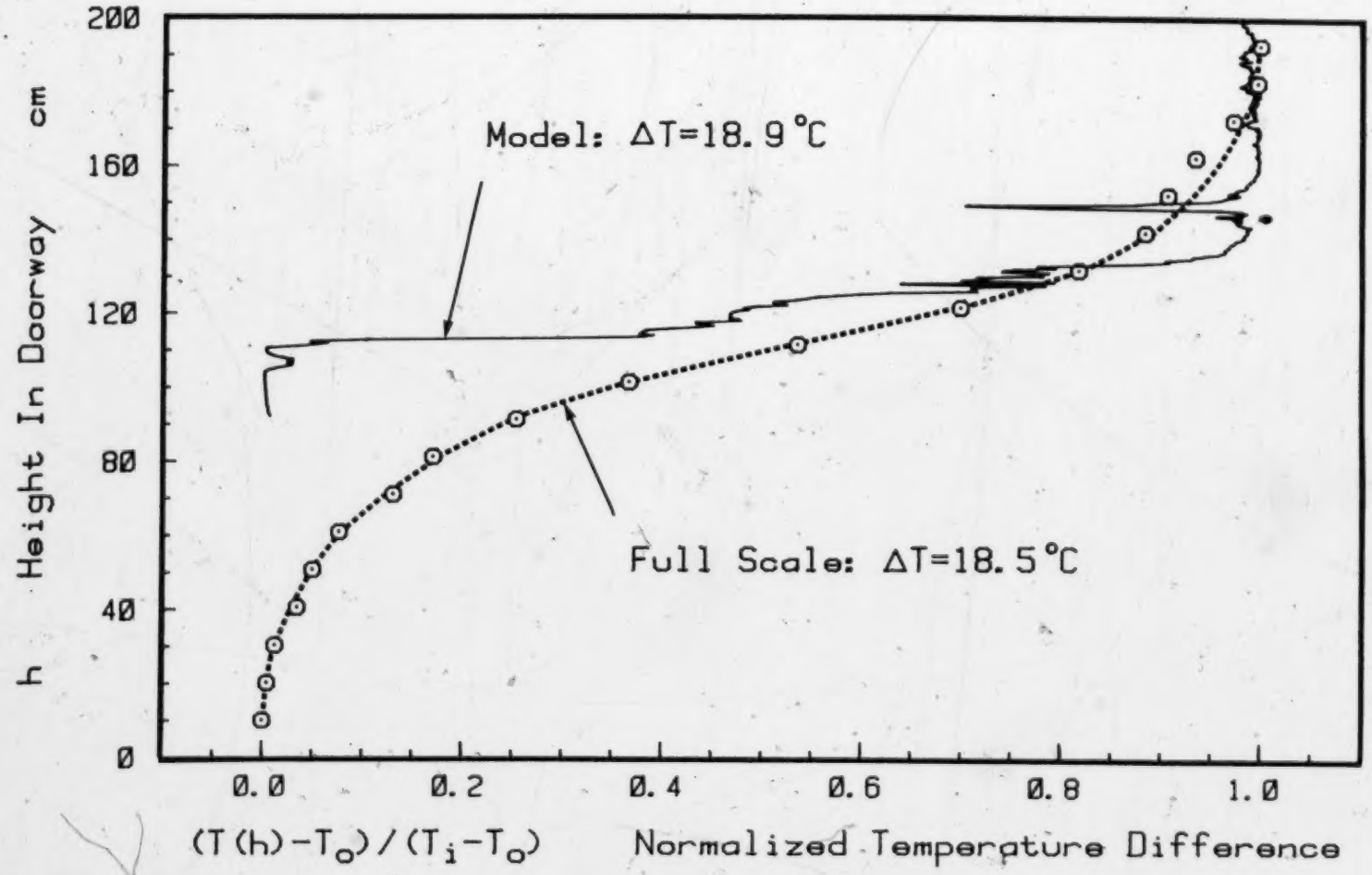

FIGURE 6-6: Comparison of a Model Salinity Profile with a Full Scale Temperature Profile Measured on the Doorway Vertical Centerline at an Equivalent Full Scale ΔT Model =18.9°C and ΔT Full Scale =18.5°C

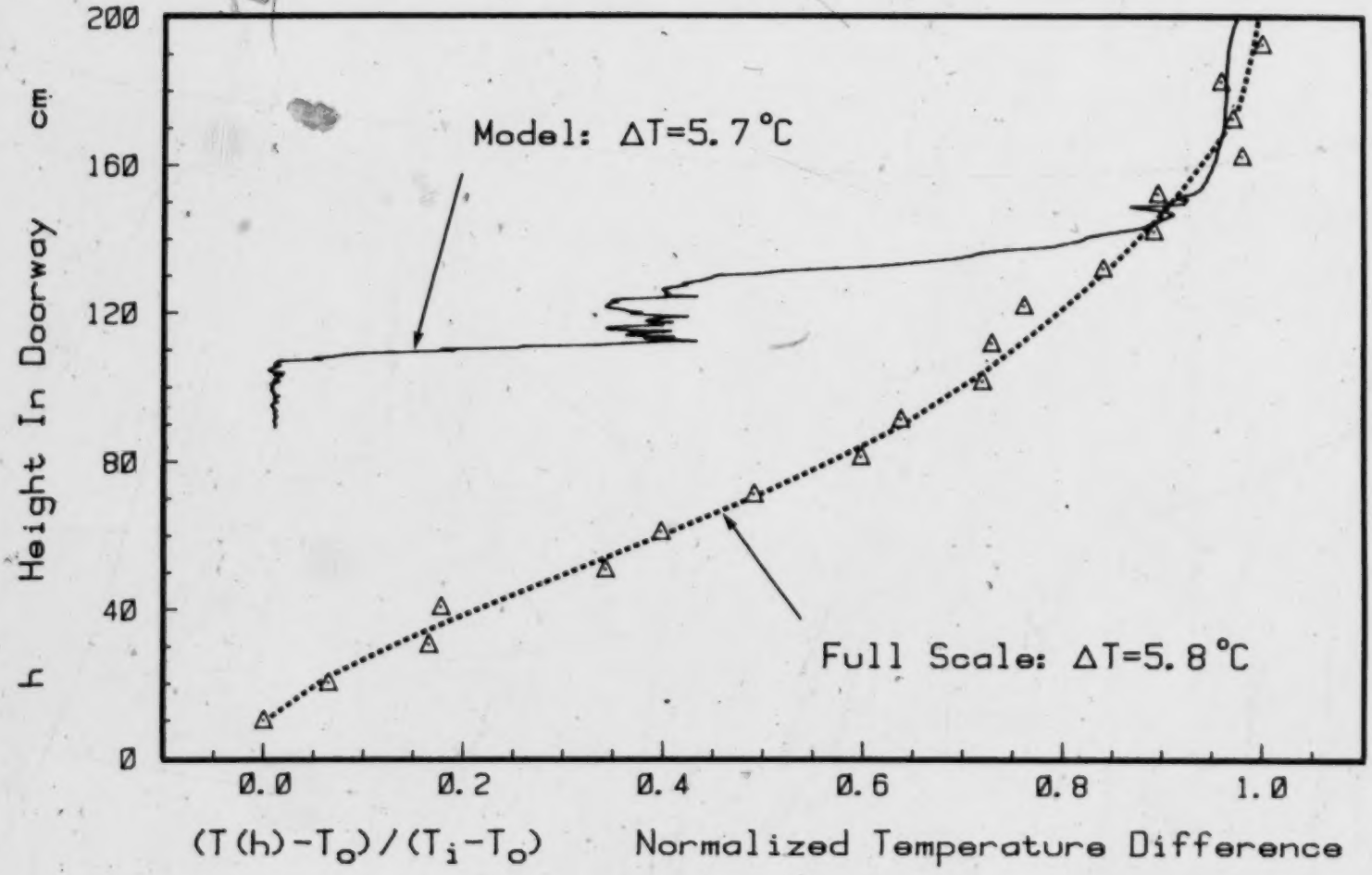

FIGURE 6-7: Comparison of a Model Salinity Profile with a Full Scale Temperature Profile Measured on the Doorway Vertical Centerline at an Equivalent Full Scale ΔT Model =5.7°C and ΔT Full Scale =5.8°C

The model profile in Figure 6-5 for $\Delta T \sim 26.5^{o}C$, indicates that the inflow stream is virtually unmixed over the entire lower half of the door implying no interfacial mixing outside the house. The outflow stream is unmixed over the upper 3/8 of the door but a thin mixing region is apparent just above the neutral level between h=110 cm and 140 cm. This layer is the result of a small amount of interior interfacial mixing. The full scale profile indicates slightly more mixing in the inflow stream as indicated by the smoother curvature between h=80 cm and 100 cm. This curvature may be in part due to the effect of time averaging. The full scale outflow profile indicates interior interfacial mixing right to the top of the door. These profiles suggest slightly more mixing in the full scale compared to the model at this temperature difference.

Figures 6-6 and 6-7 show the profiles for $\Delta T \sim 18.7^{o}C$ and $5.7^{o}C$ respectively. There is very little change in the shape of model profiles with decreasing temperature difference, The full scale profiles however show a dramatic increase in exterior interfacial mixing as discussed at length in Chapter 4. This is precisely the information required to confirm the hypothesis. The model orifice coefficient is constant at K=0.6 because very little interfacial mixing is occurring such that $C_d=0.6$ and $C_m \simeq 0$. The variation of the full scale orifice coefficient is the result of increasing interfacial mixing with decreasing temperature difference such that $C_d=0.6$ and $C_m=C_m(\overline{\Delta})$.

The final question that remains to be answered is; Why does the model not exhibit the same amount of interfacial mixing as the full scale?

Interfacial Stability and Reynolds Number Mismatch

To understand the reason for the difference in the amount of interfacial mixing that occurs in the full scale compared to the model, it is necessary to consider the implications of the mismatch in Reynolds number. Studies performed by Rozovsky, Shabrin, and Markov (1972), indicated that interfacial mixing depends on the stability of the interface and that a critical stability transition region exists below which very little or no interfacial mixing takes place. They found that the critical stability region was in the range; $5x10^4 < Re_\Delta < 10^5$.

In Chapter 5, it was shown that for any particular fractional density difference, the model Reynolds number would be approximately 1/7 of the full scale Reynolds number. With these ideas in mind, the orifice coefficients for both the full scale and the model exchanges are plotted as a function of densimetric Reynolds number in Figure 6-8. The upper and lower bounds of the stability region, as proposed by Rozovsky et al. are also shown. A very important observation can now be made; the model results lie exclusively within the stable region, whereas the full scale results lie above the upper stability bound.

This result, combined with the absence of outside turbulence in the channel to actively promote mixing, accounts for the invariant orifice coefficient of 0.6 for the model results. This explains why the full scale tests exhibit substantial interfacial mixing despite the relatively low exterior wind speeds of less than 10 km/hr.

Effect of Outside Wind on Model Exchange Rates

It is important to note that the stability concept does not necessarily imply absolutely no mixing under all flow conditions. The

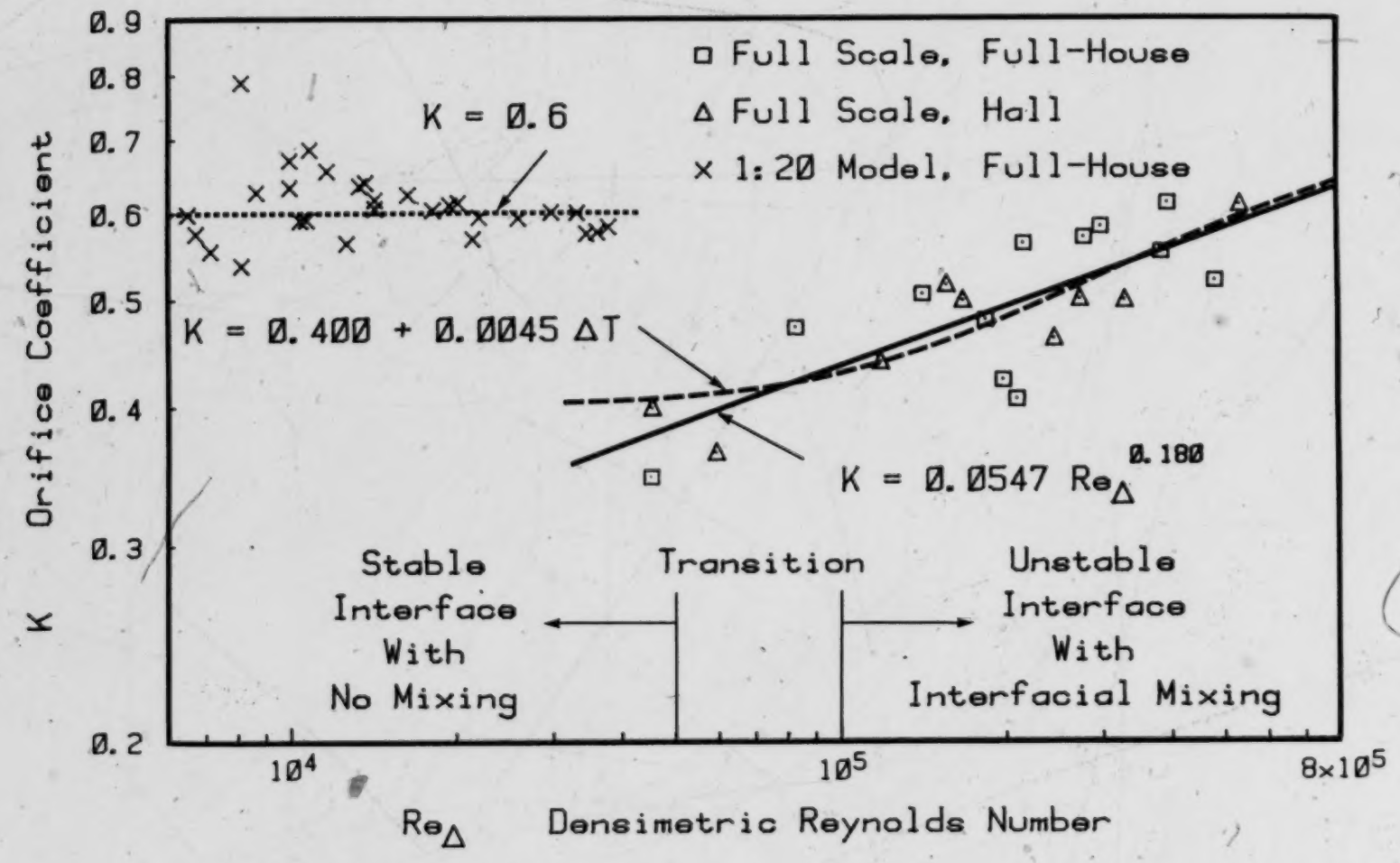

FIGURE 6-8: Comparison of Model and Full Scale Orifice Coefficients with Densimetric Reynolds Number; Stability Limits from Rozovsky, Shabrin, and Markov (1972)

important conclusion to be drawn is that for any given mixing condition in full scale, less mixing is likely to occur in the model due to its lower Reynolds number. For similar experimental parameters then, slightly higher net flow rates will occur in the model compared to the full scale.

To illustrate this point, Figure 6-9 shows the reduction in the model orifice coefficient that results when an exterior turbulent flow passes the door. The model door opening was 150 mm (3 m full scale) from the channel side wall, such that the exterior flow was parallel to the door opening. The average flow speed between the door and the side wall was found to be equivalent to a full scale speed of 20 km/hr (using the buoyancy time scale). The temptation to make an absolute comparison between the model and full scale results should be avoided because no attempt was made to match scales of turbulence or flow speeds (the lack of a windbreak in the model allowed mean flow effects to be included with turbulent effects).

The two important observations are; first, that exterior turbulence can produce mixing in the model and second, that the reduction in orifice coefficient is greater for small temperature differences than for large temperature differences which is similar to the observed effect on the full scale orifice coefficients.

Modelling of Cold Front Flow

In the previous sections, steady state flow conditions for the model and full scale have been compared. It has been shown that the theoretical time scaling is accurate but that the mismatch in Reynolds number and turbulence levels cause measurable differences in the net

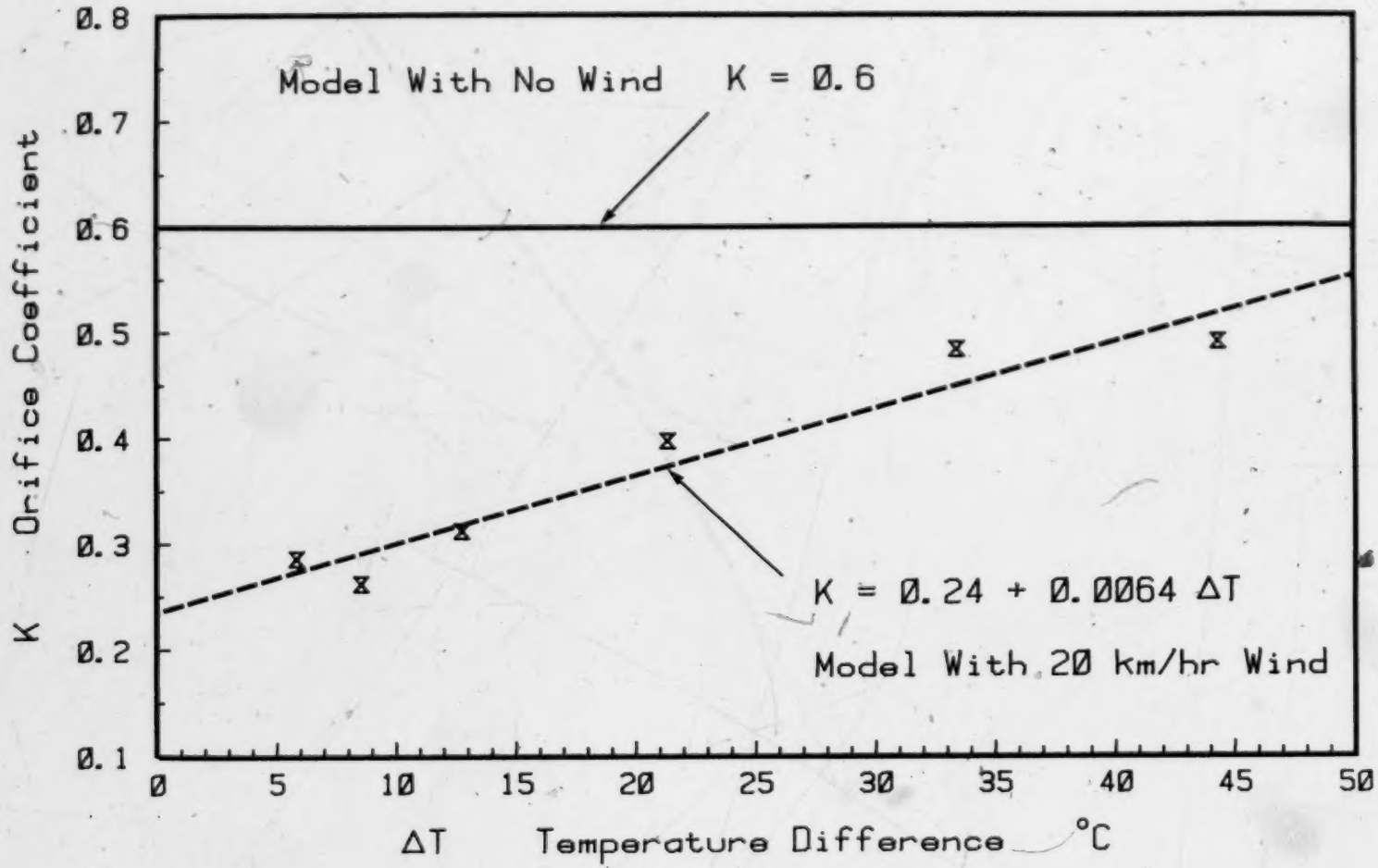

FIGURE 6-9: Reduction in Model Orifice Coefficient Due to a Parallel Wind Past the Opening at a Full Scale Equivalent Rate of 20 km/hr, Geometrically Similar to a Full Scale South Wind, No Wind Breaks Employed

flow rates. Attention will now be focused on the gravity current flow characteristics to further validate the theoretical time scale and also to determine the importance of the mismatches on these flows.

Density current velocity represents an ideal parameter for comparison between the model and full scale. The hall frontal velocity was determined in the full scale tests using thermocouples, the results of which were presented in Figure 4-17. The model frontal velocity was measured using the dual probe method described in Chapter 5. The frontal velocity results for both the model and full scale experiments are shown in Figure 6-10. Once again the results are shown in full scale units, with the model results converted to full scale using the theoretical time scale of $t_S=20^{0.5}$ and the length scale of $L_S=20$.

Although the full scale data becomes increasingly scattered for the higher frontal velocities, the agreement over the entire range of equivalent temperature differences is extremely good. These results strongly support the accuracy of the theoretical time scale. It appears that gravity current frontal velocity is unaffected by the Reynolds number mismatch. The theoretical expression for frontal velocity given by Equation 2-47 with a frontal Froude number of 0.75 was first shown with the full scale data in Figure 4-17. The expression agrees well in the moderate to large temperature difference region but is in error for both the full scale and model results below about $\Delta T=7^{o}C$.

Simpson and Britter (1979) showed that the gravity current frontal velocity is unaffected by the head entrainment rate. This probably explains why there is such good agreement between the model and full scale frontal velocities despite the Reynolds number mismatch.

If accurate full scale information is required about the motion of

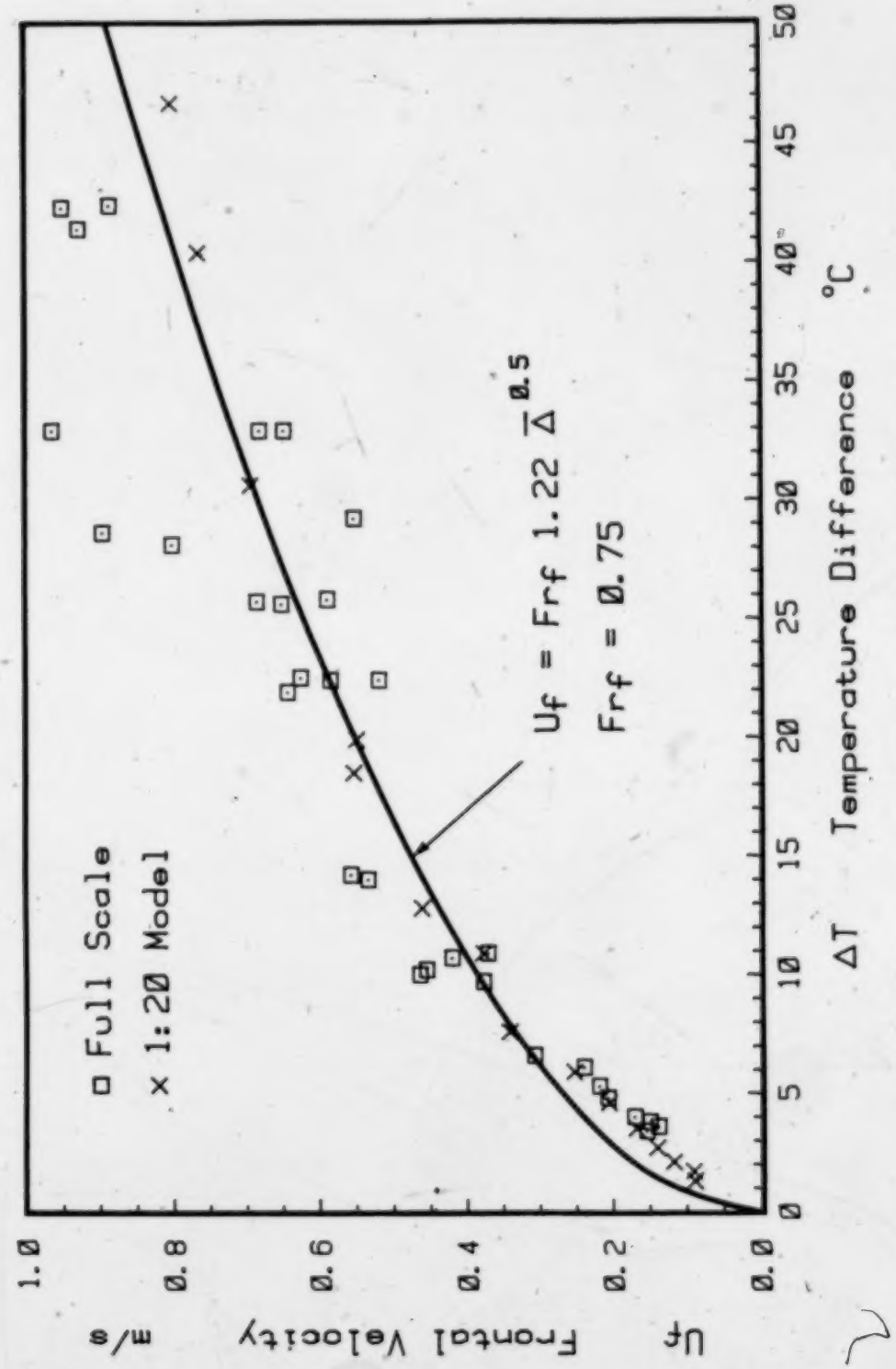

FIGURE 6-10: Comparison of Model and Full Scale Hall Frontal Velocity Variation with Temperature Difference

gravity currents for particular flow geometries, it appears that model measurements will provide accurate and valuable information. Certainly for the simple geometry configuration tested, the model results match the full scale results much better than the theoretical expression.

Decreasing Exchange Rate

The confirmation of similarity for steady state flow and frontal velocity suggests that the onset of the decreasing flow, and its functional form, also model satisfactorily. The data for several of the long duration model tests on the full-house geometry are shown in Figure 6-11. The plotting format is identical to that used in Chapter 4 in Figures 4-22 to 4-24. As with the full scale results, the normalizing procedure causes each of the individual tests to collapse to a single curve with an initial slope $(W^2H^3g/9)^{0.5}$.

The best fit correlation of the theoretical decay function given by Equation 2.52 is also shown on Figure 6.11. As was the case with the full scale results, the theoretical form can be seen to fit the model data very well. The values of E_{cr} and E_{max} that provide the best correlation are 0.38 and 0.99 respectively. Comparing full scale and model results:

	E_{cr} (fit)	E_{max} (fit)
Model (Full-House)	0.38	0.99
Full Scale (Full-House)	0.34	**
Full Scale (Entry)	0.35	1.06
Full Scale (Hall)	0.45	1.08

** Insufficient data to accurately estimate maximum normalized exchange volume E_{max}.

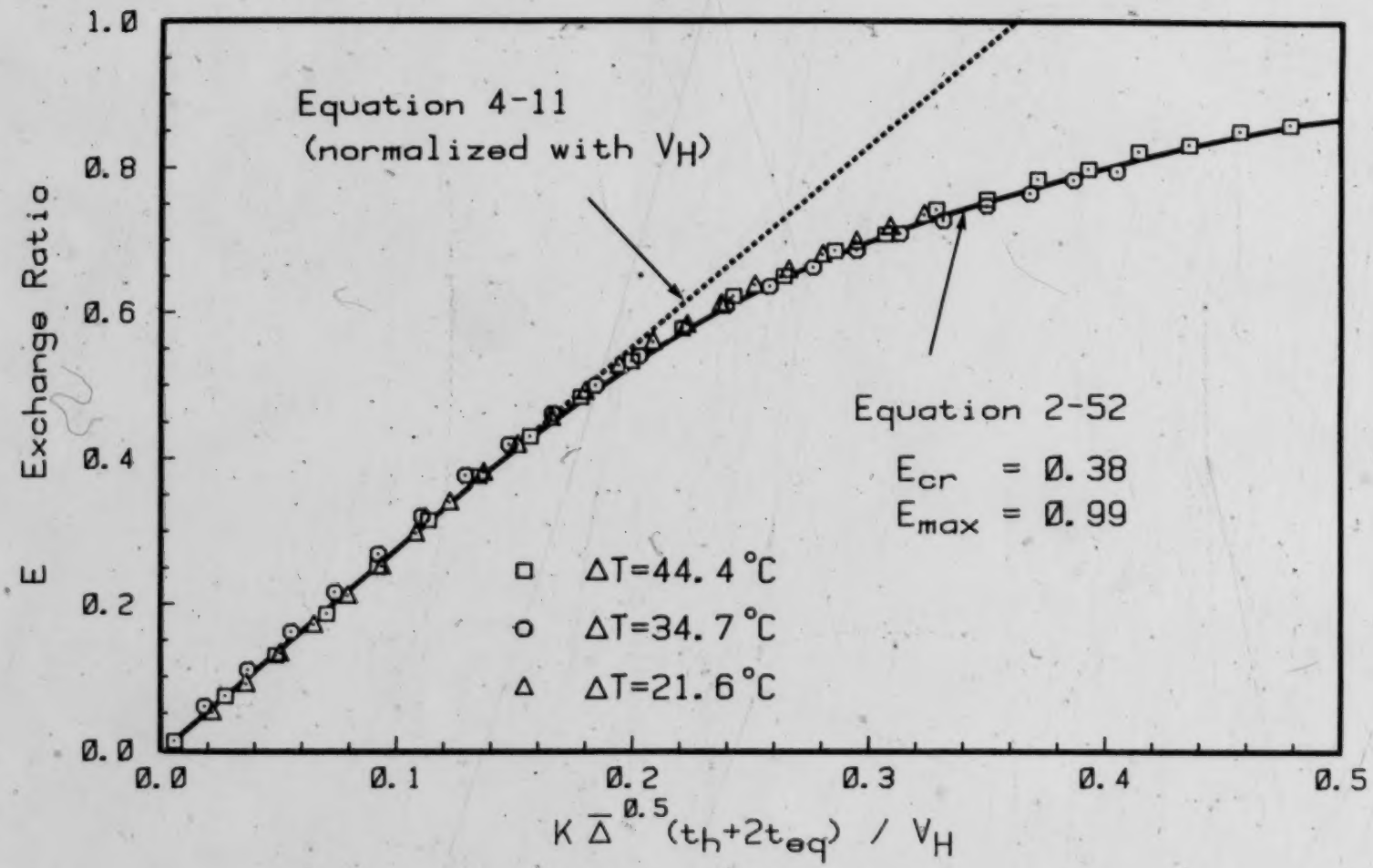

FIGURE 6-11: Model Exchange Ratio for Full-House Geometry with Exponential Decreasing Flow Correlation

The most significant difference between the model and the full scale decay curves are the maximum exchange values. The value of E_{max}=0.99 for the model implies that the maximum exchange volume is 99% of the interior volume beneath a horizontal plane which is level with the top of the entry door. The value of E_{max}=1.07 for the full scale results implies that some of the air trapped above the top of the door level must be mixing with the outgoing air. This difference is probably another result of the Reynolds number mismatch. The reduced level of mixing that has been shown to exist in the model results in less trapped fluid becoming entrained and carried outdoors.

Equivalent Opening and Closing Time

In Chapter 4, it was shown that the buoyancy exchange which takes place during the opening and closing periods can be determined using the fully open flow rate and a modified opening and closing time. The equivalent time for a constant swing motion was shown to be $t_o 2/¶$ and $t_c 2/¶$, or $2t_{eq}$ if the opening and closing motions are the same. The total buoyancy exchange for the opening and closing period was accurately predicted as $Q_n 2t_{eq}$.

In Chapter 5, the procedure for measuring the short duration pumping exchange volumes was described. It included the use of several measurement techniques including the transducer system for the large fractional density differences, a series of probes calibrated over different ranges for the moderate to small fractional density differences and the special alcohol-saltwater mixture for the $\Delta T \approx 0$ extreme.

Unlike the full scale tests, in which only one swing speed was

examined, the model pumping experiments were conducted with 4 different swing speeds. The four swing times tested in the model were 0.81, 0.69, 0.56 and 0.43 s, with a hold time of 0.24 s between opening and closing. If the buoyancy time scale is applied to these values, then the equivalent full scale opening and closing times can be calculated as, 3.6, 3.1, 2.5 and 1.9 s, and a hold time of 1.1 s, in full scale units.

Figure 6-12 illustrates the exchanged volumes over the complete equivalent temperature difference range for the swing speed of 1.9 s. Each data point represents the average of two or three exchange tests to reduce scatter produced by experimental variability. The data blends well from one measuring device range to the next.

The buoyancy predicted volume exchanged curve given by Equation 2-44 with $t_{eq}=(2/\pi)1.9$ s and $t_h=1.1$ s is also shown.

$$V_B = Q_n\ (2t_{eq} + t_h) \qquad (2\text{-}44)$$

The correlation provided by Equation 2-44 is accurate down to a critical temperature difference of approximately $6^{\circ}C$, at which point inertial pumping begins to contribute to the exchange volume. Similar correlations using Equation 2-44 are obtained for each of the other swing speeds tested, except that the critical fractional density difference and the zero ΔT exchange volume depend on swing speed and are different for each correlation. The variation of critical fractional density difference and zero ΔT exchange volume, with swing speed, are examined in the next section.

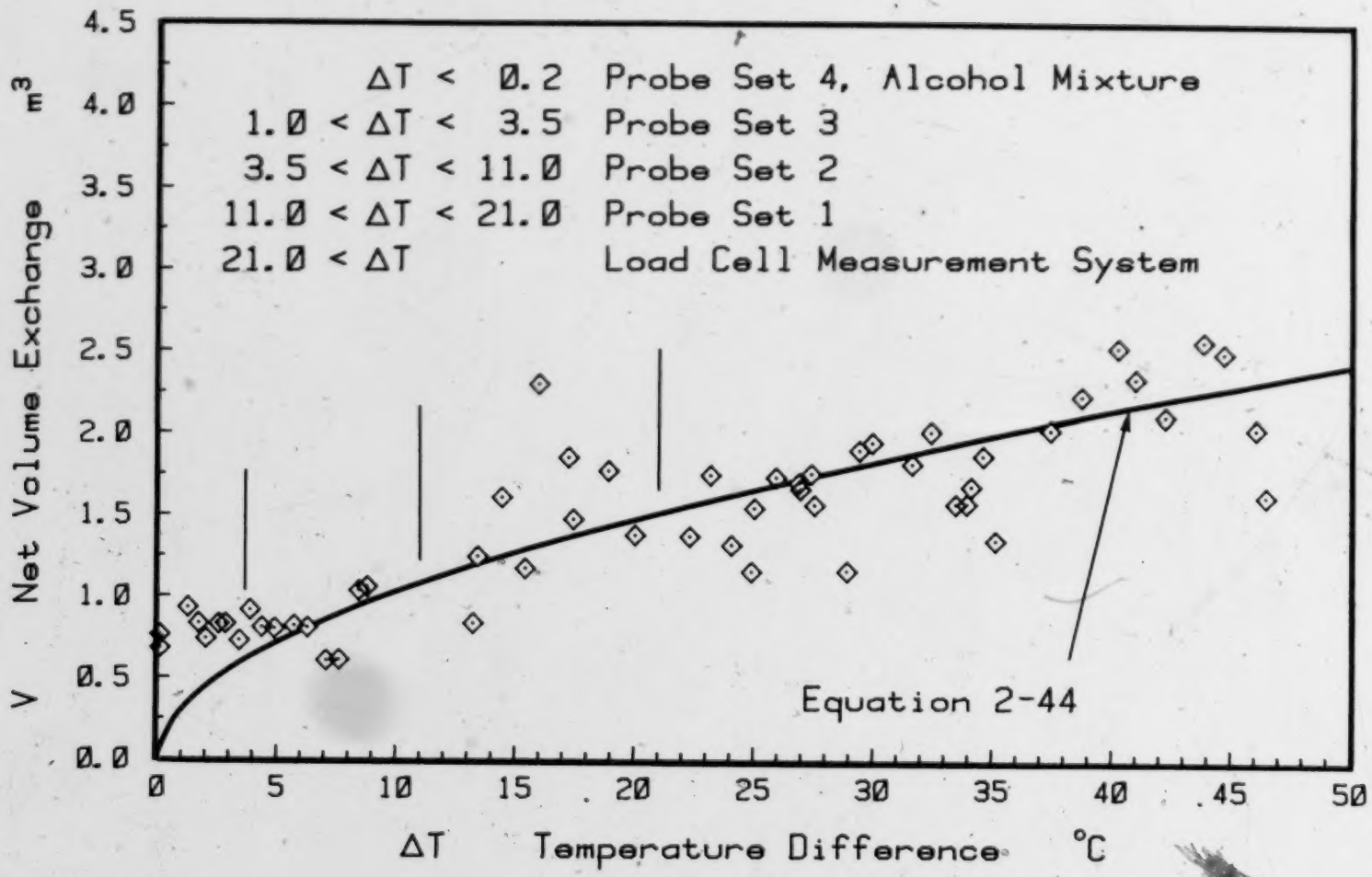

FIGURE 6-12: Typical Correlation of Short Duration Exchanges with Temperature Difference; Swing Time=1.9 s, Hold Time=1.1 s

Inertial Pumping

Both the model results and the full scale results have shown that below a critical fractional density difference the total exchange volume is in excess of the amount predicted by buoyancy alone. The additional exchange volume was identified as the residual pumping exchange volume V_p. This volume was shown the be negligible at $\overline{\Delta}_{cr}$ and to represent the total exchange volume at $\Delta T=0$, identified as V_{P_o}. These two points can be identified on Figure 6-12 as the departure point where the data diverges from the prediction line at about 6^oC, and at the data intersection with the vertical axis at a value of approximately 0.75 m^3. The relationship between these two points and swing speed will now be examined.

Critical Fractional Density Difference- The method used in Chapter 4 to enhance the critical fractional density difference departure point was to plot the ratio of total volume exchanged to the buoyancy predicted exchange, using a semi-log format as seen in Figure 4-15. Following the same procedure with the model data for each of the four swing speeds allows the critical fractional density difference to be determined for each. Figure 6-13 illustrates this for the fastest swing time of 1.9 s, with the critical fractional density difference identified as approximately 0.019. In a similar manner the critical fractional density differences were determined for the other swing speeds as 0.013, 0.011 and 0.009 for the swing speeds of 2.5, 3.1 and 3.6 s respectively. The full scale critical fractional density difference for a swing time of 3.75 s was determined in Chapter 4 as approximately 0.012.

The critical fractional density difference is found to vary

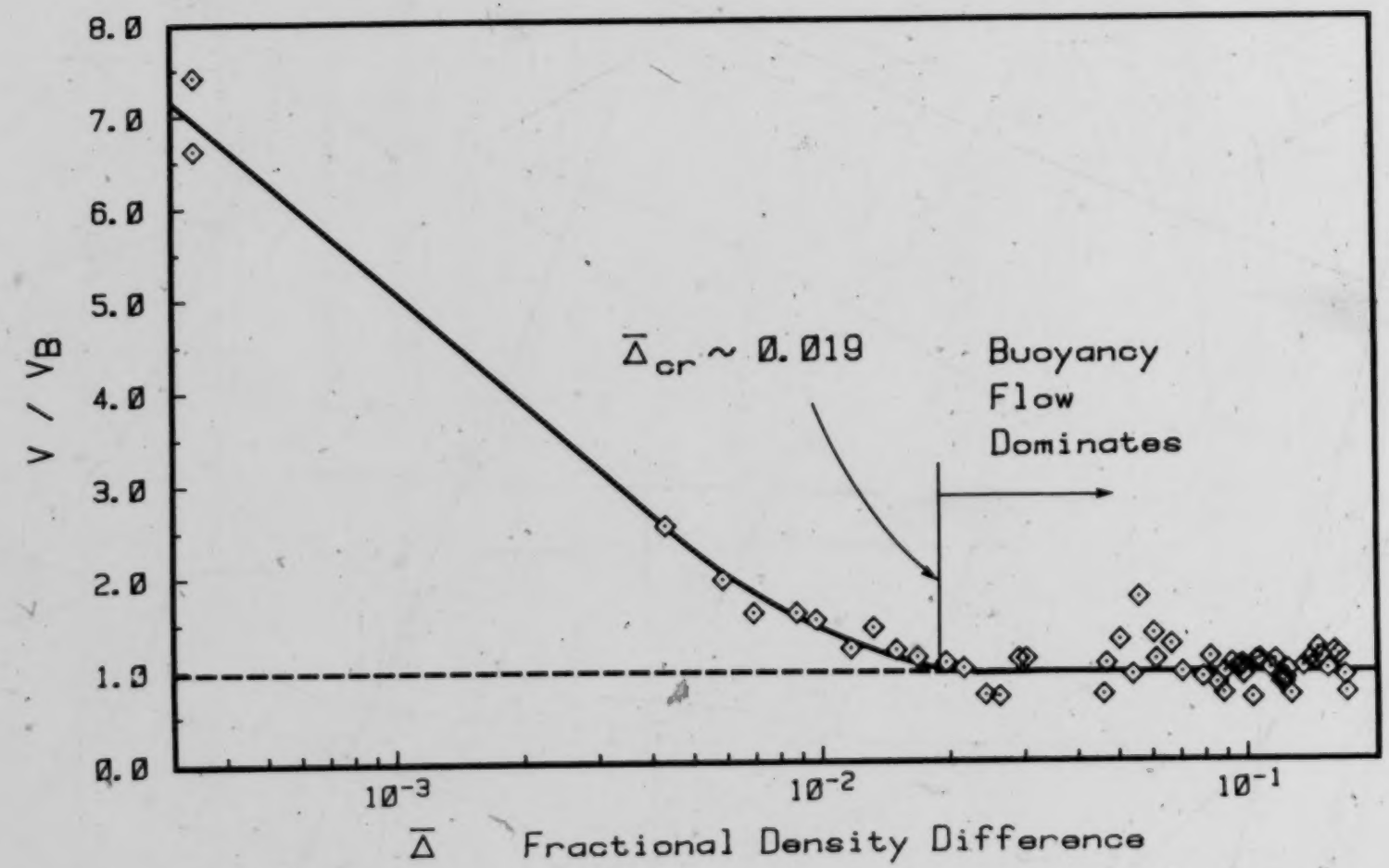

FIGURE 6-13: Critical Fractional Density Difference Determined from the Ratio of Total Exchange to Buoyancy Predicted Exchange for Short Duration Openings; Swing Time=1.9 s, Hold Time=1.1 s

inversely with the swing time, with a constant of proportionality P_1, of approximately 0.0325 where:

$$P_1 = 0.0325 = \bar{\Delta}_{cr}\, t_o \qquad (6\text{-}1)$$

It is important to note that even for the fastest swing speed the critical temperature difference at which the inertial effect just begins to contribute is only 5 to 6°C. Observing Figure 6-13, the point at which predicted buoyancy driven exchange equals the residual volume exchange occurs at a fractional density difference of 0.006, this is equivalent to a temperature difference of approximately 1.8°C. Clearly from the view of energy losses, even for the fastest swing speed, pumping exchange contributes can be neglected.

The model and full scale critical fractional density differences are similar considering that the accuracy of the full scale temperature measurements are only within 1 to 2 degrees.

ΔT=0 Volume Pumped- The pumping experiments were also conducted for very small fractional density differences using the alcohol-salt water solution and salinity probes. The volumes pumped at each of the swing speeds were determined to be 0.43, 0.52, 0.61 and 0.72 m^3 for the swing speeds of 3.6, 3.1, 2.5 and 1.9 s respectively. The full scale pumping volume was determined in Chapter 4 to be 0.45 m^3 for the swing speed of 3.75 s.

The pumped exchange volume at a zero fractional density difference was also found to vary proportionally to swing speed with a constant of proportionality P_2, of approximately 1.55, where:

$$P_2 = 1.55 = V_{Po}\, t_o \qquad (6\text{-}2)$$

The buoyancy time scale appears to apply at $\Delta T=0$, as indicted by the similar exchange volumes of 0.43 m^3 in the model compared to 0.45 m^3 in full scale for swing times of 3.6 s and 3.75 s respectively, where the model swing time is converted to full scale using the buoyancy time scale. This is very convenient, however, it does not agree with the inertia time scale of 31 determined in Chapter 2 by matching Reynolds numbers.

Combined Buoyancy-Pumping Region- An empirical relationship can now be developed between the residual volume, swing speed, and fractional density difference by noting that $V_p t_o$ must diminish from a value of P_2 at $\bar{\Delta}t_o=0$, to zero at $\bar{\Delta}t_o=P_1$. Figure 6-14 illustrates $V_p t_o$ as a function of $\bar{\Delta}t_o$. The data converge at the vertical intercept of $P_2=1.55$ sm^3 and the horizontal intercept of $P_1=0.0325$ s. The intermediate data was approximated by the following linear relationship.

$$V_p t_o = P_2 - \frac{P_2}{P_1} \bar{\Delta}to$$

or rearranging

$$V_p = \frac{P_2}{t_o} \left[1 - \frac{\bar{\Delta}t_o}{P_1} \right] \qquad (6.3)$$

Caution must be used when determining residual volumes with this relationship for it only applies for doors with H≈206 cm and W≈91 cm, and is largely based on model results which have not been fully confirmed in full scale. Further experimental work with varying sized doors may allow a complete dimensional treatment such that the constants are nondimensional and functionally dependent on the values of W and H.

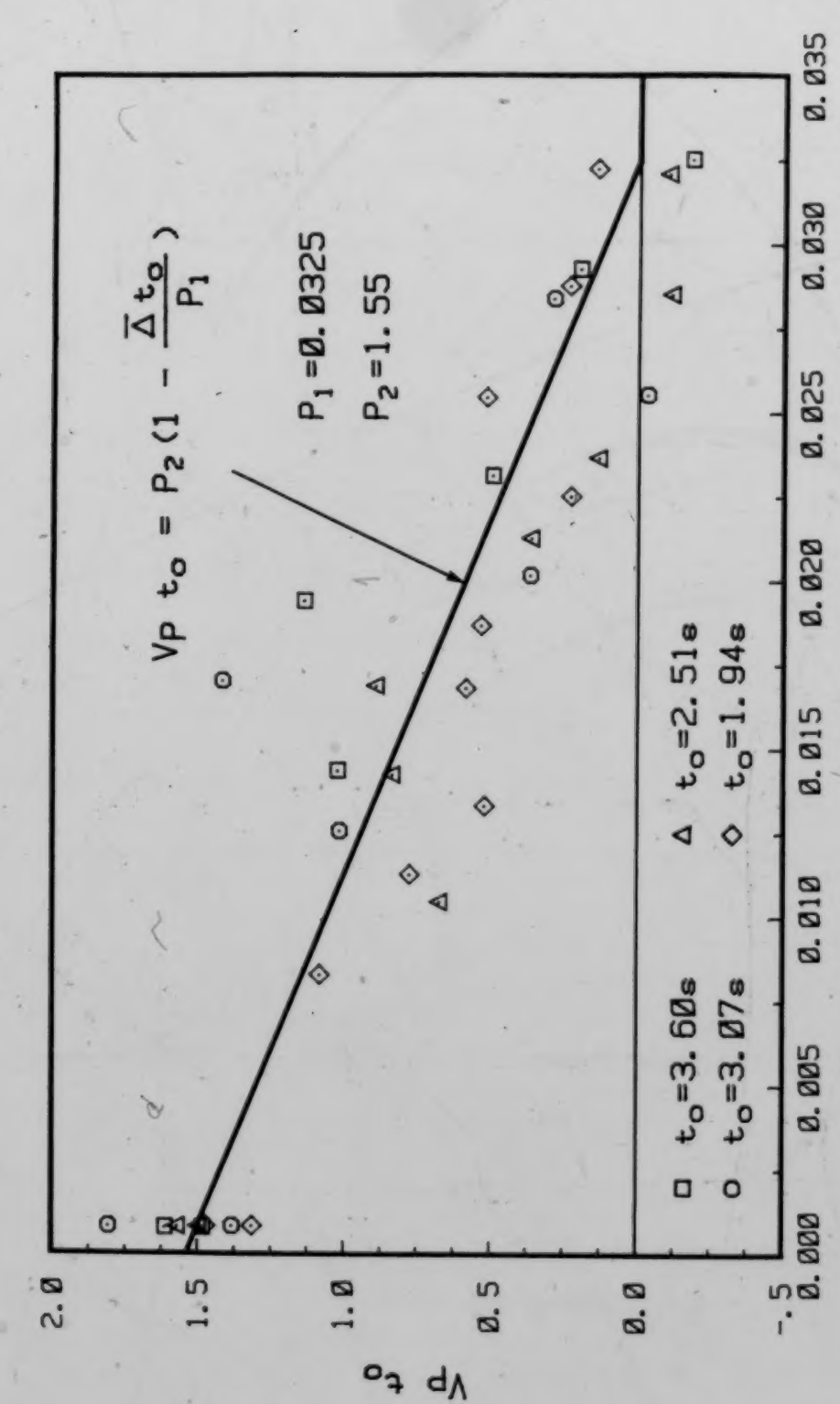

FIGURE 6-14: Correlation of Residual Pumping Exchange Volume with Door Swing Time and Fractional Density Difference

One final caution; the residual volumes given by these equations assume a relatively short hold time, but if the hold time is large, then the actual value of V_p may be greater because the turbulence would have a greater period of time to promote exchange.

CHAPTER 7

CONCLUSIONS AND RECOMMENDATIONS

Full scale air exchange experiments were conducted at the Alberta Home Heating Research Facility using tracer gas and thermocouple techniques. Similar experiments were then conducted using a 1:20 scale model with salt water and fresh water solutions to simulate full scale indoor-outdoor temperature differences. The following conclusions and recommendations are based on the experimental results obtained during the course of these experimental studies.

Steady State Buoyancy-Driven Flow

1) Steady state buoyancy-driven flow is proportional to the square root of the indoor-outdoor fractional density difference as predicted by the theoretical inviscid analysis.

2) Viscous, contraction and velocity effects can be accounted for by a mixing coefficient C_m, and a discharge coefficient C_d, where $K=C_d(1-C_m)$. The discharge coefficient was found to be approximately 0.6. The mixing coefficient was found to vary from zero to 0.35 over a temperature difference range of 40°C to 0°C, for wind speeds less than 10 km/hr. The variation in mixing coefficient was found to correlate linearly with temperature difference and as a power function with densimetric Reynolds number to the 0.18 power.

3) The variation in the mixing coefficient C_m, was caused by interfacial mixing of fluid across the counterflow interface. At large temperature differences, virtually no exterior mixing occurs due to the

rapid upward flow of outgoing fluid but a small amount of interior interfacial mixing occurs due to the large interfacial contact surface. At small temperature differences, substantial interior and exterior interfacial mixing takes place, causing a large reduction in net exchange rates, reflected in a reduced orifice coefficient, K.

4) Exterior and interior turbulence tend to increase the amount of interfacial mixing, reducing the net exchange rate and orifice coefficient. Smaller temperature differences are more significantly affected by a given turbulence level compared to large temperature differences. This reflects the relative strength of the buoyancy forces promoting stability and the inertial forces promoting mixing.

5) Buoyancy flow exists during the period when the door is opening and closing, and can be accurately predicted by integrating the steady flow buoyancy equation for varying orifice width.

Steady State Flow Departure and Decreasing Flow Rate

1) Frontal velocity flow rates down a long hall agree with the theoretical predictions from lock exchange theory with a frontal Froude number of approximately 0.75, which is near the pure counterflow limit of 0.707.

2) Long hall experiments confirm the theoretical model which predicts that departure from steady state flow will begin when the gravity current has traveled the length of the hall, reflected off the end wall and returned to the entry at frontal speed U_f. Simple one dimensional flow produces a well defined inflection point in the volume exchange curve at the wave return time.

3) For complicated geometries which have two dimensional spreading

flow, the return of numerous reflected waves from multiple reflection surfaces tends to blur the distinct inflection point observed in the one dimensional case.

4) A critical departure volume can be roughly estimated as 60% to 70% of the air volume trapped beneath a horizontal plane level with the top of the opening. Estimating the flow rate allows a critical time to be approximated without considering frontal velocity or characteristic flow length.

5) After the critical time, the flow rate decreases until the exchange volume asymptotically approaches a maximum exchange volume slightly larger than the gaseous volume beneath a horizontal plane level with the top of the entry, V_H. The volume exchange in excess of V_H depends on the amount of buoyantly trapped air above the horizontal plane which is mixed downwardly. The values obtained in this study indicate total exchanges of approximately $1.07V_H$, for limited interior circulation. If interior circulation is strong, the total exchange volume may approach the total interior volume.

Inertial Pumping Exchange

1) The exchange produced by the pumping action of a typical residential swinging door is totally negligible below a critical fractional density difference. The relationship between the critical fractional density difference and 90 degree swing time was determined empirically as $\bar{\Delta}_{cr} = 0.0324s/t_o$, for a typically sized residential door. For a typical swing time of 2.5 s, the critical temperature difference is approximately 4^oC and the temperature difference at which the residual exchange produced by pumping is equal to the theoretical

buoyancy exchange is approximately $1^{o}C$ (during opening and closing). Pumping contributions can be totally neglected in calculating heating energy losses.

2) At the extreme of a zero temperature difference the pumping volume exchange was also found to be inversely proportional to the swing time. The constant of proportionality was determined empirically for a typically sized residential door resulting in $V_{P_o}=1.55sm^3/t_o$.

3) The value of residual exchange V_P, (that is the exchange volume during opening and closing over and above that predicted using the buoyancy exchange analysis) was found to vary linearly with fractional density difference, decreasing from a value of $1.55sm^3/t_o$ at a fractional density ratio of zero, to a value of zero at the critical density ratio of $\overline{\Delta}_{cr}=0.0325/t_o$.

Model Similitude

1) The theoretical buoyancy time scale based on matching Froude numbers was determined as $L_S^{0.5}$ and was confirmed for both the gross flows and local frontal flows.

2) A densimetric Reynolds number mismatch of approximately a factor of 7 resulted from the combination of selected length scale and modelling fluid. The primary effect lay with relative interfacial stability. Model densimetric Reynolds numbers were smaller than the stability transition range of $5x10^4 - 10^5$ as defined by Rozovsky, Shabrin and Markov (1972) and the full scale densimetric Reynolds numbers were larger than the stability transition range. For this reason, the full scale tests exhibited significantly more interfacial mixing than the model. These results were confirmed by temperature and

salinity profiles. Full scale results exhibited more interfacial mixing at small temperature differences than at large temperature differences. For these reasons the model will over predict the full scale exchange rates due to the relative lack of interfacial mixing, particularly at small fractional density differences. If however, the local model and full scale Reynolds number are both above the transition range, then the mismatch may become less significant.

3) The theoretical time scale of 31 for inertial pumping, based on a Reynolds number match at a zero fractional density difference, was found to be incorrect. The experimentally determined inertial pumping time scale of 4.78 is only 6% different than the buoyancy time scale. This allows the same time scale to be used over the entire fractional density difference range.

4) The time of departure from steady flow and the functional form of decreasing flow were found to be similar for the model and full scale using the theoretical time scale of $L_S^{0.5}$. The only significant difference was that the maximum volume exchange in the model was V_H compared to approximately $1.07V_H$ in full scale. This was the result of interfacial stability in the model limiting the mixing of fluid above the horizontal plane level with the top of the door.

Recommendations

1) For air exchange calculations in houses the orifice coefficient should not be taken as constant at 0.6 but as $K = 0.4 + 0.0045\Delta T$. Further study should be conducted to determine the quantitative influence of wind on interfacial mixing as a function of wind speed and wind angle. Because wind induced turbulence reduces buoyancy exchange, the calculated exchange using the expression above will result in an overestimate of both energy requirements and fresh air supply.

2) Further model studies should be performed to examine the merits of modified entry configurations such as sunken entries.

3) Model studies of larger structures would require increased model length scales resulting in increased Reynolds number mismatches. Further study should be directed toward determining the possibility of generating model turbulence levels to induce the correct amount of interfacial mixing. The dependence of interfacial mixing on door height should also be examined.

4) A vibration damping system for the model should be developed to improve the weight measurement system for small weight changes.

REFERENCES

REFERENCES

Bara, B. (1985),"Ground Release Concentration Fluctuations", M.Sc. Thesis, Department of Mechanical Engineering, University of Alberta.

Barr, D.I.H., (1963), "Densimetric Exchange Flow In Rectangular Channels", La Houille Blanche, No.7, pp. 739-766.

Bassett, M.R., Shaw, C. and Evans R.G., (1981), "An Appraisal of the Sulphur Hexafluoride Decay Technique for Measuring Air Infiltration Rates in Buildings", ASHRAE Trans. Vol. 87, Pt. 2, pp. 361-371.

Bean, H.S. (1971), "Fluid Meters, Their Theory and Application", ASME Report, Sixth Edition.

Benjamin, T.B. (1968), "Gravity Currents and Related Phenomena", Jour. Fluid Mech. 31, pp. 209-248

Brown, W.G., Wilson, A.G. and Solvason, K.R., "Heat and Moisture Flow Through Openings by Convection", ASHRAE Journal, Sept. 1963, pp. 49-53.

Brown, W.G. and Solvason, K.R., "Natural Convection Through Rectangular Openings in Partitions-1", Int. J. Heat Mass Transfer, Vol. 5, pp. 859-868.

Fritzsche, C. and Lilienblum, W. (1968), "New Measurements for the Determination of the Cold Losses at the Doors of Cold Rooms", Kaltetechnik - Klimatisierung 20, Jahrgang Heft 9.

Roberson, J.A. and Crowe, C.T. (1980), Engineering Fluid Mechanics, 2nd Edition, Houghton Mifflin Company, pp. 531-534.

Rozovsky, I.L., Shabrin, A.N. and Markov, S.B. (1972), "Investigation of the Forms of Interface by Density Current of Salt and Fresh Water in a Rectangular Channel" Proc. of Int. Symposium on Stratified Flow Novosibirsk pp. 647-655.

Schlichting, H. (1955), Boundary-Layer Theory, 7th Edition, McGraw-Hill Book Company, p. 13.

Shaw, B.H. (1972), "Heat and Mass Transfer by Natural Convection and combined Natural Convection and Forced Air Flow Through Large Rectangular Openings in a Vertical Partition.", Institute of Mechanical Engineers Conference, Vol. CS19.

Shaw, B.H.(1976), "Heat and Mass Transfer by Convection Through Large Rectangular Openings in a Vertical Partitions.", Ph.D. Thesis, Department of Mechanical Engineering, University of Glasgow.

Simpson, J.E. and Britter, R.E. (1979), "The Dynamics of the Head of a Gravity Current Advancing Over a Horizontal Surface", Jour. Fluid Mech. 94, part3, pp. 477-495.

Wilkinson, D.L. and Wood, I.R. (1972), "Some Observations on the Motion of the Head of a Density Current", Jour. Hydraulic Research 10, pp. 305-324.

APPENDIX A

APPENDIX A

DENSITY-DRIVEN FLOW THROUGH AN OPEN DOOR

AN INVISCID ANALYSIS

Buoyancy-driven flow through an open door can be modelled as two ventilated weirs as shown in Figure A1. Making the following assumptions:

- The pressure across the outgoing fluid at ρ_i is hydrostatic at outdoor conditions across section A-C with ρ_o setting the pressure variation.
- The pressure across the incoming fluid at ρ_o is hydrostatic at indoor conditions across section B-C with ρ_i setting the pressure variation.
- The indoor and outdoor pressures P_i and P_o are in equilibruim along the interfacial streamline and for applications to this study $P_i=P_o$.

By symmetry, the solution for these two weir flows is identical with densities interchanged. Only one flow needs to be considered, which for convenience will be the infiltration flow Q_o' from the outside to inside.

Because all streamlines originate from a reservoir that is stagnant at ρ_o, they all have the same Bernoulli constant. The Bernoulli equation crossing streamlines from points "0" to "2" as indicted on Figure A1, can be written as:

$$\frac{P_o}{\rho_o} = \frac{P_2}{\rho_o} + \frac{U_2}{2} + gz_2 \qquad \text{(A1)}$$

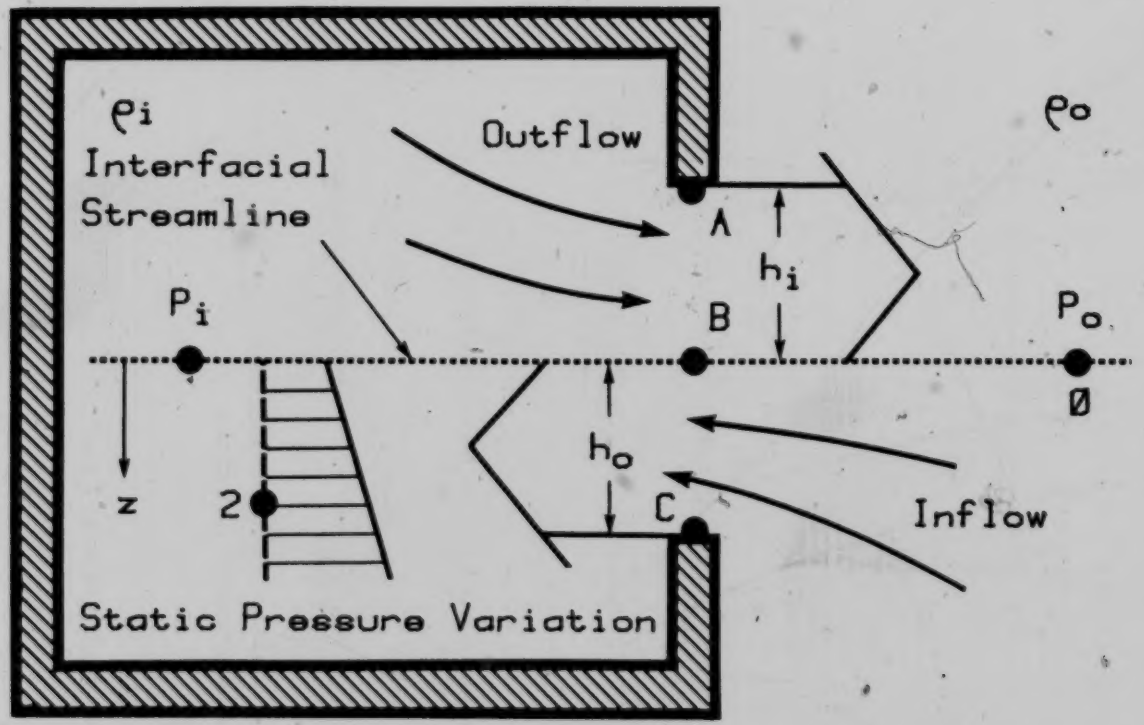

FIGURE A1: Double Weir Model of Inviscid Buoyancy-Driven Flow Through a Vertical Opening into a Sealed Room

P_2 is determined from the static pressure variation inside the room at ρ_i so that:

$$P_2 = P_i - \rho_i g z_2 \qquad (A2)$$

Combining Equations A1 and A2, and letting $\Delta\rho=\rho_o-\rho_i$ results in:

$$P_o = P_i + \frac{\rho_o U_2^2}{2} + g(\Delta\rho)z_2 \qquad (A3)$$

Solving Equation A3 for U_o' at any distance from the neutral level z and setting $P_i=P_o$ results in:

$$U_o' = \left[2g \frac{\Delta\rho}{\rho_o} z\right]^{0.5} \qquad (A4)$$

Integrating the velocity profile over width W, to find the volume flow results in :

$$Q_o' = \int_{z=0}^{z=h_o} U_o' \, W \, dz$$

$$Q_o' = \frac{2W}{3} h_o^{1.5} \left[\frac{2g\,\Delta\rho}{\rho_o}\right]^{0.5} \qquad (A5)$$

The solution for the exfiltration flow Q_i' and velocity U_i' is exactly the same with ρ_o and ρ_i interchanged so that:

$$U_i' = \left[2g \frac{\Delta\rho}{\rho_i} z\right]^{0.5} \qquad (A6)$$

$$Q_i' = \frac{2W}{3} h_i^{1.5} \left[\frac{2g\ \Delta\rho}{\rho_i}\right]^{0.5} \qquad (A7)$$

Comparing Equations A4 to A5 it is found that the velocity profiles are not symmetric but differ by $(\rho_i/\rho_o)^{0.5}$. Because the flow is incompressible the continuity equation applies for an enclosure with no other significant flows:

$$Q_i' = Q_o' \qquad (A8)$$

Using the continuity equation A8 with A5 and A7 allows h_i to be related to h_o as:

$$\frac{h_o}{h_i} = \left[\frac{\rho_o}{\rho_i}\right]^{1/3} \qquad (2\text{-}6)$$

For a total door height of $H=h_i+h_o$ Equation 2-6 can be written as:

$$h_i = \frac{H}{1 + (\rho_o/\rho_i)^{1/3}} \qquad (A9)$$

Combining Equation A7 with A9 results in the following expression for inviscid incoming and outgoing flow rate.

$$Q' = \frac{W}{3} (gH^3\ \Delta\rho/\rho')^{0.5} \qquad (2\text{-}4)$$

$$\rho' = \rho_i \frac{(1+(\rho_o/\rho_i)^{1/3})^3}{8} \qquad (2\text{-}5)$$

APPENDIX B

APPENDIX B

MIRAN A1 INFRARED ABSORPTION GAS ANALYSER CALIBRATION

A Miran A1 infrared absorption gas analyser was used in conjunction with sulphur hexaflouride (SF_6) as a tracer gas to determine air exchange volumes. The following calibration procedure was used to determine the relationship between voltage output and SF_6 concentration.

- The Miran A1 and closed loop calibration pump are purged completely with pure air and interconnected. The total internal volume is 5.64 l.
- The zero is set so that pure air registers a voltage output of 0.0 volts
- A 503 ml cylinder is purged with pure air and septums placed on the two injection ports.
- A 10 ml air sample is drawn out of the cylinder using a sample syringe, leaving it slightly depressurized.
- A 10 ml pure SF_6 sample is drawn from a storage bottle and is gently injected into the cylinder causing the pressure to return to atmospheric and is mixed completely with the aid of a ball located inside the cylinder.
- 15 consecutive 100µl samples are drawn and injected into the closed loop volume through the pump injection port. After allowing time for the sample to become thoroughly mixing the miran voltage is recorded.
- Each injection produces an increase in concentration of 0.352 ppm for a full range of 0 to ≈5.3ppm indicted by an output range from 0 to 1 volt.
- A curve of the form; $(Conc.)=A+B*(Volts)^C$, is determined for the range of 1 ppm - 5 ppm, as illustrated in Figure B2.

Standard Miran Settings:

Path length	- 1.71
Wave length	- 10.7
Slit width	- 1
Absorption	-0.1
Time Response	-10

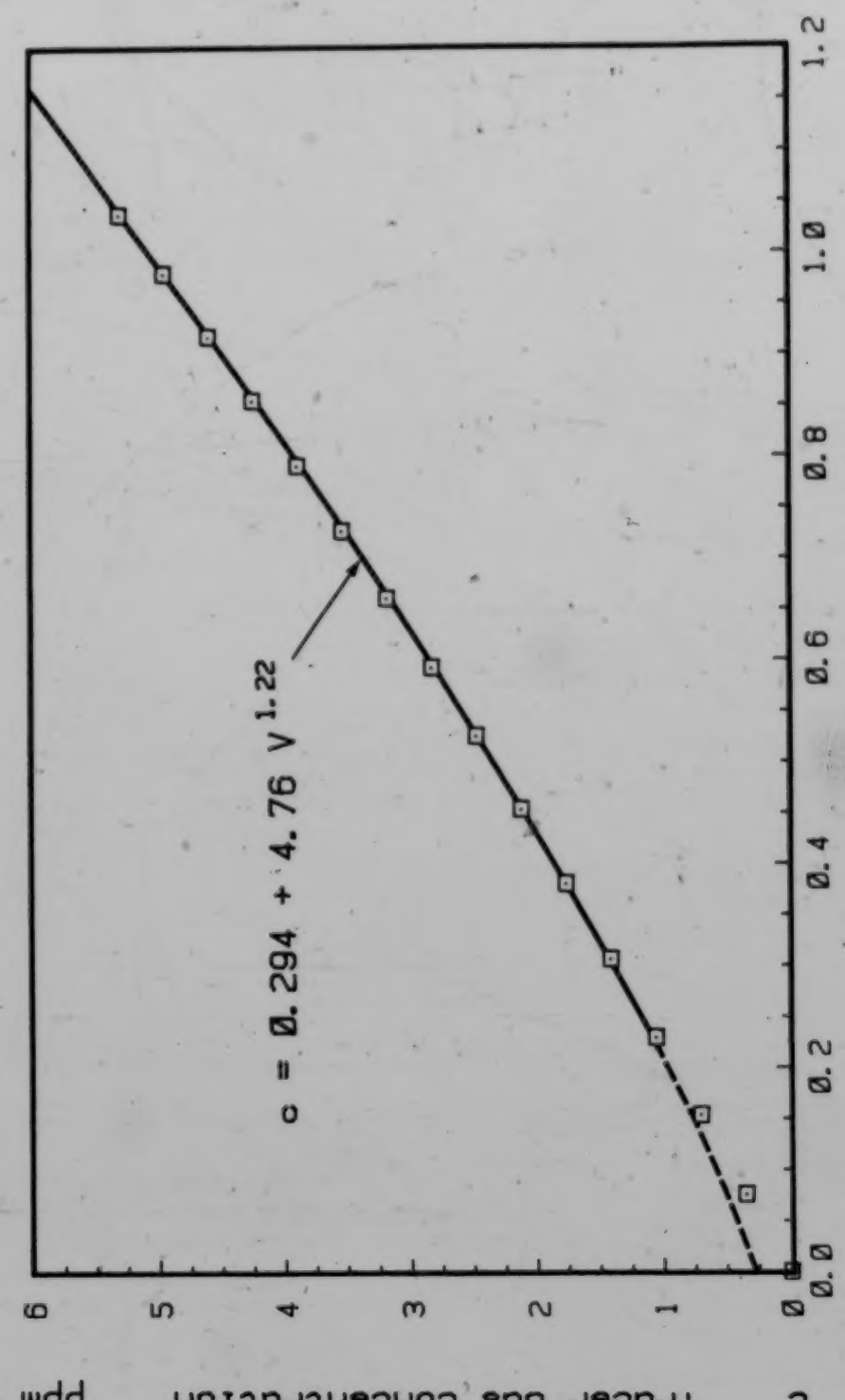

FIGURE B1: Miran 1A Infrared Gas Analyser Calibration Curve